

University of Nebraska - Lincoln

DigitalCommons@University of Nebraska - Lincoln

---

Theses and Dissertations in Biochemistry

Biochemistry, Department of

---

Fall 11-2013

## Investigation of Proline Utilization A: Kinetic Analysis of Substrate Channel-blocking Mutants and Creation of a Trifunctional Chimera Enzyme

Benjamin W. Arentson

University of Nebraska-Lincoln, ben.arentson@gmail.com

Follow this and additional works at: <https://digitalcommons.unl.edu/biochemdiss>

 Part of the [Biochemistry Commons](#)

---

Arentson, Benjamin W., "Investigation of Proline Utilization A: Kinetic Analysis of Substrate Channel-blocking Mutants and Creation of a Trifunctional Chimera Enzyme" (2013). *Theses and Dissertations in Biochemistry*. 14.

<https://digitalcommons.unl.edu/biochemdiss/14>

This Article is brought to you for free and open access by the Biochemistry, Department of at DigitalCommons@University of Nebraska - Lincoln. It has been accepted for inclusion in Theses and Dissertations in Biochemistry by an authorized administrator of DigitalCommons@University of Nebraska - Lincoln.

INVESTIGATION OF PROLINE UTILIZATION A: KINETIC ANALYSIS OF  
SUBSTRATE CHANNEL-BLOCKING MUTANTS AND CREATION OF A  
TRIFUNCTIONAL CHIMERA ENZYME

by

Benjamin W. Arentson

A DISSERTATION

Presented to the Faculty of  
The Graduate College at the University of Nebraska  
In Partial Fulfillment of Requirements  
For the Degree of Doctor of Philosophy

Major: Biochemistry

Under the Supervision of Professor Donald F. Becker

Lincoln, Nebraska

November 2013

INVESTIGATION OF PROLINE UTILIZATION A: KINETIC ANALYSIS OF  
SUBSTRATE CHANNEL-BLOCKING MUTANTS AND CREATION OF A  
TRIFUNCTIONAL CHIMERA ENZYME

Benjamin W. Arentson, Ph.D.

University of Nebraska, 2013

Advisor: Donald F. Becker

Proline metabolism is known to be involved in many cellular processes such as cell signaling, cellular redox balance, and cell survival. One of the enzymes involved in proline catabolism, proline utilization A, plays a role in oxidizing proline to glutamate in a two-step oxidation pathway involving enzymes proline dehydrogenase (PRODH) and  $\Delta^1$ -pyrroline-5-carboxylate dehydrogenase (P5CDH).

Intermediate P5C/GSA has been shown to use an intramolecular channel to move from the PRODH active site to the P5CDH active site in a phenomenon called substrate channeling. In this work, one of the main objectives was to learn more about the channel usage. Chapter 2 demonstrates that making mutations along the channel can impede passage of intermediate, and helps describe how P5C accesses the P5CDH domain.

A second objective was to gain understanding of the structure-function relationship of the DNA-binding domain of trifunctional PutAs. Chapter 3 discusses how a chimera enzyme was created by attaching the DNA-binding domain of a trifunctional PutA to a bifunctional PutA in order to make an artificial trifunctional PutA. These results help to better understand how the DNA-binding domain orientation is important and provide clues that more residues from the DNA-binding domain may be necessary for DNA-binding *in vivo*.

Chapter 4 explores a new ubiquinone analog, and provides kinetic evidence suggesting it is a substrate for the PRODH domain. Additionally *Geobacter sulfurreducens* was kinetically characterized and was shown to substrate channel.

Collectively, this dissertation aims to provide a further understanding of usage of the substrate channel in proline oxidation and insight into the structure-function relationship of trifunctional PutAs and functional switching.

## ACKNOWLEDGEMENTS

Foremost I would like to thank Dr. Donald Becker for taking a chance on me both as an REU student and a graduate student. Without his belief in me, I know I would not be standing where I am today. I cannot say enough good things about his selflessness as a mentor, his positive attitude, and his creation of an awesome work environment. When the time comes to move on, I will always remember and try to replicate his work ethic and humble character, as these are two traits I feel have made him so successful. Dr. Becker has been a truly wonderful mentor, giving me room to grow both as a person and as a scientist. His respect and understanding of things outside of the realm of science mean more to me than he will ever know. For all these things I will be forever grateful.

I also would like to thank my committee members Dr. Melanie Simpson, Dr. Julie Stone, Dr. Jaekwon Lee, and Dr. Robert Powers for their critiques and suggestions of my research. I would especially like to thank Dr. Melanie Simpson for supporting and encouraging me to participate in the Preparing Future Faculty Program, which helped focus my career goals.

Thank you also to past and present members of the Becker Lab; the lab environment made coming to work a treat each and every day. I'd like to especially thank Nikhilesh Sanyal for helping make and share four years of substrate channeling memories. Also Navasona Krishnan was instrumental in teaching me the ropes of proline metabolism and lighting a fire beneath me for scientific research. Thank you also to friends around the Beadle Center for sharing coffee, ideas, and motivation.

Much of my work would not be possible without our PutA partners in crime from the lab of Dr. Jack Tanner. Our weekly Skype meetings have definitely challenged me to think more deeply as a scientist.

Finally I have the utmost gratitude for the support of my family. Thank you to my parents both for encouraging me to follow my interests and for providing life experiences that have shaped who I have become. Much thanks also to my wife, Nikki, daughter, Tatum, and four-legged son, Kramer who have been troopers putting up with my late nights and absences. I thank them not only for their sacrifices, but also for the continual joy they bring me.

**TABLE OF CONTENTS**

<b>TITLE</b>	<b>i</b>
<b>ABSTRACT</b>	<b>ii</b>
<b>ACKNOWLEDGEMENTS</b>	<b>iv</b>
<b>TABLE OF CONTENTS</b>	<b>vi</b>
<b>ABBREVIATIONS</b>	<b>x</b>
<b>CHAPTER 1: Introduction: Substrate Channeling in Proline Metabolism</b>	<b>1</b>
INTRODUCTION	2
PROLINE METABOLIC ENZYMES	3
Proline Catabolism	3
PutA Family	6
Structural Characterization of PutAs	8
Trifunctional PutAs and Functional Switching	11
Proline Biosynthesis	13
INTERMEDIATES OF PROLINE METABOLISM	16
OVERVIEW OF SUBSTRATE CHANNELING	18
Rationale for Substrate Channeling	18
Kinetic Approaches to Test for Substrate Channeling	20
Transient Time Estimation	20
Trapping the Intermediate	22
Inactive Mutants	22
Designing Fusion Proteins	23
CHANNELING OF P5C/GSA	23
CHANNELING OF $\gamma$ -GLUTAMYL PHOSPHATE	28
SUMMARY	31

	vii
REFERENCES	33
<b>CHAPTER 2: Kinetic Characterization of Channel-blocking Mutants in <i>Bradyrhizobium japonicum</i> Proline Utilization A (PutA)</b>	<b>40</b>
ABSTRACT	41
INTRODUCTION	42
MATERIALS AND METHODS	46
Chemicals	46
Expression and Purification of BjPutA	46
Site-Directed Mutagenesis	47
Steady-State Kinetic Assays	48
Channeling Assays	51
Single Turnover Rapid-reaction Kinetics	52
Kinetic Parameters of Alternative Substrates	53
RESULTS	54
Identification and Purification of Channeling Mutants.	54
Channeling Assays of BjPutA Mutants	56
PRODH and P5CDH Kinetic Properties of BjPutA Mutants	59
Single Turnover Rapid-reaction Kinetics	63
Alternative P5CDH Substrates	66
DISCUSSION	68
REFERENCES	72
<b>CHAPTER 3: Fusing the DNA-binding Domain of <i>Escherichia coli</i> Proline Utilization A (PutA) onto the Bifunctional PutA Enzyme from <i>Rhodobacter capsulatus</i> Nearly Mimics a Genuine Trifunctional PutA</b>	<b>75</b>
ABSTRACT	76

	viii
INTRODUCTION	77
MATERIALS AND METHODS	82
Materials	82
Expression Constructs and Protein Purification	82
PRODH Kinetic Assays	84
DNA-binding	84
PRODH-P5CDH Coupled Assay	85
Oligomeric Structure Determination	85
Membrane Interactions and Lipid Pull-down Assays	86
Cell-based Functional Switching Assays	88
RESULTS	88
General Properties and Steady-state Kinetic Parameters	88
Oligomeric State Determination	91
DNA-binding and Lipid Pull-down Assays of EcRHH-RcPutA	93
Cell-based Testing of EcRHH-RcPutA Functional Switching	97
DISCUSSION	99
REFERENCES	104
<b>CHAPTER 4: Kinetic Exploration of the Proline Dehydrogenase Active Sites of <i>Geobacter sulfurreducens</i> Proline Utilization A and <i>Deinococcus radiodurans</i> Proline Dehydrogenase</b>	<b>107</b>
ABSTRACT	108
PART I: GsPutA Characterization	108
INTRODUCTION	108
MATERIALS AND METHODS	110
Chemicals	110

Steady State Kinetic Assays	110
Product Inhibition Assays	112
Channeling Assays	112
RESULTS AND DISCUSSION	113
Kinetic Characterization of GsPutA	113
Kinetic Mechanism of Proline:ubiquinone Oxidoreductase	114
Coupled Channeling Assay	114
BbPutA Proline:ubiquinone Oxidoreductase Activity	116
Ubiquinone Active Site Mutants	118
SUMMARY	120
PART II: DrPRODH Characterization	121
INTRODUCTION	121
MATERIALS AND METHODS	123
Enzyme Activity Assays	123
RESULTS AND DISCUSSION	124
REFERENCES	128
<b>CHAPTER 5: Conclusions and Future Directions</b>	<b>130</b>
SUMMARY AND FUTURE DIRECTIONS	131
REFERENCES	136

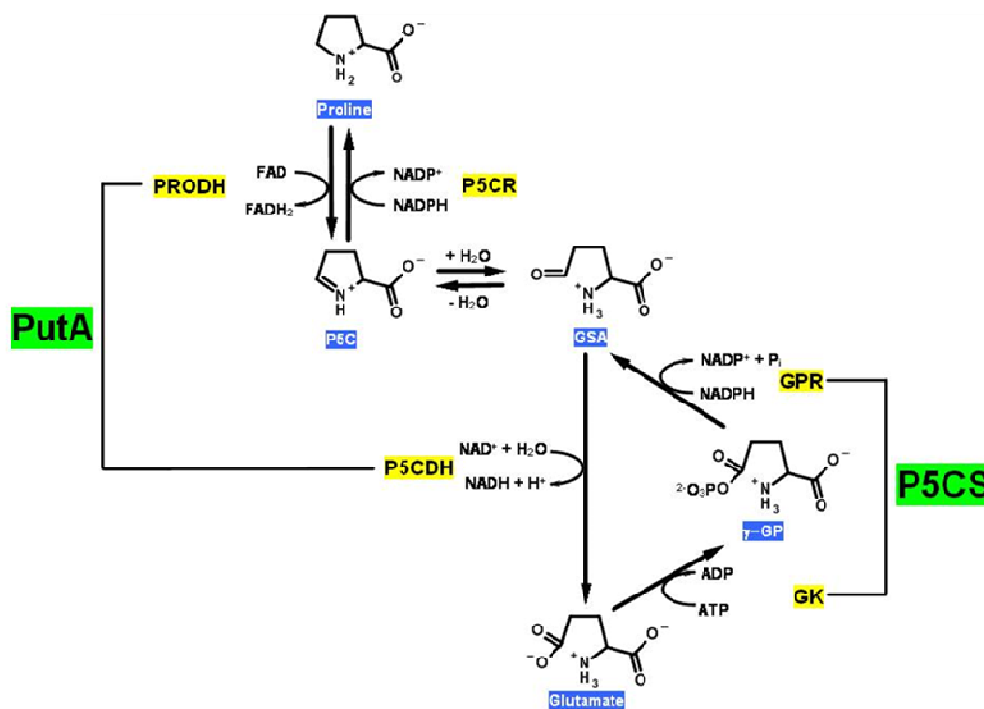
**ABBREVIATIONS**

AAK	amino acid kinase
ATP	adenosine-5'-triphosphate
BjPutA	proline utilization A from <i>Bradyrhizobium japonicum</i>
CoQ <sub>1</sub>	ubiquinone-1
CTD	C-terminal domain
DAPA-AT	diaminopelargonic acid aminotransferase
DTBS	dethiobiotin synthetase
EcPutA	proline utilization A from <i>Escherichia coli</i>
EDTA	ethylenediaminetetraacetic acid
FAD	flavin adenine dinucleotide
$\gamma$ -GP	$\gamma$ -glutamyl phosphate
GK	$\gamma$ -glutamyl kinase
GPR	$\gamma$ -glutamyl phosphate reductase
GSA	glutamate- $\gamma$ -semialdehyde
IPTG	isopropyl $\beta$ -D-thiogalactopyranoside
<i>M</i>	molecular mass
NAD <sup>+</sup>	nicotinamide adenine dinucleotide
NADH	reduced nicotinamide adenine dinucleotide
NADPH	nicotinamide adenine dinucleotide phosphate
MB	menadione bisulfite
<i>o</i> -AB	<i>o</i> -aminobenzaldehyde
PRODH	proline dehydrogenase
PutA	proline utilization A
P5C	$\Delta^1$ -pyrroline-5-carboxylate
P5CDH	$\Delta^1$ -pyrroline-5-carboxylate dehydrogenase
P5CR	pyrroline-5-carboxylate reductase

P5CS	pyrroline-5-carboxylate synthase
RcPutA	proline utilization A from <i>Rhodobacter capsulatus</i>
RHH	Ribbon-helix-helix
SAXS	small-angle X-ray scattering
SDS-PAGE	sodium dodecyl sulfate polyacrylamide gel electrophoresis
THFA	tetrahydro-2-furoic acid
TTC	triphenyltetrazolium chloride

# CHAPTER 1

## Introduction: Substrate Channeling in Proline Metabolism



Note: Much of this chapter has been published as a review article: “Substrate channeling in proline metabolism.” Arentson BW, Sanyal N, Becker DF. *Front Biosci.* 2012 Jan 1;17:375-88. Frontiers in Bioscience granted permission for use in dissertation.

## INTRODUCTION

It is well known that proline metabolism has important roles in carbon and nitrogen flux and protein synthesis. Proline metabolism has also emerged as a relevant pathway in other processes such as cell signaling, cellular redox balance, and apoptosis (1-3). Proline homeostasis is important in human disease, where inborn errors in proline metabolism are thought to lead to neurological dysfunctions such as schizophrenia and febrile seizures, as well as errors in systemic ammonia detoxification and developmental disorders such as skin hyperelasticity (4-7). Recently it was shown that mutations disrupting proline biosynthesis are linked with progeroid features and osteopenia that are part of the autosomal recessive cutis laxa syndrome (8). In bacteria and plants, proline metabolism is responsive to various environmental stresses such as drought, osmotic pressure, or ultraviolet irradiation leading to proline accumulation as a survival mechanism (9-11). Overall proline has become a very important metabolite that is thought to be involved in many cellular processes.

Fundamental to understanding the roles of proline metabolism in various processes is knowledge of the relevant enzymes and mechanisms used to maintain proper proline homeostasis. In this chapter, the unique aspect of substrate channeling in proline metabolism will be explored. Insights into the channeling mechanisms of enzymes responsible for the catabolism and biosynthesis of proline are helping to reveal the many roles of proline within the cell. Reviewed here are the structural and kinetic data that support substrate channeling of P5C/GSA and  $\gamma$ -glutamyl phosphate in the proline catabolic and biosynthetic pathways, respectively. The data indicate that both intermediates are channeled, which increases the efficiency of proline metabolic flux.

## PROLINE METABOLIC ENZYMES

### Proline Catabolism

The catabolic and anabolic reactions of proline metabolism are shown in Figure 1. The catabolic pathway generates glutamate from the four electron oxidation of proline, which occurs in two catalytic steps (12). In the first step, proline dehydrogenase (PRODH; EC 1.5.99.8) uses a flavin adenine dinucleotide (FAD) cofactor as an electron acceptor to remove two electrons from proline, rendering the intermediate  $\Delta^1$ -pyrroline-5-carboxylate (P5C). P5C then undergoes a non-enzymatic hydrolysis, which opens the ring structure and generates glutamate- $\gamma$ -semialdehyde (GSA). Pyrroline-5-carboxylate dehydrogenase (P5CDH; EC 1.5.1.12) next removes two additional electrons from GSA using nicotinamide adenine dinucleotide ( $\text{NAD}^+$ ) to complete the conversion of proline to glutamate (12).

The PRODH and P5CDH enzymes involved in the oxidation of proline are highly conserved in both eukaryotes and prokaryotes, but differ in whether they are fused into a bifunctional enzyme called proline utilization A (PutA). As reviewed by Tanner, PRODH enzymes can be divided into three branches (Figure 2) (13). One branch consists of monofunctional enzymes, where the PRODH and P5CDH domains are found as separate enzymes. The other two branches contain the PRODH and P5CDH domains on a single PutA polypeptide (13). Originally it was thought that all prokaryotes contain bifunctional PutAs, and that all eukaryotes contain monofunctional enzymes. However, it is now known that Gram-positive bacteria generally contain monofunctional enzymes, thus limiting PutAs to Gram-negative bacteria (14).

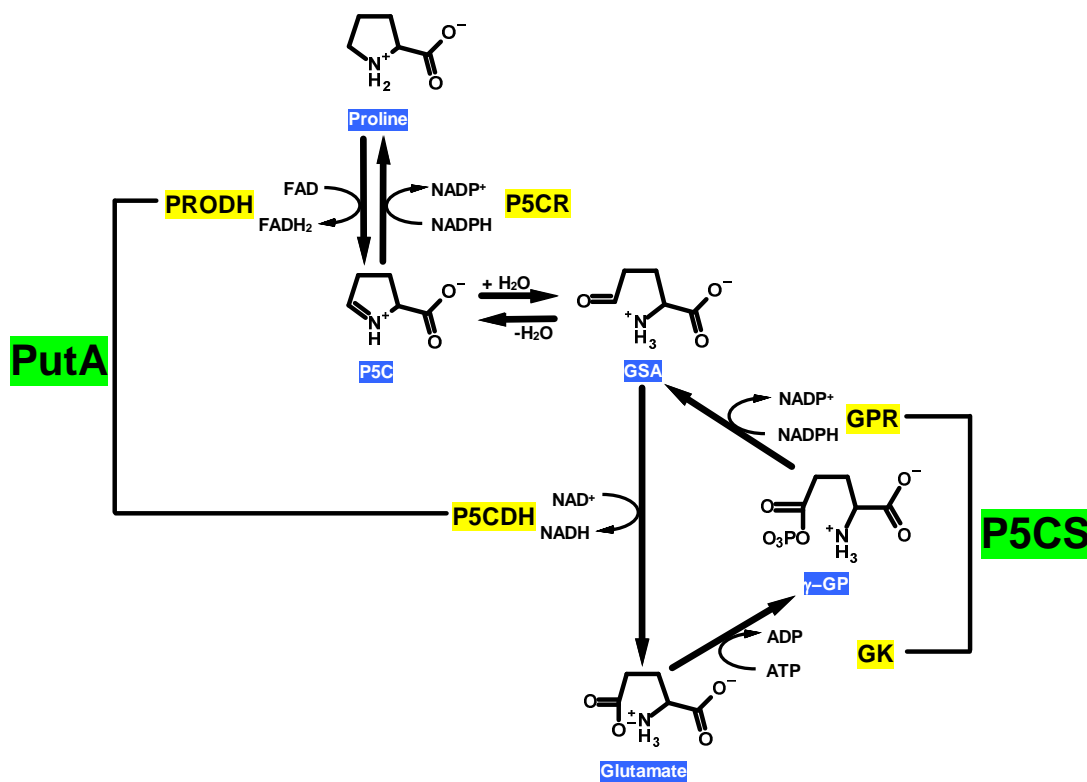


**Figure 1:** Reactions of the proline metabolic pathway. In the catabolic pathway, proline is converted to glutamate via a four electron oxidation process. Proline dehydrogenase (PRODH) performs the first oxidative step, resulting in the intermediate pyrroline-5-carboxylate (P5C). P5C is subsequently hydrolyzed to glutamate- $\gamma$ -semialdehyde (GSA), which is then further oxidized by P5C dehydrogenase (P5CDH) to generate glutamate. In Gram-negative bacteria, PRODH and P5CDH are fused together on a bifunctional enzyme called proline utilization A (PutA). Proline anabolism begins with phosphorylation of glutamate by  $\gamma$ -glutamyl kinase (GK) to generate  $\gamma$ -glutamyl phosphate ( $\gamma$ -GP).  $\gamma$ -GP is reduced by  $\gamma$ -glutamyl phosphate reductase (GPR) to GSA, which cyclizes to form P5C. P5C is then reduced to proline via pyrroline-5-carboxylate reductase (P5CR). In higher eukaryotes such as plants and animals, GPR and GK are fused together in the bifunctional enzyme pyrroline-5-carboxylate synthase (P5CS).



## PutA Family

As mentioned above, PutAs are divided into two branches. Branch 1 PutAs include  $\alpha$ ,  $\beta$ ,  $\gamma$  proteobacteria, while branch 2 is composed of Gram-negative cyanobacteria,  $\delta$  and  $\epsilon$  proteobacteria, and corybacterium (15). Normally branch 1 and branch 2 PutAs share sequence identities of less than 30%, suggesting significant diversity between branches (16). Based on amino acid sequence and domain organization (Table 1 and Figure 3), branch 1 and branch 2 can be further subdivided into five different subfamilies 1A, 1B, 1C, 2A, and 2B (15). Branch 1A and 2A are composed

Table 1. PutA subfamily organization and characteristics\*

Subfamily	Phylogenetic Branch	Functional Designation	Functional Domains	Representative Member	Oligomeric State
1A	1	Bifunctional	PRODH, P5CDH	BjPutA	Tetramer
1B	1	Bifunctional	PRODH, P5CDH, CTD	RcPutA	Monomer <sup>†</sup>
1C	1	Trifunctional	RHH, PRODH, P5CDH, CTD	EcPutA	Dimer
2A	2	Bifunctional	PRODH, P5CDH	GsPutA	Dimer <sup>‡</sup>
2B	2	Bifunctional	PRODH, P5CDH, CTD	HpPutA	Dimer <sup>‡</sup>

\*Table adapted from (15).

<sup>†</sup>Data described in Chapter 3 of this thesis.

<sup>‡</sup>Dr. John Tanner, personal communication.

of minimalist bifunctional PutAs that only contain PRODH and P5CDH, ranging in size from 980-1100 amino acid residues (15). *Bradyrhizobium japonicum* PutA (BjPutA, 999 AA) is a branch 1A example from literature that has been characterized both structurally and kinetically and will be the focus of Chapter 2. Branch 1B and 2B consist of long bifunctional PutAs that contain an additional ~175 residue C-terminal domain (CTD)

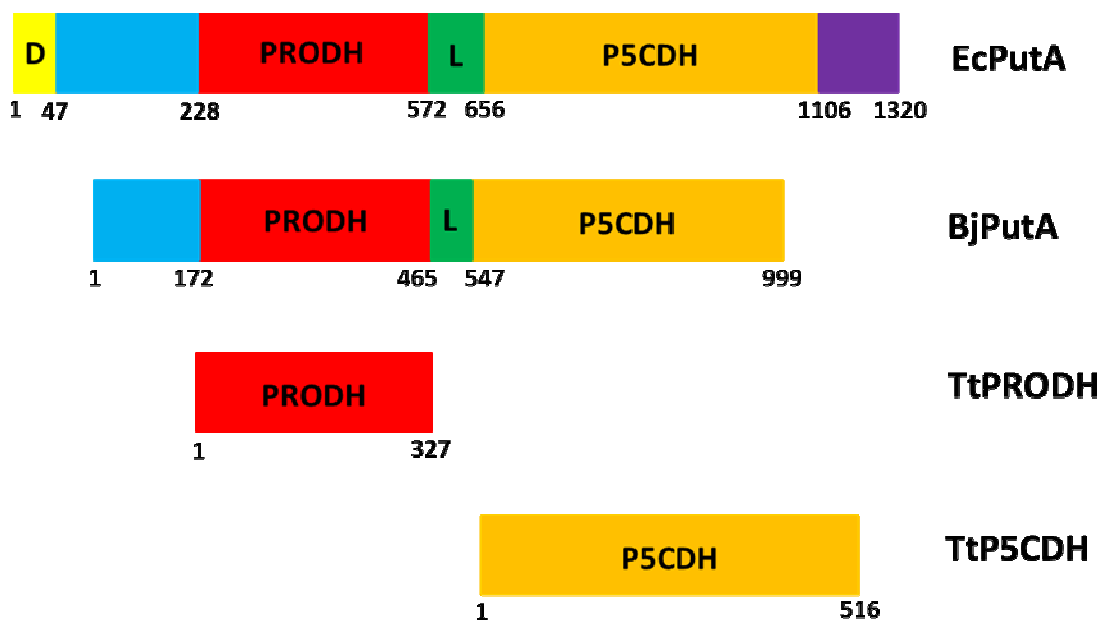


**Figure 3:** Domain mapping of PRODH and P5CDH from *E. coli* (EcPutA), *B. japonicum* (BjPutA), and *T. thermophilus*. In PutAs, the PRODH and P5CDH domains are connected by a linker region (L). Trifunctional PutAs such as EcPutA also have a DNA binding domain (D). TtPRODH and TtP5CDH are separate enzymes (monofunctional) in the Gram-positive bacteria, *T. thermophilus*. Figure adapted from (17).

of unknown function. Long bifunctional PutAs normally contain between 1100-1200 residues (15). *Rhodobacter capsulatus* PutA (RcPutA, 1127 AA) is a representative PutA from branch 1B and will be the focus of Chapter 3. Branch 1C consists of trifunctional PutAs that contain the PRODH, P5CDH, and CTD, but are distinct from all other PutAs by the addition of a DNA-binding domain at the N-terminus. Trifunctional PutAs are generally 1300-1400 residues in length (16). The DNA-binding domain is composed of a ribbon-helix-helix (RHH) domain that interacts with the *put* control region and will be discussed shortly (18, 19). *E. coli* PutA (EcPutA, 1320 AA) is a highly studied member of the trifunctional PutA subfamily. As previously mentioned, eukaryotes and many Gram-positive bacteria express PRODH and P5CDH as separate enzymes. Typically monofunctional PRODHs are between 200-600 amino acids, while monofunctional P5CDHs are 400-600 residues. The evolutionary divergence from bifunctional PutA to monofunctional PRODH and P5CDH is of interest due to substrate channeling between the active sites of PutAs. Substrate channeling between monofunctional enzymes would necessitate functional PRODH-P5CDH interactions which have not yet been reported.

### **Structural Characterization of PutAs**

Currently, only one three-dimensional structure of a full length PutA has been published--the minimalist bifunctional PutA from *Bradyrhizobium japonicum* (BjPutA) (PDB ID 3HAZ) (20). However, the full-length structure of a second minimalist PutA from *Geobacter sulfurreducens* (PDB ID 4F9I) has been deposited in the Protein Data Bank. The X-ray crystal structure of BjPutA provided the first structural details about domain organization and overall arrangement of PutAs. Truncated EcPutA structures

have also been solved of the PRODH domain of EcPutA (PDB ID 1K87, 1TJ2, ITIW, 1TJ0, 3ITG), but the entire structure of a trifunctional PutA remains elusive (21-24). Additionally, the RHH DNA binding domain was solved by solution NMR (*Pseudomonas putida*, PDB ID 2JXI, 2JXG) and X-ray diffraction (*E. coli*, PDB ID 2GPE, 2RBF) (25-27). Though a full length trifunctional structure does not exist, small-angle X-ray scattering (SAXS) was used to determine the 3-dimensional molecular envelope of EcPutA (28). Additionally, several structures of monofunctional PRODH and P5CDH exist, including PRODH from *Thermus thermophilus* (2G37) and *Deinococcus radiodurans* (PDB ID 4H6R) and P5CDH from human (PDB ID 3V9G), mouse (PDB ID 3V9J), and *T. thermophilus* (PDB ID 1UZZ) (29-32).

Crystal structures of BjPutA and EcPutA both show the PRODH active site is located within a distorted ( $\beta\alpha$ )<sub>8</sub> barrel, where the *re* face of a non-covalently bound flavin is packed against the barrel, leaving the *si* face accessible for substrate binding and catalysis (Figure 4) (20, 22). As mentioned, trifunctional PutAs also contain a DNA-binding domain composed of a RHH domain that provides the point of dimerization (21). The P5CDH active site is found at the interface between a Rossmann-like NAD<sup>+</sup> binding domain and the activity domain that provides the catalytic cysteine (28).

While the active site domain folds are thought to be conserved throughout the PutA superfamily, the oligomeric structures are not conserved. Within branch 1A, the oligomeric state of minimalist PutAs BjPutA and *Legionella pneumophila* (LpPutA) are tetrameric and dimeric, respectively (15, 20). In branch 1B, SAXS data suggests RcPutA

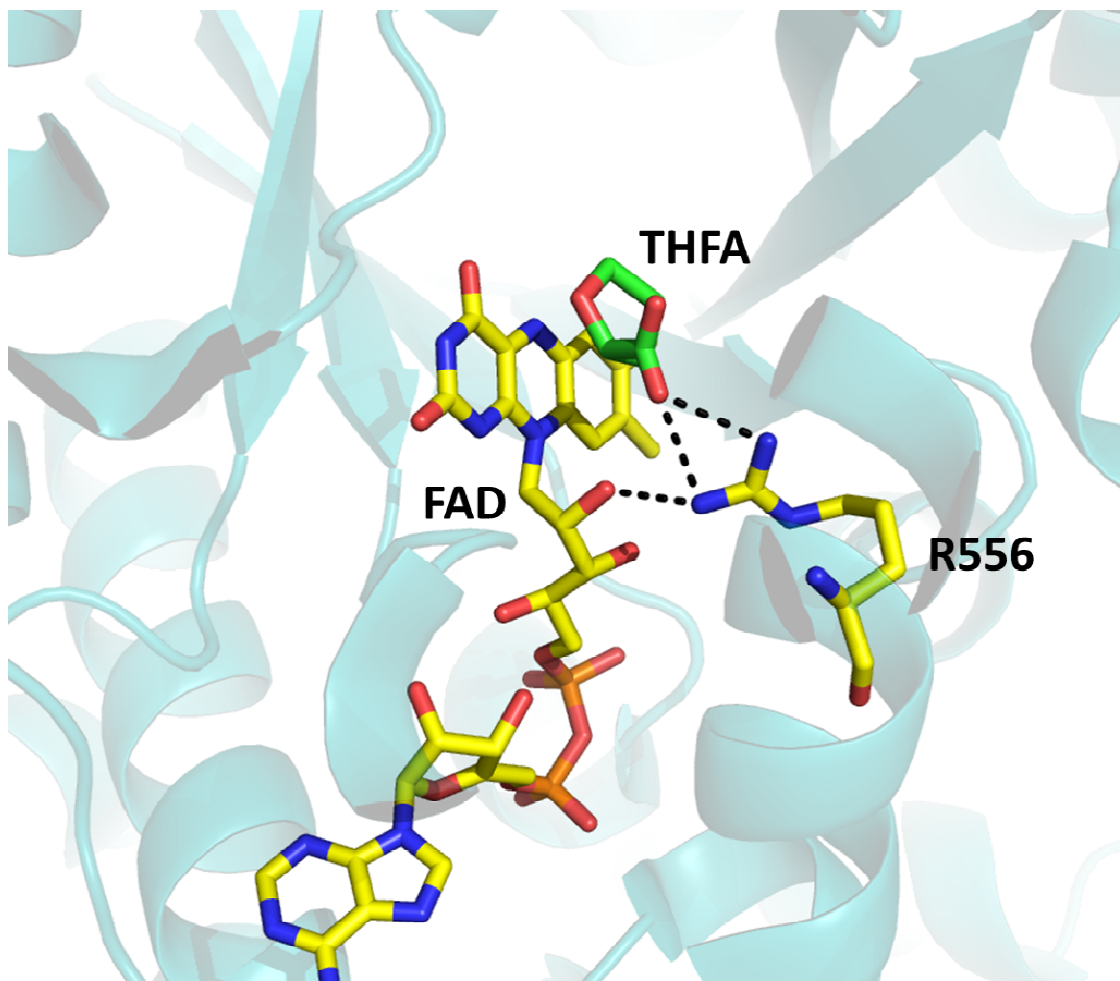


**Figure 4:** PRODHD active site from EcPutA (residues 86-669) coordinating proline analog L-tetrahydro-2-furoic acid (THFA). The *re* face of flavin is shown packed against the  $(\beta\alpha)_8$  barrel, exposing the *si* face to substrate catalysis. R556 is an active site residue known to coordinate the carboxyl group of proline for catalysis. Flavin is colored in yellow, THFA in green, and R556 in yellow. Black dashed lines represent hydrogen bonds between R556 and THFA and flavin. Figure generated using PDB code 1TIW and PyMOL (23).

is a monomer, while branch 1C representative EcPutA is a dimer (28). However, early evidence suggests more parity within branch 2, as representatives of subfamilies 2A (*G. sulfurreducens*) and 2B (*H. pylori*) are both dimers (Tanner, personal communication) (15).

A  $\beta$ -hairpin extending from the NAD<sup>+</sup> binding domain may provide some clues about the oligomerization state in PutAs. The  $\beta$ -hairpin, along with a C-terminal  $\beta$ -strand form a point of dimerization through domain swapping for minimalist PutAs, as well as all other aldehyde dehydrogenases (15). However, in long bifunctional and trifunctional PutAs, multiple sequence alignments indicate the  $\beta$ -hairpin is truncated or nonexistent (16). Due to this truncation, it is unlikely that dimerization through domain swapping occurs in long bifunctional PutAs and trifunctional PutAs. This has been verified in trifunctional PutAs, which dimerize through the RHH domain as well as the long bifunctional PutA member RcPutA, which is monomeric (described in Chapter 3).

### **Trifunctional PutAs and Functional Switching**

Early work on *Salmonella typhimurium* revealed that PutA is a membrane bound flavoprotein and also a negative regulator of the *put* operon (33, 34). Later, it was shown that PutA interaction with the *put* control region was abolished by two conditions, when proline and either an electron acceptor or membrane was present or when the flavin was reduced by dithionite (35). Around the same time, work on the *E. coli* PutA enzyme indicated functional switching from a DNA-bound state to a catalytically active, membrane bound state occurred via a redox dependent mechanism (36). Parallel with this observation were chymotryptic digestions of *E. coli* PutA (EcPutA) in the presence and

absence of proline that revealed different digestion patterns (37). Therefore, it was hypothesized that the binding of proline in the presence of a flavin electron acceptor induces a conformational change and, under these conditions, PutA becomes more hydrophobic leading to enhanced membrane association and catalysis (35, 38). Membrane association and DNA-binding were shown to be two mutually exclusive events that are dependent on environmental proline levels. When proline levels are low, PutA remains in the cytoplasm where it interacts with the *put* control region and represses expression of *putA* and *putP* (a high affinity Pro/Na<sup>+</sup> symporter) genes (39). When proline levels increase, PutA associates with the membrane where it becomes catalytically active (39). The conformational change was shown to be reversible, as catalytically active enzyme could be re-oxidized and lose its ability to interact with the membrane (40). Thus, the interaction between the DNA-binding domain and the *put* control region is dependent on environmental proline levels, linking transcription to metabolism.

Alongside proteolysis experiments, structural evidence also supports both global and redox-dependent conformational changes in PutA. An X-ray crystal structure of the PRODH domain of EcPutA treated with sodium dithionite revealed structural changes in the flavin adenine dinucleotide (FAD) cofactor. The isoalloxazine ring of the FAD was observed to be bent 22° along the N(5)-N(10) axis, whereas the ring is planar when the FAD is oxidized. In addition, the ribityl chain was rotated and a new hydrogen bond network was formed between ribityl hydroxyl groups and the surrounding residues in PutA (41). Similar changes in the flavin and the surrounding hydrogen bond network are also seen when inactivating the PRODH domain with the mechanism-based inhibitor N-

propargylglycine (PPG) (24). The conformational change in the ribityl moiety caused by dithionite is thought to help initiate global conformational changes in PutA that ultimately leads to functional switching between DNA and membrane binding. Recently it was reported that the  $\beta$ 3- $\alpha$ 3 loop of the PRODH ( $\beta\alpha$ )<sub>8</sub> barrel domain of EcPutA is part of the electrostatic network disrupted upon flavin reduction, and may be involved in propagating the flavin redox state to the peripheral membrane binding domain (42). Mutating  $\beta$ 3- $\alpha$ 3 loop residue D370 to alanine or asparagine disrupted functional switching, allowing EcPutA to associate with the membrane in the presence and absence of proline (42). Crystal structures of the mutants reveal no significant changes in the  $\beta$ 3- $\alpha$ 3 loop region or within the PRODH domain, concluding that the mutants disrupt the flavin redox signal transmission to peripheral regions of PutA. It should be noted that outside the  $\beta$ 3- $\alpha$ 3 loop region, little else is understood regarding how the conformational change radiates from the reduced flavin to the rest of the enzyme (43).

### **Proline Biosynthesis**

Proline biosynthesis from glutamate involves three enzymatic steps (Figure 1). The initial two steps are catalyzed by  $\gamma$ -glutamyl kinase (GK; EC 2.7.2.11) and  $\gamma$ -glutamyl phosphate reductase (GPR; EC 1.2.1.41). GK uses adenosine-5'-triphosphate (ATP) to generate  $\gamma$ -glutamyl phosphate, which is subsequently reduced by GPR using nicotinamide adenine dinucleotide phosphate (NADPH) to produce GSA (12). GSA next cyclizes to P5C, which is a crossroads intermediate that, in principle, can be converted not only to proline, but also to ornithine or back to glutamate via P5CDH (12). The reduction of P5C to proline is catalyzed by P5C reductase (P5CR; EC 1.5.1.2), while the

production of ornithine from P5C requires ornithine aminotransferase (OAT; EC 2.6.1.13), an enzyme that is important for balancing cellular nitrogen levels (12).

In bacteria and lower eukaryotes such as yeast, GK and GPR are discrete monofunctional enzymes. In animals and plants, the GK and GPR domains are fused together into the bifunctional enzyme P5C synthase (P5CS) (Figure 5). The GK and GPR domains are well conserved in lower eukaryotes and bacteria. The GK domain is normally between 250-450 residues in length with an N-terminal amino acid kinase (AAK) domain. In bacteria, GK contains a C-terminal pseudo uridine synthase and archaeosine-specific transglycosylase (PUA) domain, which has no known function (44). It has been suggested, however, that the PUA domain may enable bacterial GK to have a gene regulatory role (45). The structures of GK enzymes from *E. coli* and *Campylobacter jejuni* have been solved (PDB ID 2J5T, 2AKO) (46). *E. coli* GK is composed of an N-terminal catalytic domain made up of eight nearly parallel  $\beta$ -sheets sandwiched by two layers of three and four  $\alpha$ -helices. It is connected by a linker region to the PUA domain, which contains a distinctive  $\beta$  sandwich (46).

GPR typically contains 400-500 residues and consists of an N-terminal Rossmann fold domain for NADPH binding, a catalytic domain, and an oligomerization domain at the C-terminus (47). The X-ray crystal structure of GPR from *Thermotoga maritima* reveals that the catalytic domain has an  $\alpha/\beta$  architecture with a five-stranded parallel  $\beta$ -sheet (PDB ID 1O20) (47). To date, no complete structure of bifunctional P5CS has been reported. However, the structure of the isolated GPR domain (PDB ID 2H5G; unpublished) from human P5CS is available. The last enzyme of the proline biosynthetic pathway, P5CR, ranges from 400-500 residues in length and has a conserved N-terminal

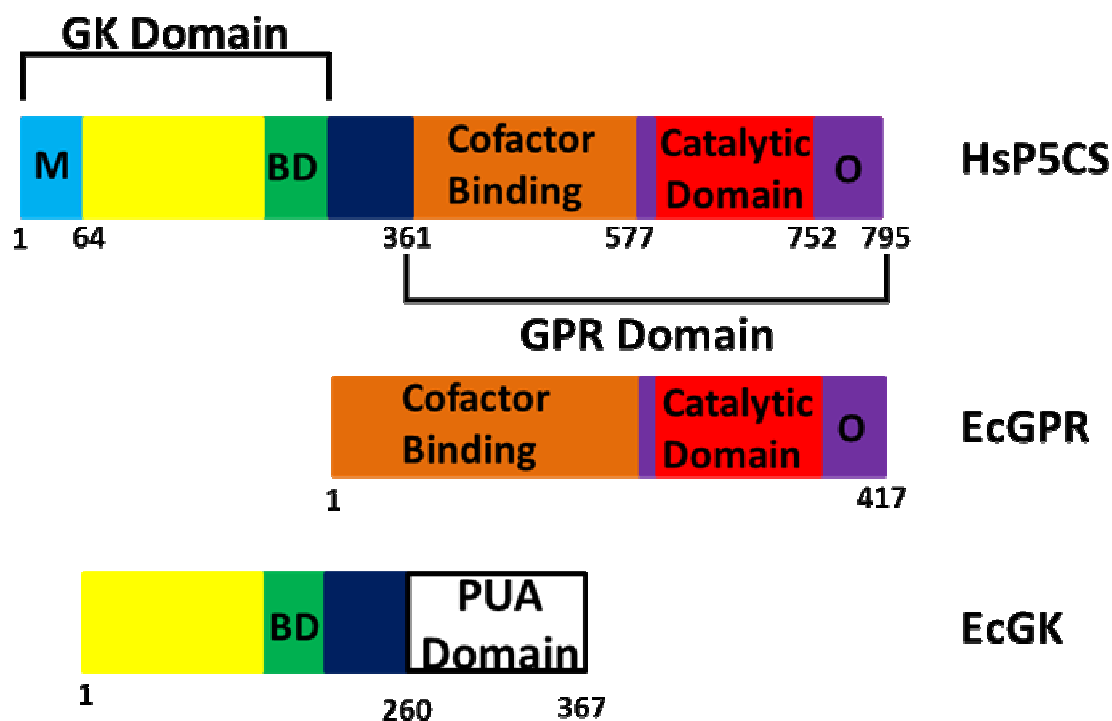


**Figure 5:** Domain mapping of monofunctional  $\gamma$ -glutamyl phosphate reductase (EcGPR) and  $\gamma$ -glutamyl kinase (EcGK) enzymes from *E. coli* and bifunctional pyrroline-5-carboxylate synthase (P5CS) from *Homo sapiens*. **M**, putative mitochondrial signaling peptide, **BD**, binding domain for glutamate and ATP, **O**, oligomerization domain, and **PUA**, pseudo uridine synthase and archaeosine-specific transglycosylase domain with no known function in EcGK. Figure adapted from (17).

Rossmann fold for NADPH binding. Several crystal structures of P5CR have been determined including the human form (PDB ID 2GRA) (48). Human P5CR has an active site cleft made of an 8-stranded  $\beta$ -sheet sandwiched by  $\alpha$ -helices on either side and oligomerizes to form a decameric structure of dimers (48).

## **INTERMEDIATES OF PROLINE METABOLISM**

The P5C/GSA and  $\gamma$ -glutamyl phosphate intermediates of proline metabolism are appreciably labile and reactive. Figure 6 shows examples of undesirable fates that can occur with these intermediates. The instability of the intermediates implies substrate channeling may be important for maintaining efficient proline metabolic flux. The intermediate shared by the catabolic and biosynthetic pathways, P5C/GSA, has been shown to inhibit other enzymes, react with metabolites, and act as a signaling molecule. GSA has been reported to inhibit glucosamine-6-phosphate synthase from *E. coli*, cytidine 5'-triphosphate synthase, and the amidotransferase domain of carbamoyl phosphate synthetase (49-51). Additionally, P5C forms adducts with other metabolites such as pyruvic acid, oxaloacetic acid, and acetoacetic acid (52). P5C can also react with pyridoxal phosphate in patients with type II hyperprolinemia. Type II hyperprolinemia is characterized by elevated plasma levels of P5C/GSA due to deficient P5CDH activity (53). The high levels of P5C/GSA generates inactive adducts with pyridoxal phosphate, leading to lower amounts of functional vitamin B6 in patients (Figure 6) (52). P5C also acts as a signaling molecule in eukaryotes and is thought to induce apoptosis by

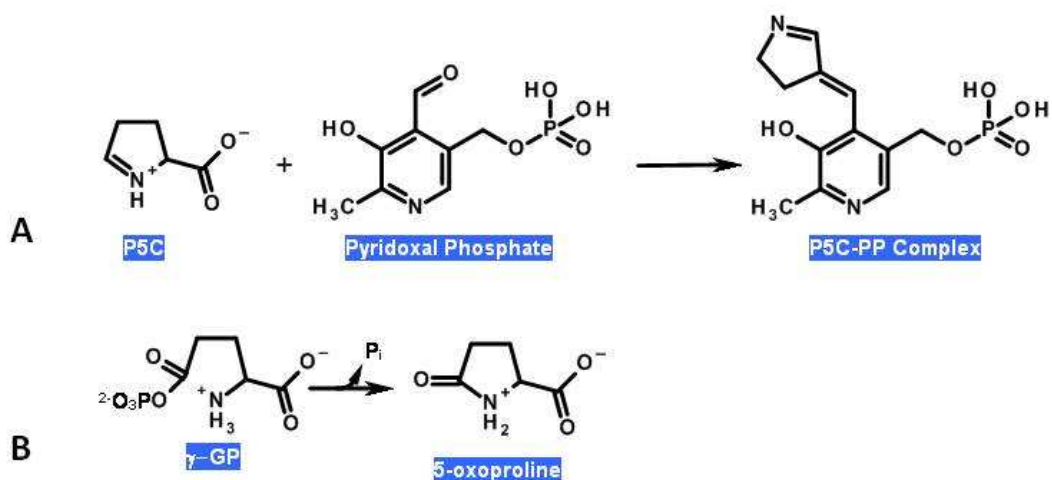


**Figure 6:** Side reactions of intermediates pyrroline-5-carboxylate (P5C) and  $\gamma$ -glutamyl phosphate ( $\gamma$ -GP). (A) P5C can deactivate pyridoxal phosphate by forming an adduct, resulting in vitamin B6 deficiency in individuals with hyperprolinemia type II. The P5C-pyridoxal phosphate adduct structure is from reference 38. (B)  $\gamma$ -GP can cyclize and dephosphorylate to form 5-oxoproline, which is suggested to be a neurotoxin in rats. Figure adapted from (17).

increasing intracellular reactive oxygen species (54, 55). Altogether, it seems that controlling levels of free P5C/GSA would be beneficial.

The reactive intermediate in proline biosynthesis is  $\gamma$ -glutamyl-phosphate. The carbonyl phosphate group is susceptible to nucleophilic attack, resulting in the spontaneous cyclization of  $\gamma$ -glutamyl-phosphate into 5-oxoproline as shown in Figure 6 (56, 57). It has been suggested that 5-oxoproline is a neurotoxin. Interstitial injection of 5-oxoproline into rats produces behavioral and neuropathological effects that resemble Huntington's disease (58, 59). The instability of  $\gamma$ -glutamyl phosphate seems to necessitate its channeling between GK and GPR during proline biosynthesis.

## **OVERVIEW OF SUBSTRATE CHANNELING**

### **Rationale for Substrate Channeling**

Substrate channeling is a phenomenon where the product of one reaction is transported to a second active site without equilibrating into bulk solvent (60). Three mechanisms of substrate channeling have been defined, two of which are reviewed by Miles *et al.* (61). The most common form of substrate channeling occurs when a cavity exists within a protein that sequesters the intermediate from solvent, allowing for a means of travel between active sites (61). To date, several enzymes are known to utilize these intramolecular tunnels, with the classic example being tryptophan synthase (62). The second form of channeling does not use intramolecular cavities; rather, electrostatic residues on the surface of the enzyme guide the intermediate from the first active site to the second active site (61). Dihydrofolate reductase-thymidylate synthase complex stands as the common example for this form of channeling (63). A third form of

channeling exists in protein complexes such as pyruvate dehydrogenase, which uses cofactor lipoic acid to transfer substrate to multiple active sites without contacting solvent (64).

Substrate channeling has been proposed to be advantageous in the cellular environment for several reasons, as outlined by Ovadi and others (60, 65). First and foremost it increases the efficiency of coupled reactions both by preventing the loss of intermediates to diffusion and by decreasing transit time between active sites. This allows the steady-state flux through the coupled steps to be attained more rapidly (60). Secondly, it prevents labile intermediates from decaying and reacting with other metabolites or enzymes within the cell (60). Third, channeling segregates intermediates that may require a specific environment (e.g., pH) to retain structure or reactivity. Channels can provide an environment that facilitates an equilibrium step that normally would be unfavorable in the bulk solution. Finally, channeling limits intermediates from being siphoned out into competing reactions or pathways (60).

All of the benefits listed above are not necessarily relevant for every channeling system. In the proline catabolic pathway, channeling of P5C/GSA may be most critical for making the hydrolysis of P5C to GSA more favorable at physiological pH. The P5C/GSA equilibrium is highly pH dependent (49). GSA is favored only below pH 6.5 due to protonation of the pyrrolinium ring, which facilitates the hydrolysis of P5C to GSA. Thus, one benefit of channeling between PRODH and P5CDH would be to increase the  $pK_a$  of the pyrrolinium species above pH 6.5, making the hydrolysis of P5C to GSA more favorable at physiological pH. If we only consider the P5C/GSA hydrolysis step, substrate channeling is likely more critical for the proline catabolic pathway than for

proline biosynthesis, since P5C formation is favored at physiological pH. In the proline biosynthetic pathway, protecting the highly labile  $\gamma$ -glutamyl phosphate would be a clear benefit of substrate channeling between GK and GPR.

### **Kinetic Approaches to Test for Substrate Channeling**

Different strategies have been devised to examine whether channeling occurs between enzymes. Before reviewing the evidence for substrate channeling in proline metabolism, a short description of various experimental methods is described here.

#### **Transient Time Estimation**

A common strategy to test for channeling is to evaluate whether there is a lag time in reaching steady-state formation of the final product in a coupled assay. Figure 7 shows substrate (S) being converted to the final product (P) via the coupled action of two enzymes (E1 and E2). The lag time or transient time, Tau ( $\tau$ ), is the time preceding the build-up to steady-state formation of the final product using the substrate of the first enzyme (66). If no channeling occurs,  $\tau$  should be equal to the ratio of  $K_m/V_{max}$  of the second enzyme. If the observed lag time is shorter than the  $K_m/V_{max}$  ratio, then it infers that the intermediate is transferred between the enzymes, E1 and E2. The extent of the observed lag time may vary among different channeling systems with a shorter transient time being interpreted as more efficient transfer or channeling (67). Along with steady-state assays, pre-steady state measurements can also be made to evaluate the lag time prior to product formation.

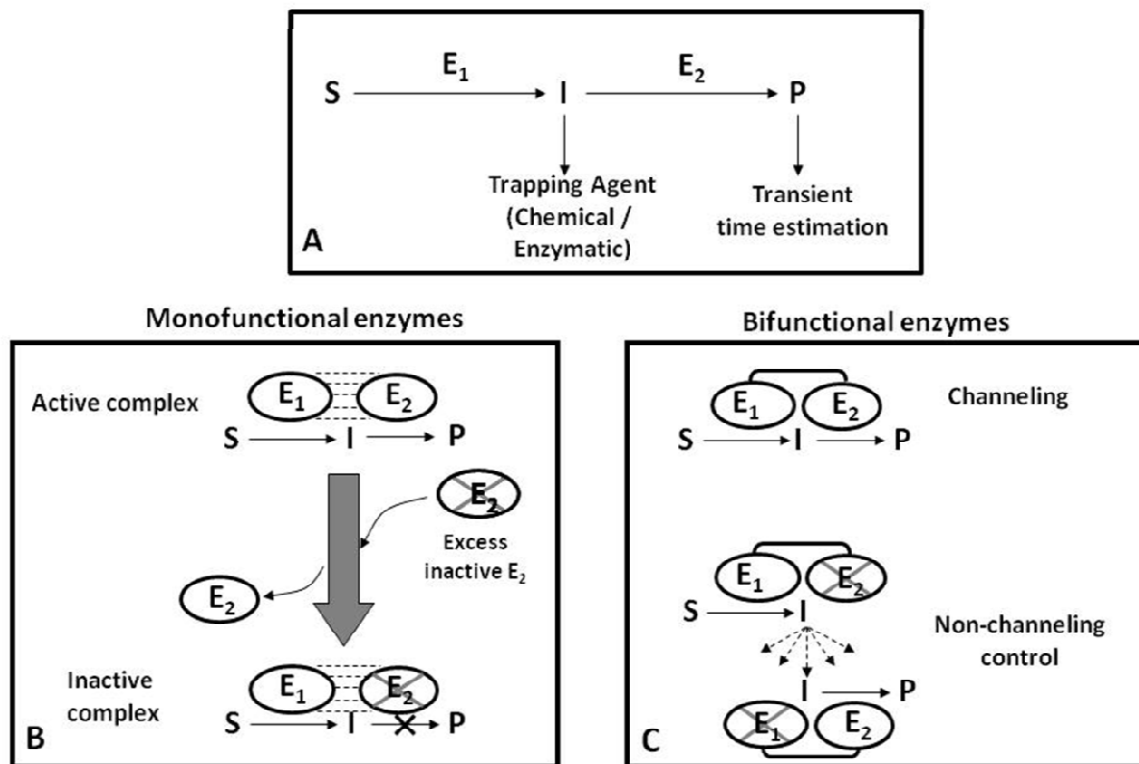


**Figure 7:** Strategies for examining substrate channeling. (A) Transient time analysis of a coupled reaction involving two enzymes, E1 and E2, which convert substrate S into product P. A trapping agent can also be used to test whether intermediate I is released into bulk solvent during the reaction. (B) Inactivation of one of the enzyme pairs by site-directed mutagenesis. If channeling occurs, adding inactive E2 would disrupt the active E1-E2 complex resulting in lower steady-state activity. (C) Testing channeling in bifunctional enzymes. Inactivation of the individual domains results in monofunctional variants that can only catalyze the coupled reaction via a diffusion mechanism. The mixture of monofunctional variants is thus a non-channeling control. Figure adapted from (17).

### **Trapping the Intermediate**

The effect of a reagent that specifically traps the intermediate species (I, Figure 7) on the kinetics of product formation can also be used to evaluate channeling. For example, *o*-aminobenzaldehyde (*o*-AB) which reacts with P5C to form a yellow complex can be used as a trapping agent for the PRODH and P5CDH coupled reaction. *o*-AB would be anticipated to decrease the overall rate of glutamate formation if no channeling occurs, while in a channeling system *o*-AB would have a negligible effect on the reaction kinetics. Using a third enzyme that competes with E2 for the intermediate can also be an effective strategy to test for substrate channeling.

### **Inactive Mutants**

Another useful tool is to generate active site mutants of the two enzymes being studied (Figure 7B). In the case of suspected channeling partners, an active site mutant (e.g., E2) would be expected to compete with its native counterpart for interaction with the cognate enzyme (E1). If channeling occurs, adding the inactive E2 mutant in amounts excess to that of native E2 would decrease product formation. If no channeling occurs, adding the inactive E2 mutant to the coupled enzyme assay would have no effect on the rate of product formation. This strategy was effectively used to rule out channeling between aspartate aminotransferase (AAT) and malate dehydrogenase (MDH) (68).

If the channeling involves two enzyme active sites that are covalently linked, active site mutants can be used to generate a non-channeling control. Figure 7C illustrates that combining active site mutants of E1 and E2 creates a mixture of monofunctional enzyme variants that can only generate product via a diffusion mechanism. The transient

times of the native enzyme and the mixed enzyme variants can then be compared to distinguish between channeling and non-channeling mechanisms. This strategy was used recently to demonstrate channeling in bifunctional PutA.

### **Designing Fusion Proteins**

Two active sites that are in close proximity can sometimes exhibit kinetic behavior that resembles direct channeling (69). One strategy for distinguishing between active channeling and proximity effects is to change the relative orientation of two active sites, which is important for interacting enzymes (70). A polypeptide linker can be engineered to covalently link the two enzymes with various degrees of flexibility and in different orientations (69). If the enzymes are truly channeling, changes in the orientation of the active sites will have a dramatic effect on the kinetics of production formation.

### **CHANNELING OF P5C/GSA**

The oxidation of proline to glutamate is catalyzed in consecutive reactions by PRODH and P5CDH (Figure 1). Avoiding release of P5C/GSA into bulk solvent during proline oxidation may be beneficial due to the chemical properties of P5C/GSA as discussed in the previous section. Evidence for channeling P5C/GSA has recently been shown for bifunctional PutA from *BjPutA*. Srivastava *et al.* reported a 2.1 Å resolution crystal structure of *BjPutA* (999-residue polypeptide) that reveals an interior channel connecting the PRODH and P5CDH active sites (PDB ID 3HAZ) (24). Figure 8 shows a structural model of *BjPutA*, which purifies as a homodimer. Both PRODH and P5CDH domains contribute to the formation of the channel, with the two active sites separated by a distance of 41 Å. The connecting channel appears to start at the *si* face of the

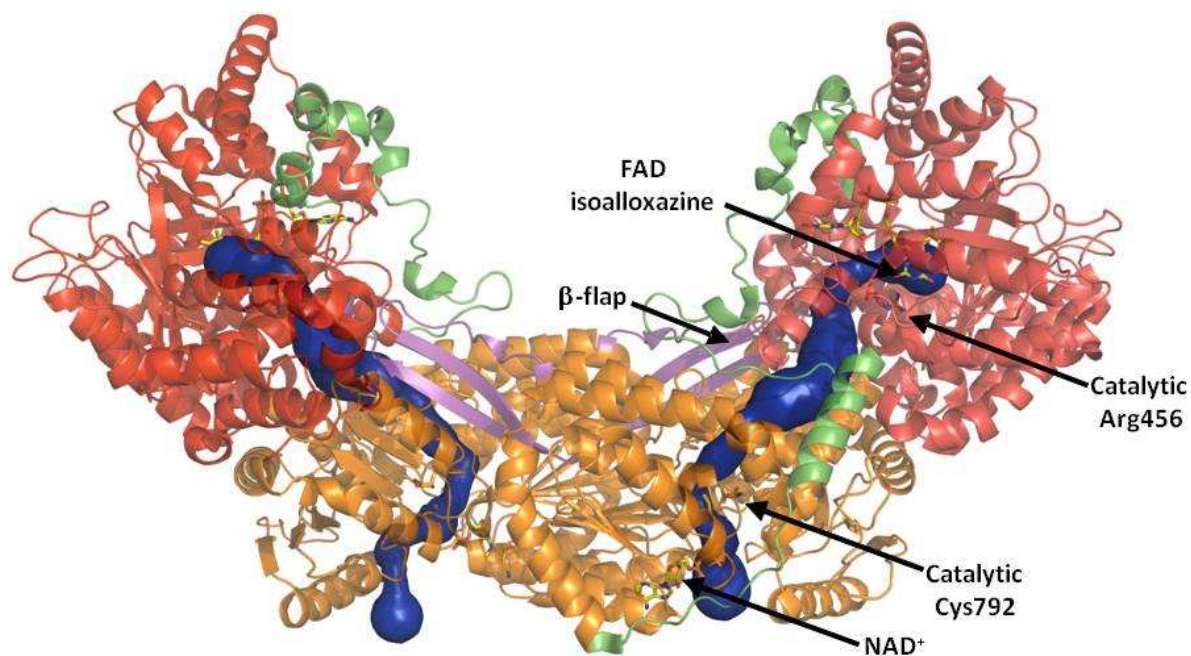


**Figure 8:** Structure of dimeric BjPutA shown in ribbon representation. The PRODH domain (red) and the P5CDH domain (orange) of each protomer are connected by a linker region (green). Active site residues (Arg456, Cys792), FAD and NAD<sup>+</sup> are displayed as sticks.  $\beta$ -flap of each protomer is colored as magenta. The substrate channel of each BjPutA protomer is shown as blue surface. This model was made using PyMol and PDB 3HAZ.

isoalloxazine ring of FAD and end at the catalytic cysteine (Cys792) of the P5CDH domain (Figure 8). Within the channel, the central cavity is lined by fifteen basic residues (Lys and Arg) and seventeen acidic residues (Glu and Asp), imparting a hydrophilic nature to the channel. Each of the PutA protomers has an individual channel connecting the PRODH and P5CDH active sites.

Interestingly, the dimeric structure of BjPutA seems to be critical for sealing the channel and minimizing access to bulk solvent. A  $\beta$ -flap protrudes from the P5CDH domain ( $\beta$  strand residues 628-646, 977-989) from one protomer and forms intermolecular interactions with the P5CDH domain of the second protomer (Figure 8). This  $\beta$ -flap is structurally conserved in *Thermus thermophilus* P5CDH (PDB ID 1UZZ, residues 163-174,506-516) as well as a class I aldehyde dehydrogenase isolated from sheep liver (PDB ID 1BXS, residues 147-159, 486-498) (71, 72). Thus, in BjPutA, the  $\beta$ -flap not only helps stabilize dimer formation but is also important for sealing the central cavity.

Along with these structural features of channeling, kinetic evidence for channeling was also reported for BjPutA by Srivastava *et al.* (24). Different experiments have provided strong evidence for channeling. First, the amount of P5C released into bulk solvent was quantitated by using *o*-aminobenzaldehyde (*o*-AB) as a trapping agent. P5C and *o*-AB react to form a yellow complex that can be monitored at 443 nm (73). In the absence of  $\text{NAD}^+$ , the P5CDH domain is inactive and leads to significant release of P5C into the bulk solvent, as detected by yellow complex formation. In the presence of  $\text{NAD}^+$ , however, the P5CDH domain is active, resulting in significantly lower *o*-AB-P5C complex formation, as the majority of P5C is converted into glutamate (24). The apparent

fraction of P5C that is channeled in BjPutA from PRODH to P5CDH was estimated to be 0.7 by these measurements.

Substrate channeling in BjPutA was also examined by estimating the transient time to reach steady-state turnover of the second enzyme, P5CDH, using proline as a substrate (24, 74, 75). With native BjPutA, steady-state formation of NADH (product of the P5CDH reaction) occurred without any apparent lag time (24). The absence of a lag time in the approach to steady-state indicates substrate channeling. A non-channeling control was also analyzed using active site mutants of BjPutA that lack PRODH (R456M) and P5CDH (C792A) activity (24). The R456M mutation inactivates PRODH but does not impair P5CDH activity, whereas the C792A mutation inactivates P5CDH but does not impair PRODH activity. The mixture of these monofunctional variants was used as a non-channeling control as described above. In this non-channeling control, P5C formed by the C792A variant must diffuse out into bulk solvent and bind to the R456M variant before NADH is formed. In the assays with the non-channeling variants, a lag time of about seven minutes for NADH formation was observed (24). The observed lag time was similar to the theoretical  $\tau$  value calculated from the independent PRODH activity and P5CDH kinetic parameters. An example of these steady-state assays is shown in Figure 9. Figure 9 illustrates the clear difference in the kinetic behavior of native BjPutA and the non-channeling control. With native BjPutA, NADH formation is observed without a lag time, while with the mixed variants a lag time of around 6.5 minutes is observed. The results from these assays are consistent with a substrate channeling mechanism in BjPutA. Kinetic profiles of native BjPutA and the mixed variants were also compared by rapid-reaction kinetics under anaerobic, single-turnover

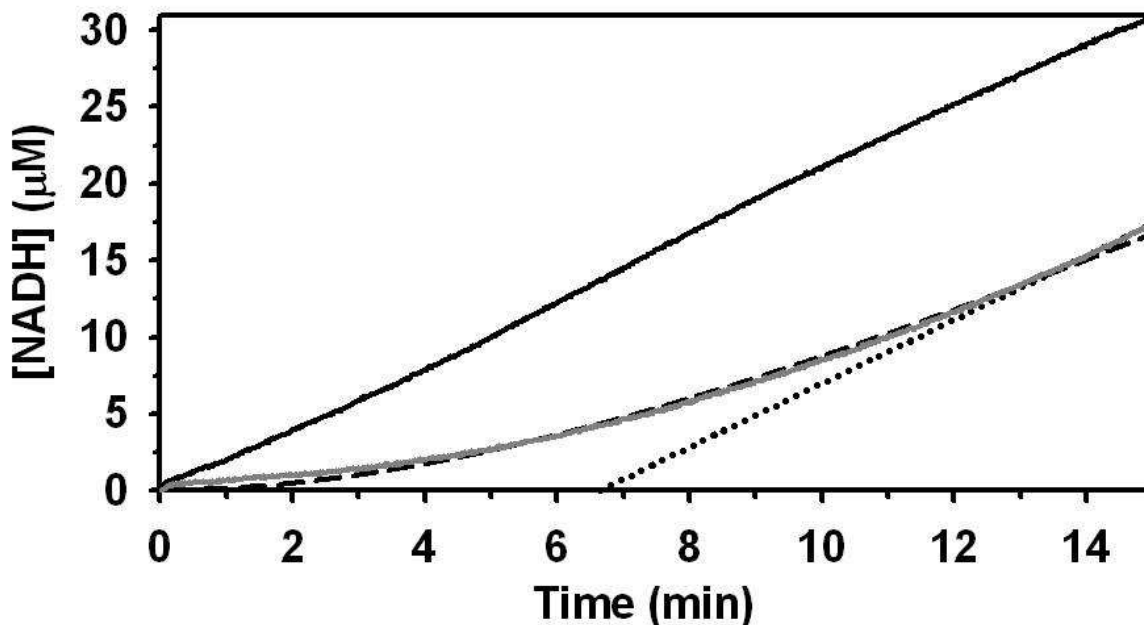


**Figure 9:** Example of transient time analysis of BjPutA. Steady-state formation of NADH using proline as a substrate by native BjPutA (solid black curve) and an equimolar mixture of monofunctional variants R456M and C792A (solid grey curve). The mixture of the monofunctional variants serves as a non-channeling control. The dotted line represents the extrapolation used for estimating the lag-time. Native BjPutA shows no apparent lag in NADH formation, while a lag time of about 6.5 min is observed for the non-channeling control. The dashed line overlaying the grey curve of the non-channeling control reaction was simulated using the kinetic parameters of PRODH and P5CDH as described previously and the following equation:  $[NADH] = v_1 t + (v_1/v_2) K_m (e^{-v_2 t/K_m} - 1)$  (76). Assays were performed at pH 7.5. Figure adapted from (17).

conditions. Rapid mixing of native BjPutA and proline generated NADH with no apparent lag time. For the non-channeling variants, a 10 s lag time for NADH formation was observed after mixing the enzymes with proline. These results show native BjPutA efficiently channels P5C/GSA.

Evidence for channeling in PutA has also been reported from *Salmonella typhimurium* PutA (StPutA). Similar to EcPutA, StPutA contains the N-terminal DNA binding domain and is thus trifunctional. Maloy *et al.* demonstrated that the P5CDH domain shows a 14-fold greater steady-state production of NADH using P5C generated endogenously from proline by PRODH, as compared to exogenously added P5C (77). In addition, they showed exogenous P5C was unable to compete against endogenous P5C. Due to a lack of structural information on trifunctional PutAs, it is not clear whether a channel similar to that characterized in BjPutA exists. Future structural and kinetic experiments will need to be performed to fully address the channeling mechanism in trifunctional PutAs.

### **CHANNELING OF $\gamma$ -GLUTAMYL PHOSPHATE**

As mentioned previously, channeling of the intermediate  $\gamma$ -glutamyl phosphate would be beneficial because of its instability. Channeling of  $\gamma$ -glutamyl phosphate is also implicated by the fusion of GK and GPR in bifunctional P5CS. Kinetically speaking, data has existed for over forty years suggesting that a complex forms between bacterial GK and GPR in order to conceal  $\gamma$ -glutamyl-phosphate from solvent (78, 79). A typical assay to measure GK activity is to add hydroxylamine along with the substrates, glutamate and ATP. Hydroxylamine reacts with the product  $\gamma$ -glutamyl phosphate to make  $\gamma$ -glutamyl

hydroxamate, which can be measured at 535 nm (78). Multiple groups have documented that GK activity is dependent on the presence of GPR. GK is inactive or exhibits very low activity in the absence of GPR, suggesting GPR is required for GK activity (56, 57, 78, 80, 81). It was found that a 10:1 GPR:GK ratio was necessary to obtain maximal GK activity, indicating that a GK/GPR complex forms with excess GPR (80). To test for a complex, Smith *et al.* tried incubating different ratios of bacterial GK and GPR, then looked for co-elution of the enzymes by chromatography (80). Both proteins eluted separately meaning either a complex does not form or complex formation is transient and is dependent on substrate binding. Other work suggesting a GK-GPR complex includes assays which contained GK and GPR, but lacked NADPH, the cofactor necessary for GPR activity (57). In this case the GPR enzyme was inactive, but it still activated GK. GK has also been shown to be activated by incubation with GPR mutants, further demonstrating that GK activation by GPR does not require GPR activity (82). Other experiments that have explored GK/GPR interactions include Chen *et al.*, who created a mutant GK/GPR fusion protein that was able to over-produce proline, making the host *E. coli* strain more resistant to osmotic stress (83). While this work does not support channeling directly, it does show that enhancing the proximity of two active sites can significantly increase the efficiency of a metabolic pathway (83).

Structural data supporting channeling is not directly available for GK and GPR enzymes (84). Figure 10 shows the individual structures of *E. coli* GK (EcGK) and *T. maritima* GPR (TtGPR). Marco-Marin *et al.* modeled a possible interaction between monofunctional GK and GPR, showing GPR in both an open and closed conformation, depending on the binding status of the substrate (46). The model shows a tetrameric form

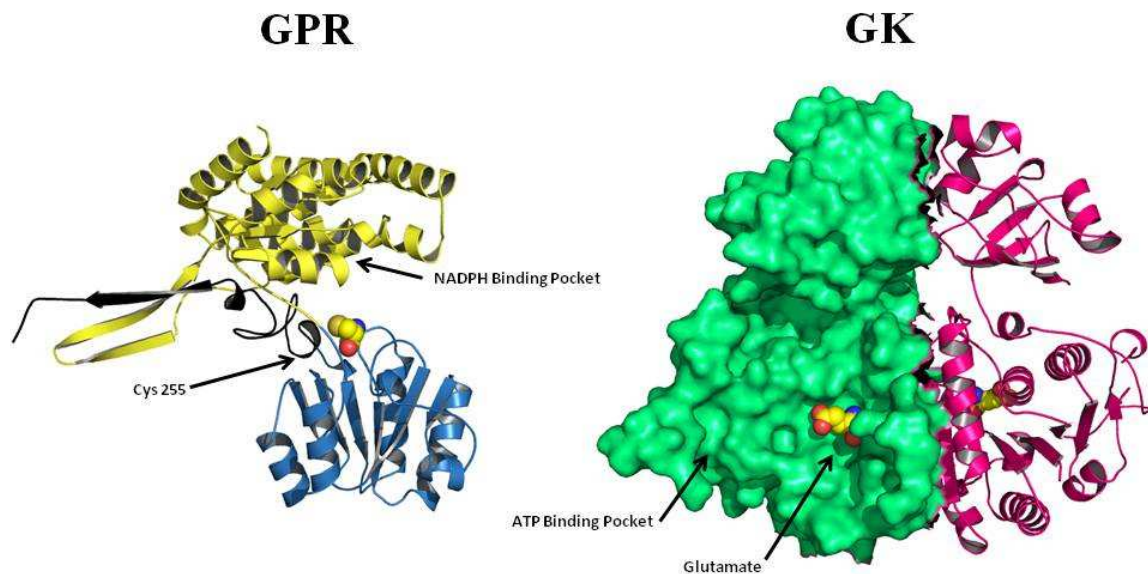


**Figure 10:** Structures of GPR from *T. maritima* (TmGPR) and GK from *E. coli* (EcGK). EcGK is shown as a dimer with one monomer shown in surface representation and the other monomer as a ribbon cartoon illustration. Glutamate is shown as spheres in the substrate binding pocket, which is solvent accessible. Only one monomer of GPR (open conformation) is shown, which contains three domains: NADPH binding domain (yellow), catalytic domain (blue) with the catalytic cysteine shown in spheres, and the oligomerization domain (black). The solvent-exposed glutamate binding pocket of GK suggests that the  $\gamma$ -glutamyl phosphate intermediate would be accessible to GPR in a potential GK-GPR complex. A GK-GPR complex in which the catalytic domain of GPR is aligned with the glutamate binding pocket of GK has been proposed and modeled by Marco-Marin *et al* (46). Models shown here were made using PyMol and PDBs 2J5T (EcGK) and 1O20 (TmGPR). Figure adapted from (17).

of GK from *E. coli* complexed with a dimer of GPR from *T. maritime* (46). In solving the crystal structure EcGK, Marco-Marin *et al.* noted that GK was well suited for channeling (46). They suggested that channeling is possible if the GK and GPR active sites are positioned so that the active site cysteine of GPR is able to react with  $\gamma$ -glutamyl phosphate while still bound at the GK active site. A complex as described would allow for a favorable environment and timely transfer of  $\gamma$ -glutamyl-phosphate to the second active site thereby preventing cyclization to 5-oxoproline (46). Additionally it has been suggested that leucine zipper motifs found in the GK and GPR domains of plants, as well as the GK and GPR enzymes of some bacteria are evidence for a functional complex (85). The leucine zipper of plant P5CS may help with oligomerization or it may be an artifact of evolution. Several domain swapping experiments have shown that leucine zippers mediate protein-protein dimerization in eukaryotic and prokaryotic enzymes. Thus, the leucine zippers in bacterial GK and GPR enzymes and plant P5CS may support a possible channeling complex (86).

## **SUMMARY**

As presented in this chapter, there is solid evidence of substrate channeling in proline metabolism, particularly in the catabolic pathway where structural and kinetic evidence both exist. However, there are many outstanding questions left to answer such as must P5C use the channel to access the P5CDH domain, how does exogenous P5C enter the cavity, and where does the hydrolysis step occur. To help answer these questions, Chapter 2 of this dissertation will further explore the substrate channel by making bulky mutations along the cavity to impede passage of P5C. Kinetic

characterizations will be used to determine the effects of the mutations and whether they change the overall structure of the enzyme, allowing conclusions to be drawn regarding how P5C accesses the second active site. Chapter 3 helps to further understand the structure-function relationship of the DNA binding domain and the functional switching mechanism employed by trifunctional PutAs. An artificial trifunctional PutA was created by fusing the DNA-binding domain of EcPutA to a monomeric, long bifunctional PutA (RcPutA). This fusion enzyme provides further knowledge of the DNA-binding domain and hints that more residues may be necessary to form a functional DNA-binding domain *in vivo*. Finally, Chapter 4 will be divided into two parts. The first part will provide kinetic evidence supporting a new ubiquinone analog as a functional substrate in PutAs. It also presents kinetic results suggesting a newly purified PutA, GsPutA, also uses a substrate channeling mechanism. The second half will kinetically explore a PRODH domain in order to better understand how proline enters and leaves the active site. Ultimately this dissertation will help further the knowledge of the proline metabolic field by using steady-state kinetics to investigate different aspects of proline utilization A.

## REFERENCES

1. Phang, J. M., Liu, W., and Zabirnyk, O. (2010) Proline metabolism and microenvironmental stress, *Annu Rev Nutr* 30, 441-463.
2. Donald, S. P., Sun, X. Y., Hu, C. A., Yu, J., Mei, J. M., Valle, D., and Phang, J. M. (2001) Proline oxidase, encoded by p53-induced gene-6, catalyzes the generation of proline-dependent reactive oxygen species, *Cancer Res* 61, 1810-1815.
3. Krishnan, N., Dickman, M. B., and Becker, D. F. (2008) Proline modulates the intracellular redox environment and protects mammalian cells against oxidative stress, *Free Radic Biol Med* 44, 671-681.
4. Chakravarti, A. (2002) A compelling genetic hypothesis for a complex disease: PRODH2/DGCR6 variation leads to schizophrenia susceptibility, *Proc Natl Acad Sci U S A* 99, 4755-4756.
5. Baumgartner, M. R., Hu, C. A., Almashanu, S., Steel, G., Obie, C., Aral, B., Rabier, D., Kamoun, P., Saudubray, J. M., and Valle, D. (2000) Hyperammonemia with reduced ornithine, citrulline, arginine and proline: a new inborn error caused by a mutation in the gene encoding delta(1)-pyrroline-5-carboxylate synthase, *Hum Mol Genet* 9, 2853-2858.
6. Mitsubuchi, H., Nakamura, K., Matsumoto, S., and Endo, F. (2008) Inborn errors of proline metabolism, *J Nutr* 138, 2016S-2020S.
7. Kamoun, P., Aral, B., and Saudubray, J. M. (1998) [A new inherited metabolic disease: delta1-pyrroline 5-carboxylate synthetase deficiency], *Bull Acad Natl Med* 182, 131-137; discussion 138-139.
8. Reversade, B., Escande-Beillard, N., Dimopoulou, A., Fischer, B., Chng, S. C., Li, Y., Shboul, M., Tham, P. Y., Kayserili, H., Al-Gazali, L., Shahwan, M., Brancati, F., Lee, H., O'Connor, B. D., Schmidt-von Kegler, M., Merriman, B., Nelson, S. F., Masri, A., Alkazaleh, F., Guerra, D., Ferrari, P., Nanda, A., Rajab, A., Markie, D., Gray, M., Nelson, J., Grix, A., Sommer, A., Savarirayan, R., Janecke, A. R., Steichen, E., Sillence, D., Hausser, I., Budde, B., Nurnberg, G., Nurnberg, P., Seemann, P., Kunkel, D., Zambruno, G., Dallapiccola, B., Schuelke, M., Robertson, S., Hamamy, H., Wollnik, B., Van Maldergem, L., Mundlos, S., and Kornak, U. (2009) Mutations in PYCR1 cause cutis laxa with progeroid features, *Nat Genet* 41, 1016-1021.
9. Wood, J. M., Bremer, E., Csonka, L. N., Kraemer, R., Poolman, B., van der Heide, T., and Smith, L. T. (2001) Osmosensing and osmoregulatory compatible solute accumulation by bacteria, *Comp Biochem Physiol A Mol Integr Physiol* 130, 437-460.
10. Yoshiba, Y., Kiyosue, T., Katagiri, T., Ueda, H., Mizoguchi, T., Yamaguchi-Shinozaki, K., Wada, K., Harada, Y., and Shinozaki, K. (1995) Correlation between the induction of a gene for delta 1-pyrroline-5-carboxylate synthetase and the accumulation of proline in *Arabidopsis thaliana* under osmotic stress, *Plant J* 7, 751-760.

11. Szabados, L., and Savoure, A. (2010) Proline: a multifunctional amino acid, *Trends Plant Sci* 15, 89-97.
12. Adams, E., and Frank, L. (1980) Metabolism of proline and the hydroxyprolines, *Annu Rev Biochem* 49, 1005-1061.
13. Tanner, J. J. (2008) Structural biology of proline catabolism, *Amino Acids* 35, 719-730.
14. White, T. A., Krishnan, N., Becker, D. F., and Tanner, J. J. (2007) Structure and kinetics of monofunctional proline dehydrogenase from *Thermus thermophilus*, *J Biol Chem* 282, 14316-14327.
15. Tanner, J. J., and Becker, D. F. (2013) PutA and proline metabolism, In *Handbook of Flavoproteins* (Hille, R., Miller, S. M., and Palfey, B., Eds.), pp 31-56, Walter De Gruyter, Boston.
16. Singh, R. K., and Tanner, J. J. (2012) Unique structural features and sequence motifs of proline utilization A (PutA), *Front Biosci (Landmark Ed)* 17, 556-568.
17. Arentson, B. W., Sanyal, N., and Becker, D. F. (2012) Substrate channeling in proline metabolism, *Front Biosci (Landmark Ed)* 17, 375-388.
18. Gu, D., Zhou, Y., Kallhoff, V., Baban, B., Tanner, J. J., and Becker, D. F. (2004) Identification and characterization of the DNA-binding domain of the multifunctional PutA flavoenzyme, *The Journal of biological chemistry* 279, 31171-31176.
19. Zhou, Y., Larson, J. D., Bottoms, C. A., Arturo, E. C., Henzl, M. T., Jenkins, J. L., Nix, J. C., Becker, D. F., and Tanner, J. J. (2008) Structural basis of the transcriptional regulation of the proline utilization regulon by multifunctional PutA, *J Mol Biol* 381, 174-188.
20. Srivastava, D., Schuermann, J. P., White, T. A., Krishnan, N., Sanyal, N., Hura, G. L., Tan, A., Henzl, M. T., Becker, D. F., and Tanner, J. J. (2010) Crystal structure of the bifunctional proline utilization A flavoenzyme from *Bradyrhizobium japonicum*, *Proceedings of the National Academy of Sciences of the United States of America* 107, 2878-2883.
21. Larson, J. D., Jenkins, J. L., Schuermann, J. P., Zhou, Y., Becker, D. F., and Tanner, J. J. (2006) Crystal structures of the DNA-binding domain of *Escherichia coli* proline utilization A flavoprotein and analysis of the role of Lys9 in DNA recognition, *Protein Sci* 15, 2630-2641.
22. Lee, Y. H., Nadaraia, S., Gu, D., Becker, D. F., and Tanner, J. J. (2003) Structure of the proline dehydrogenase domain of the multifunctional PutA flavoprotein, *Nat Struct Biol* 10, 109-114.
23. Zhang, M., White, T. A., Schuermann, J. P., Baban, B. A., Becker, D. F., and Tanner, J. J. (2004) Structures of the *Escherichia coli* PutA proline dehydrogenase domain in complex with competitive inhibitors, *Biochemistry* 43, 12539-12548.
24. Srivastava, D., Zhu, W., Johnson, W. H., Jr., Whitman, C. P., Becker, D. F., and Tanner, J. J. (2010) The structure of the proline utilization a proline dehydrogenase domain inactivated by N-propargylglycine provides insight into conformational changes induced by substrate binding and flavin reduction, *Biochemistry* 49, 560-569.

25. Halouska, S., Zhou, Y., Becker, D. F., and Powers, R. (2009) Solution structure of the *Pseudomonas putida* protein PpPutA45 and its DNA complex, *Proteins* 75, 12-27.
26. Larson, J. D., Jenkins, J. L., Schuermann, J. P., Zhou, Y., Becker, D. F., and Tanner, J. J. (2006) Crystal structures of the DNA-binding domain of *Escherichia coli* proline utilization A flavoprotein and analysis of the role of Lys9 in DNA recognition, *Protein Sci* 15, 2630-2641.
27. Zhou, Y., Larson, J. D., Bottoms, C. A., Arturo, E. C., Henzl, M. T., Jenkins, J. L., Nix, J. C., Becker, D. F., and Tanner, J. J. (2008) Structural basis of the transcriptional regulation of the proline utilization regulon by multifunctional PutA, *J Mol Biol* 381, 174-188.
28. Singh, R. K., Larson, J. D., Zhu, W., Rambo, R. P., Hura, G. L., Becker, D. F., and Tanner, J. J. (2011) Small-angle X-ray scattering studies of the oligomeric state and quaternary structure of the trifunctional proline utilization A (PutA) flavoprotein from *Escherichia coli*, *The Journal of biological chemistry* 286, 43144-43153.
29. White, T. A., Krishnan, N., Becker, D. F., and Tanner, J. J. (2007) Structure and kinetics of monofunctional proline dehydrogenase from *Thermus thermophilus*, *J Biol Chem* 282, 14316-14327.
30. Luo, M., Arentson, B. W., Srivastava, D., Becker, D. F., and Tanner, J. J. (2012) Crystal structures and kinetics of monofunctional proline dehydrogenase provide insight into substrate recognition and conformational changes associated with flavin reduction and product release, *Biochemistry* 51, 10099-10108.
31. Srivastava, D., Singh, R. K., Moxley, M. A., Henzl, M. T., Becker, D. F., and Tanner, J. J. (2012) The three-dimensional structural basis of type II hyperprolinemia, *J Mol Biol* 420, 176-189.
32. Inagaki, E., Ohshima, N., Takahashi, H., Kuroishi, C., Yokoyama, S., and Tahirov, T. H. (2006) Crystal structure of *Thermus thermophilus* Delta1-pyrroline-5-carboxylate dehydrogenase, *J Mol Biol* 362, 490-501.
33. Maloy, S. R., and Roth, J. R. (1983) Regulation of proline utilization in *Salmonella typhimurium*: characterization of put::Mu d(Ap, lac) operon fusions, *J Bacteriol* 154, 561-568.
34. Menzel, R., and Roth, J. (1981) Purification of the putA gene product. A bifunctional membrane-bound protein from *Salmonella typhimurium* responsible for the two-step oxidation of proline to glutamate, *The Journal of biological chemistry* 256, 9755-9761.
35. Ostrovsky de Spicer, P., and Maloy, S. (1993) PutA protein, a membrane-associated flavin dehydrogenase, acts as a redox-dependent transcriptional regulator, *Proceedings of the National Academy of Sciences of the United States of America* 90, 4295-4298.
36. Wood, J. M. (1987) Membrane association of proline dehydrogenase in *Escherichia coli* is redox dependent, *Proceedings of the National Academy of Sciences of the United States of America* 84, 373-377.
37. Brown, E. D., and Wood, J. M. (1993) Conformational change and membrane association of the PutA protein are coincident with reduction of its FAD cofactor by proline, *The Journal of biological chemistry* 268, 8972-8979.

38. Muro-Pastor, A. M., and Maloy, S. (1995) Proline dehydrogenase activity of the transcriptional repressor PutA is required for induction of the put operon by proline, *The Journal of biological chemistry* 270, 9819-9827.
39. Muro-Pastor, A. M., Ostrovsky, P., and Maloy, S. (1997) Regulation of gene expression by repressor localization: biochemical evidence that membrane and DNA binding by the PutA protein are mutually exclusive, *J Bacteriol* 179, 2788-2791.
40. Surber, M. W., and Maloy, S. (1999) Regulation of flavin dehydrogenase compartmentalization: requirements for PutA-membrane association in *Salmonella typhimurium*, *Biochim Biophys Acta* 1421, 5-18.
41. Zhang, W., Zhang, M., Zhu, W., Zhou, Y., Wanduragala, S., Rewinkel, D., Tanner, J. J., and Becker, D. F. (2007) Redox-induced changes in flavin structure and roles of flavin N(5) and the ribityl 2'-OH group in regulating PutA--membrane binding, *Biochemistry* 46, 483-491.
42. Zhu, W., Haile, A. M., Singh, R. K., Larson, J. D., Smithen, D., Chan, J. Y., Tanner, J. J., and Becker, D. F. (2013) Involvement of the beta3-alpha3 Loop of the Proline Dehydrogenase Domain in Allosteric Regulation of Membrane Association of Proline Utilization A, *Biochemistry* 52, 4482-4491.
43. Becker, D. F., Zhu, W., and Moxley, M. A. (2011) Flavin redox switching of protein functions, *Antioxid Redox Signal* 14, 1079-1091.
44. Perez-Arellano, I., Rubio, V., and Cervera, J. (2006) Mapping active site residues in glutamate-5-kinase. The substrate glutamate and the feed-back inhibitor proline bind at overlapping sites, *FEBS Lett* 580, 6247-6253.
45. Perez-Arellano, I., Gallego, J., and Cervera, J. (2007) The PUA domain - a structural and functional overview, *FEBS J* 274, 4972-4984.
46. Marco-Marin, C., Gil-Ortiz, F., Perez-Arellano, I., Cervera, J., Fita, I., and Rubio, V. (2007) A novel two-domain architecture within the amino acid kinase enzyme family revealed by the crystal structure of *Escherichia coli* glutamate 5-kinase, *J Mol Biol* 367, 1431-1446.
47. Page, R., Nelson, M. S., von Delft, F., Elsliger, M. A., Canaves, J. M., Brinen, L. S., Dai, X., Deacon, A. M., Floyd, R., Godzik, A., Grittini, C., Grzechnik, S. K., Jaroszewski, L., Klock, H. E., Koesema, E., Kovarik, J. S., Kreusch, A., Kuhn, P., Lesley, S. A., McMullan, D., McPhillips, T. M., Miller, M. D., Morse, A., Moy, K., Ouyang, J., Robb, A., Rodrigues, K., Schwarzenbacher, R., Spraggon, G., Stevens, R. C., van den Bedem, H., Velasquez, J., Vincent, J., Wang, X., West, B., Wolf, G., Hodgson, K. O., Wooley, J., and Wilson, I. A. (2004) Crystal structure of gamma-glutamyl phosphate reductase (TM0293) from *Thermotoga maritima* at 2.0 Å resolution, *Proteins* 54, 157-161.
48. Meng, Z., Lou, Z., Liu, Z., Li, M., Zhao, X., Bartlam, M., and Rao, Z. (2006) Crystal structure of human pyrroline-5-carboxylate reductase, *J Mol Biol* 359, 1364-1377.
49. Bearne, S. L., and Wolfenden, R. (1995) Glutamate gamma-semialdehyde as a natural transition state analogue inhibitor of *Escherichia coli* glucosamine-6-phosphate synthase, *Biochemistry* 34, 11515-11520.

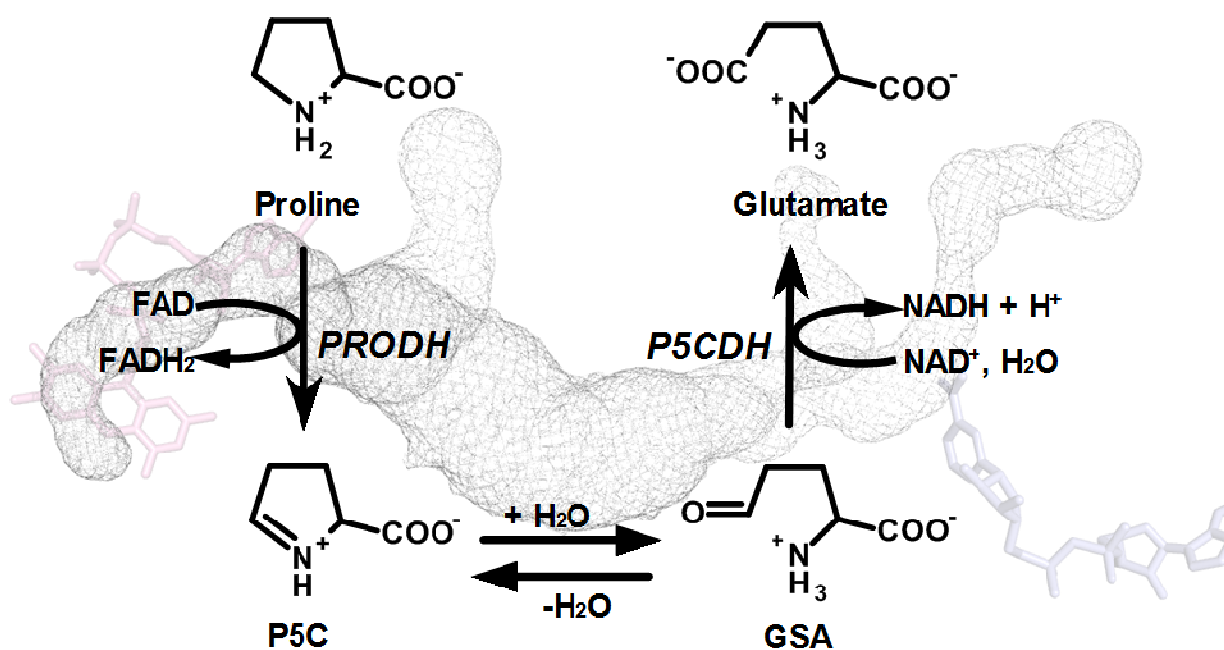
50. Bearne, S. L., Hekmat, O., and Macdonnell, J. E. (2001) Inhibition of *Escherichia coli* CTP synthase by glutamate gamma-semialdehyde and the role of the allosteric effector GTP in glutamine hydrolysis, *Biochem J* 356, 223-232.
51. Thoden, J. B., Huang, X., Raushel, F. M., and Holden, H. M. (1999) The small subunit of carbamoyl phosphate synthetase: snapshots along the reaction pathway, *Biochemistry* 38, 16158-16166.
52. Farrant, R. D., Walker, V., Mills, G. A., Mellor, J. M., and Langley, G. J. (2001) Pyridoxal phosphate de-activation by pyrroline-5-carboxylic acid. Increased risk of vitamin B6 deficiency and seizures in hyperprolinemia type II, *J Biol Chem* 276, 15107-15116.
53. Geraghty, M. T., Vaughn, D., Nicholson, A. J., Lin, W. W., Jimenez-Sanchez, G., Obie, C., Flynn, M. P., Valle, D., and Hu, C. A. (1998) Mutations in the Delta1-pyrroline 5-carboxylate dehydrogenase gene cause type II hyperprolinemia, *Hum Mol Genet* 7, 1411-1415.
54. Nomura, M., and Takagi, H. (2004) Role of the yeast acetyltransferase Mpr1 in oxidative stress: regulation of oxygen reactive species caused by a toxic proline catabolism intermediate, *Proc Natl Acad Sci U S A* 101, 12616-12621.
55. Maxwell, S. A., and Davis, G. E. (2000) Differential gene expression in p53-mediated apoptosis-resistant vs. apoptosis-sensitive tumor cell lines, *Proc Natl Acad Sci U S A* 97, 13009-13014.
56. Hayzer, D. J., and Moses, V. (1978) The enzymes of proline biosynthesis in *Escherichia coli*. Their molecular weights and the problem of enzyme aggregation, *Biochem J* 173, 219-228.
57. Seddon, A. P., Zhao, K. Y., and Meister, A. (1989) Activation of glutamate by gamma-glutamate kinase: formation of gamma-cis-cyclo-glutamyl phosphate, an analog of gamma-glutamyl phosphate, *J Biol Chem* 264, 11326-11335.
58. Rieke, G. K., Scarfe, A. D., and Hunter, J. F. (1984) L-pyroglutamate: an alternate neurotoxin for a rodent model of Huntington's disease, *Brain Res Bull* 13, 443-456.
59. McGeer, E. G., and Singh, E. (1984) Neurotoxic effects of endogenous materials: quinolinic acid, L-pyroglutamic acid, and thyroid releasing hormone (TRH), *Exp Neurol* 86, 410-413.
60. Ovadi, J. (1991) Physiological significance of metabolic channelling, *J Theor Biol* 152, 1-22.
61. Miles, E. W., Rhee, S., and Davies, D. R. (1999) The molecular basis of substrate channeling, *J Biol Chem* 274, 12193-12196.
62. Hyde, C. C., Ahmed, S. A., Padlan, E. A., Miles, E. W., and Davies, D. R. (1988) Three-dimensional structure of the tryptophan synthase alpha 2 beta 2 multienzyme complex from *Salmonella typhimurium*, *J Biol Chem* 263, 17857-17871.
63. Knighton, D. R., Kan, C. C., Howland, E., Janson, C. A., Hostomska, Z., Welsh, K. M., and Matthews, D. A. (1994) Structure of and kinetic channelling in bifunctional dihydrofolate reductase-thymidylate synthase, *Nat Struct Biol* 1, 186-194.

64. Perham, R. N. (2000) Swinging arms and swinging domains in multifunctional enzymes: catalytic machines for multistep reactions, *Annu Rev Biochem* 69, 961-1004.
65. Huang, X., Holden, H. M., and Raushel, F. M. (2001) Channeling of substrates and intermediates in enzyme-catalyzed reactions, *Annu Rev Biochem* 70, 149-180.
66. Anderson, K. S. (1999) Fundamental mechanisms of substrate channeling, *Methods Enzymol* 308, 111-145.
67. Bera, A. K., Smith, J. L., and Zalkin, H. (2000) Dual role for the glutamine phosphoribosylpyrophosphate amidotransferase ammonia channel. Interdomain signaling and intermediate channeling, *J Biol Chem* 275, 7975-7979.
68. Geck, M. K., and Kirsch, J. F. (1999) A novel, definitive test for substrate channeling illustrated with the aspartate aminotransferase/malate dehydrogenase system, *Biochemistry* 38, 8032-8037.
69. Iturrate, L., Sanchez-Moreno, I., Doyaguez, E. G., and Garcia-Junceda, E. (2009) Substrate channelling in an engineered bifunctional aldolase/kinase enzyme confers catalytic advantage for C-C bond formation, *Chem Commun (Camb)*, 1721-1723.
70. Tsuji, S. Y., Cane, D. E., and Khosla, C. (2001) Selective protein-protein interactions direct channeling of intermediates between polyketide synthase modules, *Biochemistry* 40, 2326-2331.
71. Moore, S. A., Baker, H. M., Blythe, T. J., Kitson, K. E., Kitson, T. M., and Baker, E. N. (1998) Sheep liver cytosolic aldehyde dehydrogenase: the structure reveals the basis for the retinal specificity of class 1 aldehyde dehydrogenases, *Structure* 6, 1541-1551.
72. Inagaki, E., Ohshima, N., Takahashi, H., Kuroishi, C., Yokoyama, S., and Tahirov, T. H. (2006) Crystal structure of *Thermus thermophilus* Delta1-pyrroline-5-carboxylate dehydrogenase, *J Mol Biol* 362, 490-501.
73. Mezl, V. A., and Knox, W. E. (1976) Properties and analysis of a stable derivative of pyrroline-5-carboxylic acid for use in metabolic studies, *Anal Biochem* 74, 430-440.
74. Purcarea, C., Ahuja, A., Lu, T., Kovari, L., Guy, H. I., and Evans, D. R. (2003) *Aquifex aeolicus* aspartate transcarbamoylase, an enzyme specialized for the efficient utilization of unstable carbamoyl phosphate at elevated temperature, *J Biol Chem* 278, 52924-52934.
75. Wimalasena, D. S., and Wimalasena, K. (2004) Kinetic evidence for channeling of dopamine between monoamine transporter and membranous dopamine-beta-monooxygenase in chromaffin granule ghosts, *J Biol Chem* 279, 15298-15304.
76. Meek, T. D., Garvey, E. P., and Santi, D. V. (1985) Purification and characterization of the bifunctional thymidylate synthetase-dihydrofolate reductase from methotrexate-resistant *Leishmania tropica*, *Biochemistry* 24, 678-686.
77. Surber, M. W., and Maloy, S. (1998) The PutA protein of *Salmonella typhimurium* catalyzes the two steps of proline degradation via a leaky channel, *Arch Biochem Biophys* 354, 281-287.
78. Baich, A. (1969) Proline synthesis in *Escherichia coli*. A proline-inhibitable glutamic acid kinase, *Biochim Biophys Acta* 192, 462-467.

79. Gamper, H., and Moses, V. (1974) Enzyme organization in the proline biosynthetic pathway of *Escherichia coli*, *Biochim Biophys Acta* 354, 75-87.
80. Smith, C. J., Deutch, A. H., and Rushlow, K. E. (1984) Purification and characteristics of a gamma-glutamyl kinase involved in *Escherichia coli* proline biosynthesis, *J Bacteriol* 157, 545-551.
81. Perez-Arellano, I., Rubio, V., and Cervera, J. (2005) Dissection of *Escherichia coli* glutamate 5-kinase: functional impact of the deletion of the PUA domain, *FEBS Lett* 579, 6903-6908.
82. Hayzer, D. J., and Leisinger, T. (1980) The gene-enzyme relationships of proline biosynthesis in *Escherichia coli*, *J Gen Microbiol* 118, 287-293.
83. Chen, M., Cao, J., Zheng, C., and Liu, Q. (2006) Directed evolution of an artificial bifunctional enzyme, gamma-glutamyl kinase/gamma-glutamyl phosphate reductase, for improved osmotic tolerance of *Escherichia coli* transformants, *FEMS Microbiol Lett* 263, 41-47.
84. Perez-Arellano, I., Carmona-Alvarez, F., Martinez, A. I., Rodriguez-Diaz, J., and Cervera, J. (2010) Pyrroline-5-carboxylate synthase and proline biosynthesis: from osmotolerance to rare metabolic disease, *Protein Sci* 19, 372-382.
85. Hu, C. A., Delauney, A. J., and Verma, D. P. (1992) A bifunctional enzyme (delta 1-pyrroline-5-carboxylate synthetase) catalyzes the first two steps in proline biosynthesis in plants, *Proc Natl Acad Sci U S A* 89, 9354-9358.
86. Abel, T., and Maniatis, T. (1989) Gene regulation. Action of leucine zippers, *Nature* 341, 24-25.

## CHAPTER 2

### Kinetic Characterization of Channel-blocking Mutants in *Bradyrhizobium japonicum* Proline Utilization A (PutA)



Note: Structural evidence validating kinetic characterizations was done in collaboration with Dr. John J. Tanner, University of Missouri-Columbia. However, structural results are not presented in this dissertation.

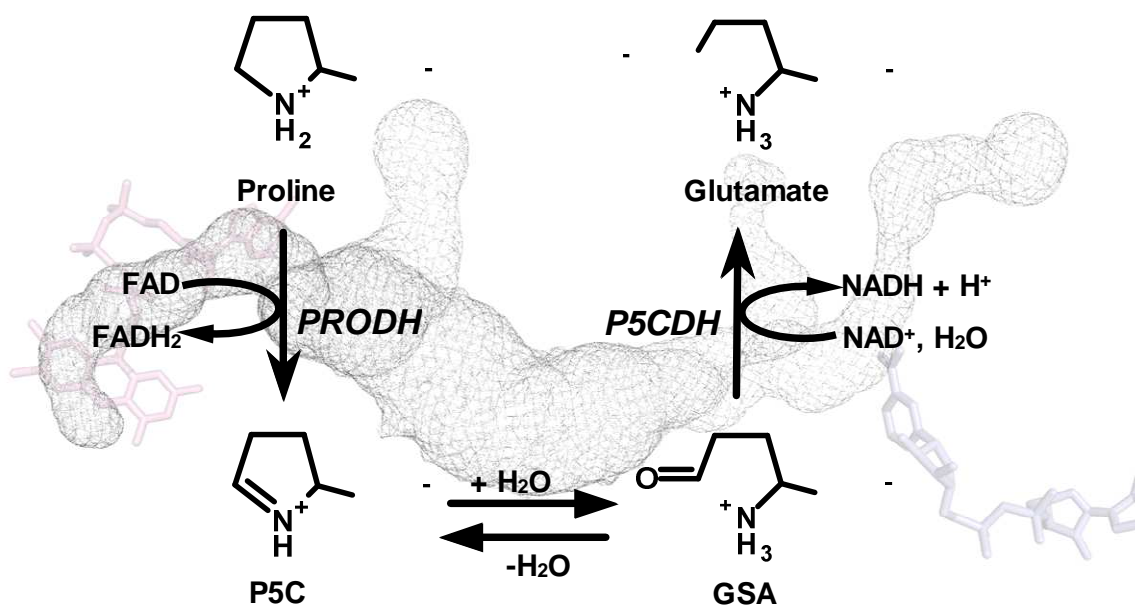
## ABSTRACT

Proline utilization A (PutA) from *Bradyrhizobium japonicum* (BjPutA) is a bifunctional flavoenzyme that catalyzes the oxidation of proline to glutamate using fused proline dehydrogenase (PRODH) and  $\Delta^1$ -pyrroline-5-carboxylate dehydrogenase (P5CDH) domains. Recent crystal structures and kinetic data suggest an intramolecular channel connects the two active sites, promoting substrate channeling of the intermediate P5C from the PRODH domain to the P5CDH domain. In this work several mutations were made along the channel in an effort to block passage of P5C to the second active site. Analysis of several site-specific mutants in the substrate channel of BjPutA revealed an important role for D779 in the channeling path. BjPutA mutants D779Y and D779W significantly decreased the overall PRODH-P5CDH channeling reaction indicating that bulky mutations at residue D779 impede travel of P5C through the channel. Interestingly, D779Y and D779W also exhibited lower P5CDH activity, suggesting that exogenous P5C must enter the channel upstream of D779. Replacing D779 with a smaller residue (D779A) had no effect on the catalytic and channeling properties of BjPutA showing that the carboxylate group of D779 is not essential for channeling. An identical mutation at D778 (D778Y) did not impact BjPutA channeling activity. Thus, D779 is optimally orientated so that replacement with the larger side chains of Tyr/Trp blocks P5C movement through the channel. The kinetic data reveal not only that bulky mutations at residue D779 hinder passage of P5C to the second active site, but also P5C must use the channel to efficiently access the P5CDH domain. Moreover, these mutants may be used to learn more about the hydrolysis event that is thought to take place within the channel.

## INTRODUCTION

Proline utilization A (PutA) catalyzes the conversion of proline to glutamate using two consecutive reactions (Scheme 1). In the first step, proline dehydrogenase (PRODH) uses a flavin cofactor as an electron acceptor to remove two electrons from proline, resulting in  $\Delta^1$ -pyrroline-5-carboxylate (P5C). P5C then undergoes a non-enzymatic hydrolysis, which opens the pyrroline ring to create glutamate- $\gamma$ -semialdehyde (GSA). GSA is a substrate for NAD<sup>+</sup>-dependent pyrroline-5-carboxylate dehydrogenase (P5CDH), where two additional electrons are removed generating glutamate. Proline and proline metabolism are important to all walks of life. For example, proline plays important roles in different pathogens including pathogenicity of *Helicobacter pylori* and *H. hepaticus* (1, 2), energy production for procyclic trypanosomes (3, 4), and regulation of metabolites linked to pathogenesis in *Photobacterium* and *Xenorhabdus* (5). In humans, inborn errors in PRODH are linked to schizophrenia (6, 7). PRODH is also regulated by p53 and has been shown to suppress cancer (8).

PutA occurs as a bifunctional enzyme in all Gram-negative bacteria and *Corynebacterium* (9). A recent crystal structure of *Bradyrhizobium japonicum* PutA (BjPutA) revealed a tunnel connecting the two active sites (10). Structural and kinetic results suggest P5C/GSA uses the channel to travel from the PRODH active site to the P5CDH active site, without equilibrating with external solvent in a phenomenon called substrate channeling (10-12). Three different mechanisms of substrate channeling have been identified in nature. The classic example includes an intramolecular channel connecting two active sites. Tryptophan synthase remains the most studied enzyme using



**Scheme 1.** Overall reaction catalyzed by proline utilization A (PutA). Flavin-dependent proline dehydrogenase catalyzes the oxidation of proline to  $\Delta^1$ -pyrroline-5-carboxylate (P5C). P5C undergoes a non-enzymatic hydrolysis, resulting in glutamic- $\gamma$ -semialdehyde (GSA). Finally, GSA is oxidized to glutamate using an  $\text{NAD}^+$  cofactor and water.

this method of channeling (13, 14). A second mechanism for channeling involves the intermediate moving across the surface of the enzyme. Two variations of surface channeling have been reported: dihydrofolate reductase-thymidylate synthase, which uses a surface “electrostatic highway” (15, 16), and dethiobiotin synthetase-diaminopelargonic acid aminotransferase, which uses a polar crevice along the enzyme’s surface (17). A third mechanism of substrate channeling involves using a swinging arm to transfer intermediate to multiple sites. The pyruvate dehydrogenase complex provides an example where a lipoic acid cofactor acts as an arm (18).

Several physiological benefits of substrate channeling versus free diffusion have been identified. Chiefly, channeling decreases transit time between active sites and prevents loss of intermediates by diffusion, making the overall reaction more efficient (11, 19). Thus, channeling enzymes can operate at maximum rates even if cellular substrate concentrations are not at saturating levels (20). Also, labile intermediates can be concealed from solvent to prevent decay or interaction with other molecules (13, 21). Finally, reaction intermediates from competing reactions can be kept separate, which dictates metabolic flux (12).

As mentioned, a crystal structure of BjPutA revealed a tunnel connecting two active sites, which is thought to channel intermediate P5C/GSA. Theoretically, the channeling of P5C/GSA is physiologically reasonable, as P5C is a substrate of three competing reactions. It can be converted to glutamate via P5CDH, ornithine via ornithine aminotransferase, or back to proline via P5C reductase. Thus, channeling of P5C in proline catabolism may be necessary to retain proper metabolic flux and avoid

metabolic cycling (21). Besides enzyme competition, free P5C/GSA is reported to be an inhibitor of glutamine in three different *E. coli* enzymes including glucosamine-6-phosphate synthase, cytidine 5'-triphosphate synthase, and the amidotransferase domain of carbamoyl phosphate synthetase (22-24). Additionally, P5C was shown to form adducts with other important metabolic intermediates including oxaloacetic acid, pyruvic acid, and acetoacetic acid (25). Considering the outcomes of liberated P5C/GSA, there appears to be a physiological advantage to sequester the intermediate during proline catabolism.

Substrate channeling in PutA was first kinetically described in *Salmonella typhimurium* (26); however, the structural and kinetic characterization of BjPutA have made this enzyme the prototype of PutA channeling. An X-ray structure of BjPutA revealed an irregularly-shaped cavity that spans 41 Å between the two active sites with a total volume of 1400 Å<sup>3</sup> (Figure 1) (10). The majority of the volume (1325 Å<sup>3</sup>) of the tunnel comes from a large central chamber with dimensions 24 Å by 14 Å by 3-7 Å, which provides adequate space to accommodate P5C (102 Å<sup>3</sup>) or GSA (120 Å<sup>3</sup>) (9). Additionally, kinetic evidence comparing native BjPutA to an equal molar mixture of two complementary active site mutants (R456M, no PRODH activity; C792A, no P5CDH activity) showed the native enzyme immediately formed NADH, while the mixed variant system had a significant lag phase before reaching steady state (10). Taken altogether, substrate channeling of P5C/GSA in BjPutA is supported by strong kinetic and structural evidence.

Using the structural and kinetic knowledge of the channel, this work further explores the cavity by mutating residues along the channel in an effort to obstruct P5C movement between the active sites. A combination of kinetic and structural results (through personal correspondence with Dr. John Tanner) provide evidence that channeling can be hindered, but the location of the mutation along the channel seems to be critical for impeding the intermediate. By making mutations along different parts of the channel, we further define the channeling path and provide novel insights into how P5C enters the channeling cavity.

## **MATERIALS AND METHODS**

### **Chemicals**

All chemicals were purchased from Sigma-Aldrich or Fisher Scientific unless otherwise noted. *E. coli* strain BL21 (DE3) pLysS was purchased from Novagen, and DH5 $\alpha$  strain was purchased from Invitrogen. All experiments used Nanopure water.

### **Expression and Purification of BjPutA**

PutA from *Bradyrhizobium japonicum* (BjPutA) was expressed as reported previously, only the incubator temperature was decreased to 20 °C for 16 hours following IPTG induction (27). Cells were harvested by centrifugation and frozen at -80°C. Frozen cells were re-suspended in 50 ml binding buffer (20 mM Tris-base, 0.5 M NaCl, 5 mM imidazole, 10% glycerol, pH 7.9) and 100  $\mu$ M flavin at 4°C. Protease inhibitors  $\epsilon$ -amino-N-caproic acid (3 mM), phenylmethylsulfonyl fluoride (0.3 mM), leupeptin (1.2  $\mu$ M), tosyl phenylalanyl chloromethyl ketone (48  $\mu$ M), and tosyllysine chloromethyl

ketone hydrochloride (78  $\mu\text{M}$ ) were added, and cells were disrupted via sonication. The cell lysate was centrifuged for 1 h at 19,000 rpm in a JA-20 rotor (Beckman) and filtered through a 0.2  $\mu\text{m}$  filter (VWR). Cell-free lysate was loaded onto a Ni-NTA Superflow resin (Qiagen) pre-equilibrated with binding buffer. Wash buffer (60 mM imidazole) then elution buffer (500 mM imidazole) were applied to the column. Protein in the elution fractions was then dialyzed into buffer containing 50 mM Tris (pH 7.5), 10 mM NaCl, 0.5 mM EDTA, 10% glycerol and loaded onto an anion exchange column (HiTrap Q HP column, GE Life Sciences) equilibrated with dialysis buffer (50 mM Tris, pH 7.5, 10 mM NaCl, 0.5 mM EDTA, 10% glycerol). A linear salt gradient comprised of dialysis buffer and dialysis buffer containing 1 M NaCl was applied to elute the PutA proteins. Purified PutA enzymes were then dialyzed into a final buffer containing 50 mM Tris (pH 7.5), 50 mM NaCl, 0.5 mM EDTA, 0.5 mM Tris(3-hydroxypropyl)phosphine, and 10 % glycerol. Enzyme concentrations were determined using 660 nm Protein Assay (Pierce) and the amount of bound flavin was quantified ( $\epsilon=13,620 \text{ M}^{-1} \text{ cm}^{-1}$ ) (27). The concentrations of the PutA proteins were normalized to the concentration of bound flavin, and the protein was flash-frozen in liquid nitrogen and stored at  $-80 \text{ }^\circ\text{C}$ .

### **Site-Directed Mutagenesis**

Mutagenic primers (Table 1) were purchased from Integrated DNA Technologies or Eurofins MWG Operon. GeneTailor Mutagenesis Kit (Invitrogen) was used to generate all mutants except T348Y, which used a Quickchange II kit (Stratagene). Mutant plasmids were transformed into DH5 $\alpha$  cells, and resulting plasmids were sequenced by

Eurofins MWG Operon to confirm mutations. Mutant BjPutA enzymes were expressed and purified as described above.

Table 1. Primers used for site-directed mutagenesis

<b>Mutant</b>	<b>Primers</b>
T348Y	5' GGCCTATTGGGACTACGAGATCAAGCGCGCG 3' 5' CGCGCGCTTGATCTCGTAGTCCCAATAGGCGC 3'
S607Y	5' AGACGCTCGACGATGCGCTCTATGAGCTGCGCG 3' 5' GAGCGCATCGTCGAGCGTCTTGCCGCCCTCG 3'
D778Y	5' GCTGCCGGAGCAGGTCGCCTACGACGTTGTCACC 3' 5' GGCGACCTGCTCCGGCAGCGCGGTGGCATCG 3'
D779A	5' TGCCGGAGCAGGTCGCCGACGCCGTTGTCACCTCC 3' 5' GTCGGCGACCTGCTCCGGCAGCGCGGTGGC 3'
D779W	5' TGCCGGAGCAGGTCGCCGACTGGGTTGTCACCTCC 3' 5' GTCGGCGACCTGCTCCGGCAGCGCGGTGGC 3'
D779Y	5' CCGGAGCAGGTCGCCGACTACGTTGTCACCTCCGC 3' 5' GCGGAGGTGACAACGTAGTCGGCGACCTGCTCCGG 3'

### **Steady-State Kinetic Assays**

All steady-state assays were performed at 23 °C. Kinetic parameters for the PRODH domain were determined for proline and ubiquinone (CoQ<sub>1</sub>) by following reduction of CoQ<sub>1</sub> at 278 nm (28). 50 mM potassium phosphate buffer (pH 7.5) and 0.5 μM enzyme were used in all kinetic assays.  $K_m$  and  $k_{cat}$  for proline were determined for

all enzymes by varying proline (1-200 mM) while holding CoQ<sub>1</sub> constant at 250 μM. CoQ<sub>1</sub> kinetic parameters were determined by varying CoQ<sub>1</sub> (10-350 μM) while holding proline constant at 150 mM. For both assays, data was collected on a Hi-Tech Scientific SF-61DX2 stopped-flow instrument using a 0.15 cm pathlength. Initial velocities were fit to the Michaelis-Menton equation using SigmaPlot 12.0.

Kinetic parameters of the P5CDH domain were determined for P5C/GSA and NAD<sup>+</sup>. Kinetic constants for P5C/GSA were determined using exogenous D,L-P5C. D,L-P5C was synthesized according to the method of Williams and Frank, and the concentration of D,L-P5C was determined as previously reported (29, 30). The concentration of L-P5C is considered as half of the total D,L-P5C concentration. It should be noted that D,L P5C is stored in 1 M HCl and it needs to be neutralized immediately before use in the assays. This leads to high NaCl concentration of ~ 600 mM after neutralization. Thus, all assays were performed with 600 mM NaCl to maintain constant ionic strength.  $K_m$  and  $k_{cat}$  for P5C/GSA were determined by varying L-P5C (0.01-6 mM) while holding NAD<sup>+</sup> constant at 0.2 mM in 50 mM potassium phosphate (pH 7.5, 600 mM NaCl) (0.25 μM enzyme). The effective concentration of GSA was estimated from the P5C-GSA pH dependence experiment reported previously (22). To determine kinetic parameters for GSA, NAD<sup>+</sup> reduction was monitored at 340 nm ( $\epsilon = 6200 \text{ M}^{-1} \text{ cm}^{-1}$ ), using a Powerwave XS 96 well plate reader (Biotek). The dissociation constant for NAD<sup>+</sup> was determined using intrinsic tryptophan fluorescence. Tryptophan was excited at 295 nm and peak emission at 330 nm was recorded. Assays initially included 50 mM potassium phosphate pH 7.5 and 0.25 μM enzyme, then NAD<sup>+</sup> (0.1-25 μM) was titrated in, which quenched tryptophan fluorescence. The observed inner filter

effect caused by the absorption of incident light by  $\text{NAD}^+$  at 295 nm was corrected using equation 1 (28).  $F_{\text{corr}}$  and  $F_{\text{obs}}$  are the corrected fluorescence and observed fluorescence, and  $A_{\text{ex}}$  and  $A_{\text{em}}$  are the absorbance values of  $\text{NAD}^+$  at the excitation and emission wavelengths.

$$F_{\text{corr}} = F_{\text{obs}} 10^{\left(\frac{A_{\text{ex}} + A_{\text{em}}}{2}\right)} \quad (1)$$

A dissociation constant for  $\text{NAD}^+$ -BjPutA complex was determined by plotting the fraction of BjPutA bound by  $\text{NAD}^+$  versus free  $[\text{NAD}^+]$  using equation 2, where  $\theta$  is the fraction of  $\text{NAD}^+$  bound and  $n$  is number of binding sites.

$$\theta = \frac{n[\text{NAD}^+]_{\text{free}}}{K_d + [\text{NAD}^+]_{\text{free}}} \quad (2)$$

The concentration of free  $\text{NAD}^+$  was determined using equation 3.

$$[\text{NAD}^+]_{\text{free}} = [\text{NAD}^+]_{\text{total}} - \theta[\text{BjPutA}]_{\text{total}} \quad (3)$$

$\theta$  is the fractional saturation of BjPutA and is calculated by  $\frac{(F_0 - F)}{(F_0 - F_{\text{max}})}$ , where  $F_0$  is fluorescence intensity without  $\text{NAD}^+$ ,  $F$  is fluorescence intensity in the presence of  $\text{NAD}^+$ , and  $F_{\text{max}}$  is the maximum fluorescence intensity under saturating concentrations of  $\text{NAD}^+$ .

Prior to performing these assays, the amount of  $\text{NAD}^+$  bound to purified BjPutA was estimated by HPLC. Purified BjPutA was denatured with 5% vol/vol trichloroacetic acid and centrifuged at 13,000 rpm for 5 min. Samples were then filtered with a 0.45 micron filter before being loaded into autosampler vials. Denatured BjPutA released

both FAD and NAD<sup>+</sup> cofactors, which were separated using a C18 column using 50 mM potassium phosphate, pH 5.3 and 100% methanol. Method of solvent application was as follows (flow rate 1 ml/min): 5 min isocratic elution with phosphate buffer, followed by a 25 min linear gradient to 50% methanol, and finally a 5 min linear gradient to 75% methanol. Both cofactors were detected at 280 nm. NAD<sup>+</sup> eluted from the column at 7.9 minutes, while FAD eluted at 16.6 min. Finally, to determine NAD<sup>+</sup> concentration, a standard curve was established using NAD<sup>+</sup> concentrations 10, 25, 50, 100, and 200  $\mu$ M. NAD<sup>+</sup> standards were treated identically to the BjPutA samples, i.e. 5% vol/vol trichloroacetic acid. Peak areas of the standards were determined and fit to a linear equation, then peak areas of NAD<sup>+</sup> from BjPutA samples were used to calculate NAD<sup>+</sup> concentration based on the linear fit of the standard curve. From this analysis, it was estimated that 74% of BjPutA was complexed with NAD<sup>+</sup>. Thus, the NAD<sup>+</sup> binding experiments reported on the remaining 26% of BjPutA that purified without NAD<sup>+</sup> bound.

### **Channeling Assays**

Channeling assays that monitor the coupled PRODH-P5CDH reaction were used to detect a lag phase in NADH formation when using proline as a substrate (10). A lag in NADH formation indicates substrate channeling is not occurring. Channeling assays were performed at 23°C by following NAD<sup>+</sup> reduction at 340 nm ( $\epsilon = 6200 \text{ M}^{-1} \text{ cm}^{-1}$ ) as previously reported (10). Assay conditions and spectral corrections were carried out identically to what was reported previously (10). All assays contained 0.1 mM CoQ<sub>1</sub>, 0.2

mM NAD<sup>+</sup>, 40 mM proline, 50 mM potassium phosphate (pH 7.5), 25 mM NaCl, 10 mM MgCl<sub>2</sub>, and 0.5 μM PutA enzyme.

Additional channeling assays were performed using increased concentrations of D779Y and D779W. Assays contained 0.1 mM CoQ<sub>1</sub>, 0.2 mM NAD<sup>+</sup>, 40 mM proline, 50 mM potassium phosphate (pH 7.5), 25 mM NaCl, and 10 mM MgCl<sub>2</sub>. Reaction progress curves were followed using a Cary Eclipse fluorescence spectrophotometer. NADH formation was monitored by exciting at 340 nm and recording the emission at 460 nm. D779Y and D778W concentrations of 0.187, 0.374, 0.935, and 1.87 μM were used in the assays and compared to assays using 0.187 μM wild-type BjPutA.

### **Single Turnover Rapid-reaction Kinetics**

Single turnover experiments were performed as described previously (10). Briefly equal volumes of enzyme (21.3 μM wild-type, 17.8 μM T348Y, and 17.9 μM D779Y) with 50 mM potassium phosphate (pH 7.5), 25 mM NaCl, 0.1 mM NAD<sup>+</sup> was rapidly mixed with 40 mM proline in 50 mM potassium phosphate buffer (pH 7.5), and 25 mM NaCl under anaerobic conditions (all concentrations reported as final concentrations after mixing) (31). Anaerobic conditions were achieved by degassing buffer, substrate, and enzyme solutions by performing repeated cycles of nitrogen flushing and vacuuming. A day prior to performing the experiment, degassed buffer was imported into an anaerobic glovebox (Belle Technology), where it was combined with protocatechuate dioxygenase (PCD) (0.05 U/mL) and protocatechuic acid (PCA) (100 μM), which help scrub dissolved oxygen. Buffer was then loaded into syringes and sealed with parafilm before exporting from glove box. Stopped-flow mixing cell and

tubing was thoroughly washed and incubated overnight with PCA/PCD buffer. Immediately prior to performing the experiment, enzyme and substrate were degassed and imported into the chamber, where PCA and PCD were added at concentrations reported above. Both enzyme and substrate were loaded into syringes and wrapped with parafilm before leaving the chamber. To collect data, anaerobic solutions were quickly loaded onto the stopped flow and syringes were parafilmed. Spectra from 300-700 nm were recorded using a Hi-Tech Scientific SF-61DX2 stopped flow instrument equipped with a photodiode array detector. FAD (451 nm) and NAD<sup>+</sup> (340 nm) reduction reactions were extracted from the spectral traces and observed rate constants were determined by single exponential fits as previously reported (10).

### **Kinetic Parameters of Alternative Substrates**

Alternative P5CDH substrates were used to determine whether BjPutA mutants D779Y and D779W exhibit higher activity with smaller substrates relative to larger substrates. Kinetic assays using GSA, succinate semialdehyde, and propionaldehyde were performed, and  $K_m$  and  $k_{cat}$  values for each were determined. All assays were performed in buffer composed of 50 mM potassium phosphate (pH 7.5, 25 mM NaCl) containing 0.2 mM NAD<sup>+</sup> and variable concentrations of GSA (L-P5C 0.01-6 mM), succinate semialdehyde (0.05-20 mM), and propionaldehyde (5-500 mM). Wild-type, D779A, D779Y, and D779W concentrations varied in the assays for each of the substrates. With GSA/P5C, all enzyme concentrations were 0.25  $\mu$ M in the assays. For succinate semialdehyde wild-type and D779A were 0.25  $\mu$ M while D779W and D779Y were 1  $\mu$ M. For propionaldehyde, wild-type and D779A were 0.25  $\mu$ M, D779W was 1

$\mu\text{M}$ , and D779W was  $2 \mu\text{M}$ . All initial velocity data was collected on a Powerwave XS 96 well plate reader (Biotek). The data were fit to the Michaelis-Menten equation using SigmaPlot 12.0.

## RESULTS

### Identification and Purification of Channeling Mutants.

The BjPutA crystal structure (PDB code: 3HAZ) and PyMOL plug-in CAVER were used to identify tunnels within BjPutA (32, 33). With a starting point at the N5 of the flavin cofactor, CAVER identified over twenty five channels leading to the bulk solvent, with a handful extending from the N5, through the predicted internal cavity, and past the catalytic cysteine in the P5CDH active site before exiting (Figure 1). By analyzing these potential channels, several residues were identified that have side chains that appear to orient into the channel at different points. These residues included T348, S607, D778, and D779. As seen in Figure 1, the side chain of T348 extends towards a bottleneck between the PRODH domain and the large internal cavity, while the side chain of S607 points to a constriction between the cavity and the P5CDH domain. The side chains of the last two residues, D778 and D779, appear to point into the main cavity.

The aforementioned residues were chosen for site-directed mutagenesis. Each residue was substituted with a tyrosine in order to retain polarity while also increasing the steric effect of the native side chain. Additionally, D779 also was mutated to tryptophan and alanine. The tryptophan further increases side chain bulk and changes polarity, whereas the alanine decreases steric size while also removing the functional property of the side chain carboxylate. All six mutant proteins, T348Y, S607Y, D778Y, and

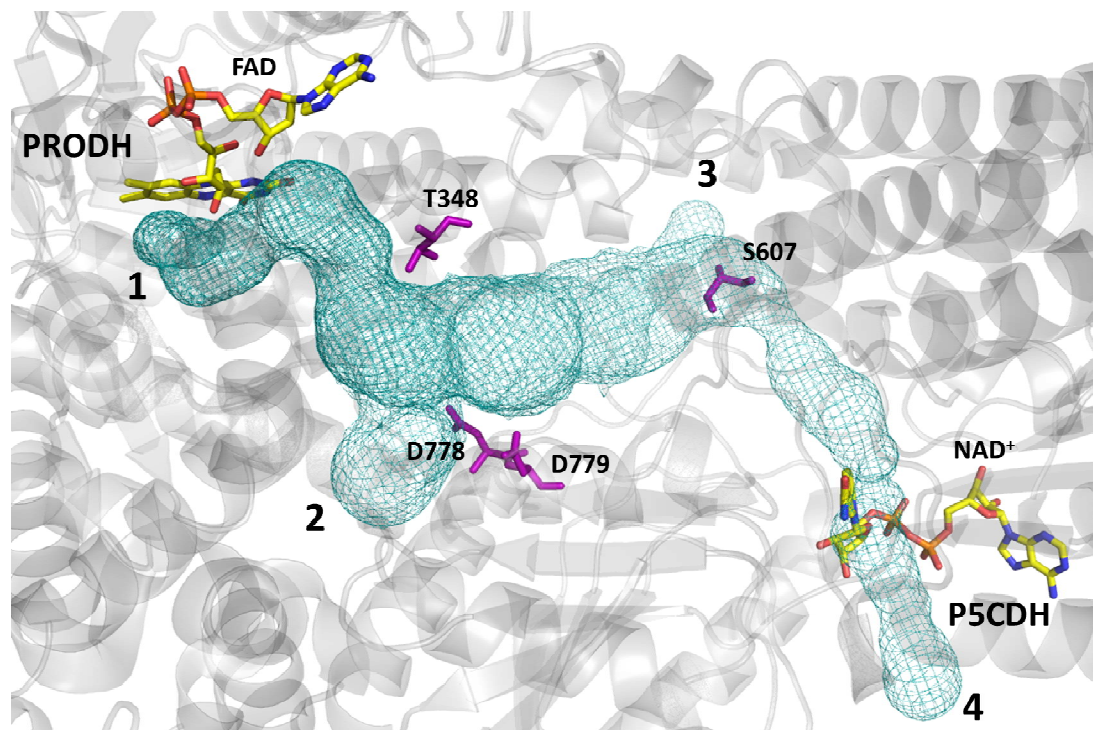


**Figure 1.** Channel connecting the PRODH active site to the P5CDH active site. FAD is shown bound within the PRODH domain, while NAD<sup>+</sup> binds at the P5CDH domain. The teal mesh channel connecting the two active sites indicates an area unoccupied by electron density that extends from the PRODH domain to the P5CDH domain. Presumably P5C travels through the channel from the PRODH active site to the P5CDH active site. The magenta sticks are native residues that appear to orient into the channel that were mutated to tyrosine residues. Numbers 1-4 label channels leading from bulk solvent to the internal cavity. Channel 1 is where proline is believed to enter, channel 2 and 3 are potential entry/exit points for water or P5C, and channel 4 is where glutamate is predicted to exit. This figure was prepared using PyMOL and CAVER using PDB code 3HAZ (32, 33).

D779Y/W/A were purified and shown to have flavin spectra similar to wild-type BjPutA with flavin peak absorbances at 380 and 451 nm. From the flavin absorbance spectra, the percent bound flavin was estimated to be 74-99% per monomer for the mutants, which is similar to 79% bound flavin for wild-type BjPutA.

### **Channeling Assays of BjPutA Mutants**

To initially screen the mutants for disruption of the channeling event, coupled PRODH-P5CDH channeling assays were performed. As described previously, these assays report on the overall oxidation of proline to glutamate by monitoring NADH formation (10). If an initial lag in NADH formation is apparent, then channeling is not likely occurring. As shown in Figure 2, channeling assays were performed on wild-type and all six BjPutA mutants. The progress curves of NADH formation in assays with T348Y, S607Y, D778Y, and D779A are very similar to wild-type with no apparent lag. The linear rate of NADH formation with the mutants is also similar to wild-type at roughly 1.4  $\mu\text{M}/\text{min}$ . In contrast, BjPutA mutants D779Y and D779W exhibit very little NADH formation over the same time course. Minor amounts of NADH were detected with D779Y and D779W even in assays extended out to 20 min. Assays were then performed with higher concentrations of D779Y and D779W, and fluorescence spectroscopy was used as a more sensitive technique to follow NADH formation. Figure 3 shows progress curves of NADH formation for D779Y and D779W relative to wild-type BjPutA. Increasing D779Y concentration 10-fold (0.187  $\mu\text{M}$  to 1.87  $\mu\text{M}$ ) generates NADH at rate comparable to wild-type BjPutA (0.187  $\mu\text{M}$ ) suggesting that D779Y is about 10-fold less active than wild-type BjPutA (Figure 3A). The extrapolated lag time

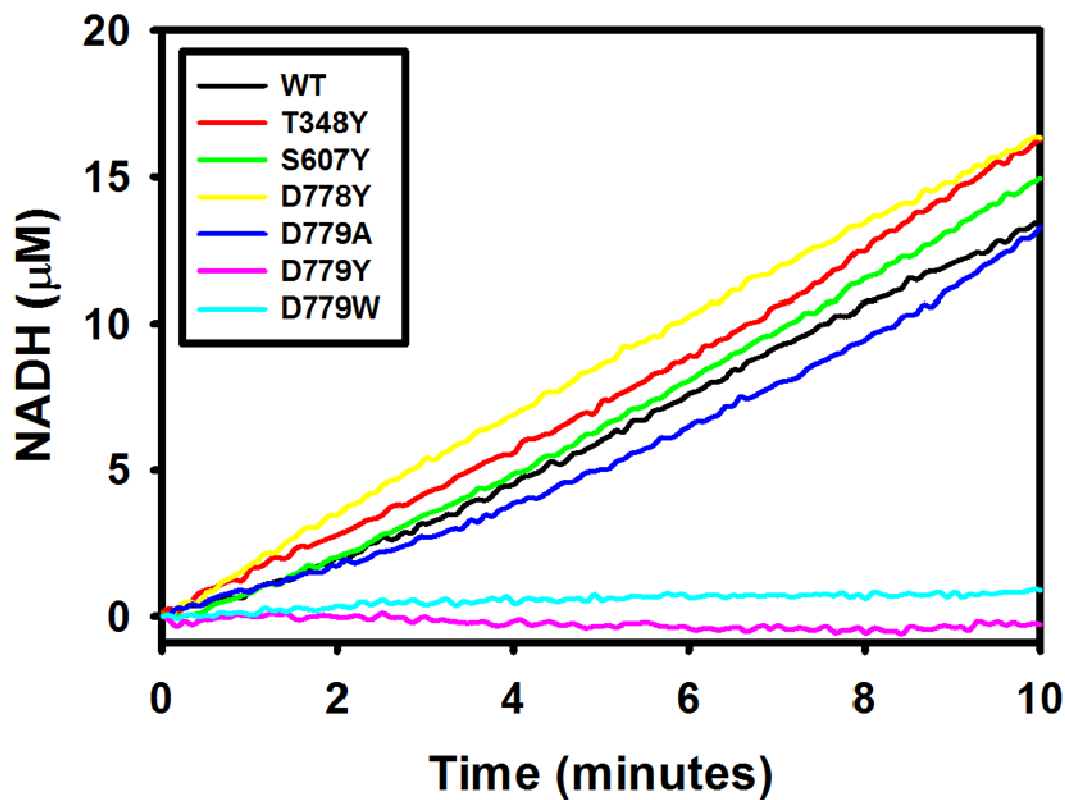


**Figure 2.** Channeling assays of wild-type, T348Y, S607Y, D778Y, D779A, D779Y, and D779W. NADH formation was monitored at 340 nm for 10 minutes. Assays performed using 40 mM proline, 100  $\mu\text{M}$  ubiquinone ( $\text{CoQ}_1$ ), 200  $\mu\text{M}$   $\text{NAD}^+$ , 50 mM potassium phosphate, 25 mM  $\text{NaCl}$ , 10 mM  $\text{MgCl}_2$ , pH 7.5

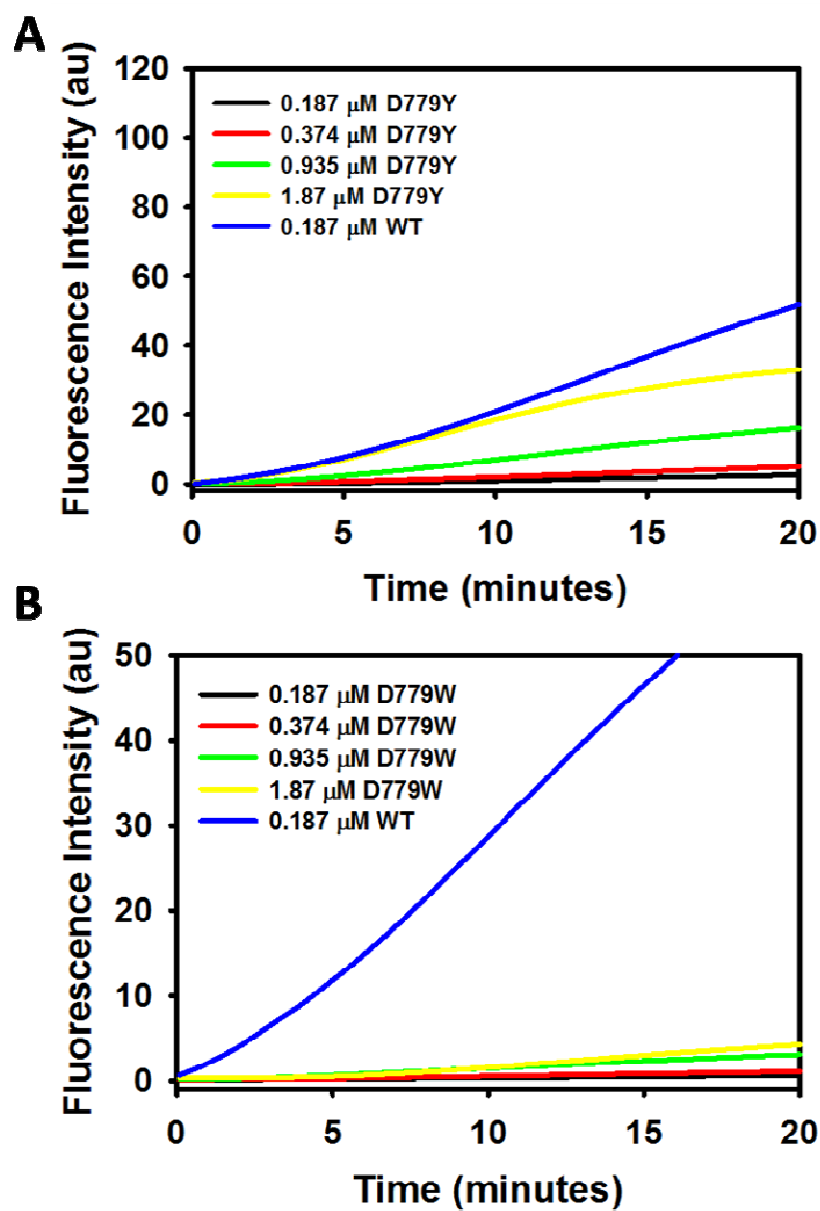


**Figure 3.** Channeling assays with increasing concentrations of D779Y (A) and D779W (B). NADH formation was monitored using fluorescence by exciting at 340 nm and recording the emission at 460 nm. In both plots 0.187  $\mu\text{M}$  of wild-type enzyme was used as a control, and four different concentrations of mutant were assayed (0.187-1.87  $\mu\text{M}$ ) to verify NADH formation. D779Y and D779W both significantly decrease NADH formation rates, with the bulkier mutation having a greater impact.

in NADH formation was 2.7 min for both wild-type and D779Y. In contrast to D779Y, NADH was essentially undetectable using a 10-fold higher concentration of the D779W mutant (Figure 3B). Thus, it appears that the D779W mutant is severely impaired.

If the channel was blocked in the D779Y and D779W mutants, P5C would be expected to exit from the PRODH active site and build up in the bulk solvent. With P5C concentration increasing in the bulk solvent over the time course of the reaction, P5C would eventually bind to the P5CDH domain leading to NADH formation. This scenario would reflect a non-channeling mechanism and would be characterized by a noticeable lag phase in NADH formation. The significantly lower NADH formation observed with D779Y and almost nonexistent NADH formation with D779W indicates that either PRODH or P5CDH activity is significantly decreased or that P5C is unable to access the P5CDH domain. To explore these possibilities, the kinetic parameters of the individual PRODH and P5CDH domains were determined for the mutants. The mutants that channeled similar to wild-type, especially D779A and T348Y, were used as channeling controls throughout the rest of this work.

### **PRODH and P5CDH Kinetic Properties of BjPutA Mutants**

The steady-state kinetic parameters of the PRODH domain were determined with proline and CoQ<sub>1</sub> as substrates (Table 2).  $K_m$  and  $k_{cat}$  values for proline (43 mM, 3.1 s<sup>-1</sup>) and CoQ<sub>1</sub> (105 μM, 2.9 s<sup>-1</sup>) were determined for wild-type BjPutA. Similar values (within two-fold) were determined for all of the mutants except D778Y. D778Y exhibited comparable  $K_m$  values for proline (91 mM) and CoQ<sub>1</sub> (82 μM), but  $k_{cat}$  was

Parameters	Proline <sup>a</sup>		Ublq	
	$k_{\text{cat}}$ (s <sup>-1</sup> )	$k_{\text{cat}}/K_m$ (M <sup>-1</sup> s <sup>-1</sup> )		$K_m$ (μM)
	3.1 ± 0.10	72 ± 8.6	105 ± 6	2.
	1.8 ± 0.01	60 ± 4.0	59 ± 2	1.
	1.6 ± 0.07	35 ± 4.8	131 ± 16	2.
	0.36 ± 0.07	4 ± 1.8	82 ± 15	0.3
	1.8 ± 0.08	32 ± 4.2	188 ± 22	2.
	2.7 ± 0.04	63 ± 3.1	56 ± 2	3.
	1.9 ± 0.06	63 ± 8.6	109 ± 12	2.

<sup>a</sup> 1 CoQ1, 0.5 μM enzyme, 50 mM potassium phosphate, pH 7.5  
<sup>b</sup> 1 M CoQ1, 0.5 μM enzyme, 50 mM potassium phosphate, pH 7.5

nearly 9-fold lower than wild-type BjPutA. This result was unexpected as shown in Figure 2 channeling assays, where D778Y exhibited a NADH formation rate that was higher than the other mutants and wild-type BjPutA. This indicates that even a 9-fold decrease in PRODH activity is not significant enough to impact the overall PRODH-P5CDH coupled reaction rate. In summary, the kinetic parameters of the D779Y and D779W mutants are similar to wild-type BjPutA and demonstrate that the lower channeling activity observed with these mutants is not caused by deficient PRODH activity.

Kinetic parameters were also determined for the P5CDH domain in all of the mutants. A  $K_m$  value of 0.42 mM GSA was determined for wild-type BjPutA (Table 3). All six mutants exhibited a similar  $K_m$  for GSA. The  $k_{\text{cat}}$  values for wild-type BjPutA and mutants T348Y, S607Y, D778Y, and D779A were similar and ranged from 3.4 – 5 s<sup>-1</sup>.

Conversely, mutants D779Y and D779W had significantly lower  $k_{\text{cat}}$  values of  $0.02 \text{ s}^{-1}$  and  $0.003 \text{ s}^{-1}$ , respectively. These turnover rates are about 200-1000 fold slower than wild-type BjPutA. The significantly lower P5CDH activity may be caused by disrupted folding of the P5CDH domain or hindered passage of P5C to the P5CDH domain.

To explore the first possibility,  $\text{NAD}^+$  binding to BjPutA was confirmed by determining the dissociation constant ( $K_d$ ) of the  $\text{NAD}^+$ -BjPutA complex using intrinsic tryptophan fluorescence. Dissociation constants of all six mutants (0.8-1.6  $\mu\text{M}$ ) were comparable to wild-type (0.6  $\mu\text{M}$ ). A  $K_d$  of 1.5  $\mu\text{M}$   $\text{NAD}^+$  was also determined for wild-type BjPutA by isothermal titration calorimetry, further validating the tryptophan fluorescence results (Figure 4). These results imply that the P5CDH domain is

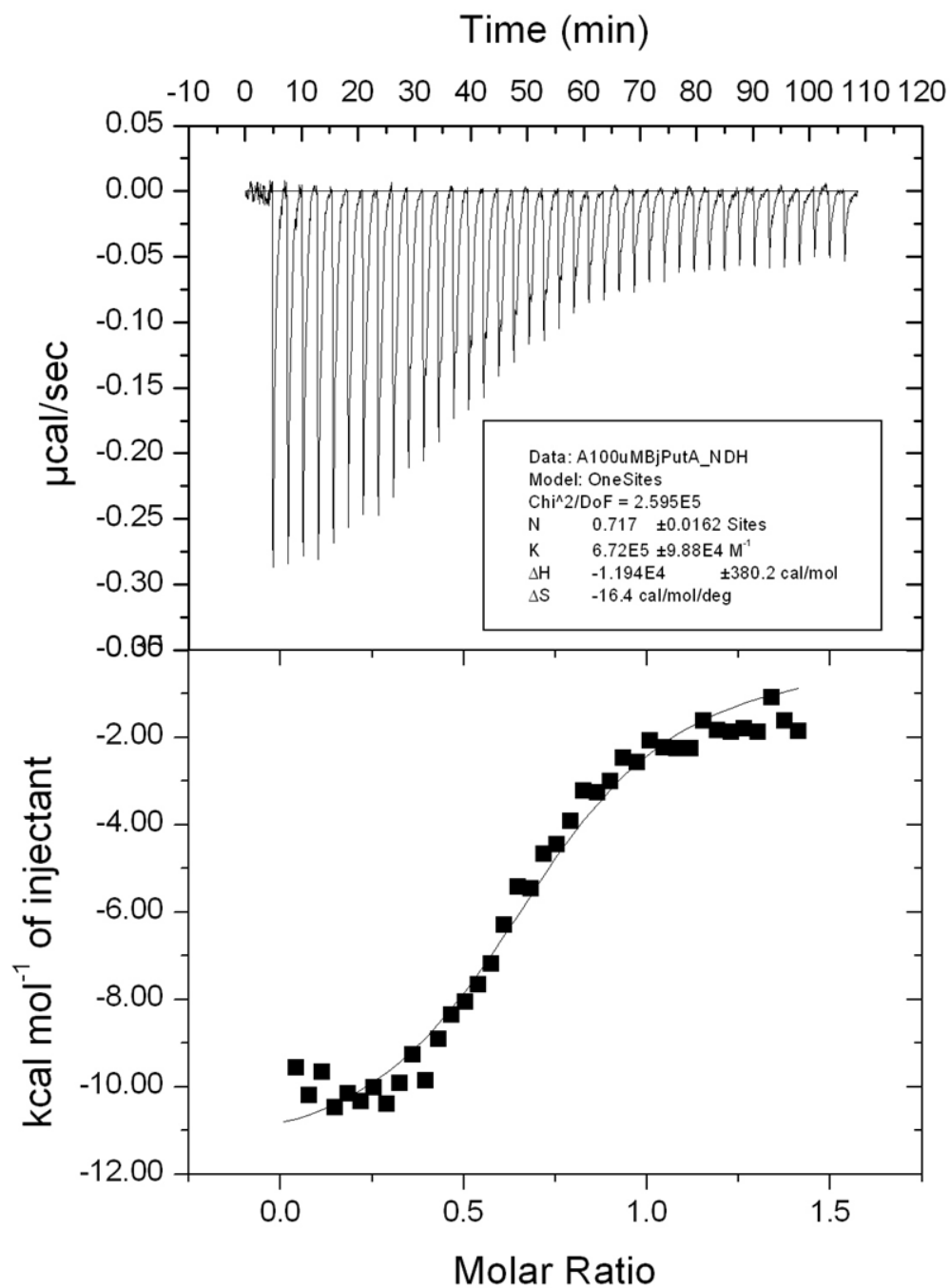


**Figure 4.** Wild-type BjPutA disassociation constant of NAD<sup>+</sup>. 23.4  $\mu\text{M}$  of BjPutA was loaded into the sample cell, and 500  $\mu\text{M}$  NAD<sup>+</sup> was injected in 2  $\mu\text{l}$  volumes for a total of 40 injections.  $N = 0.72$ .  $K_d = 1.5$   $\mu\text{M}$ .

Table 3. P5CDH kinetic parameters

Enzyme	Glutamate- $\gamma$ -Semialdehyde (GSA)			NAD <sup>+</sup> <sup>b</sup>
	$K_m$ (mM)	$k_{cat}$ (s <sup>-1</sup> )	$k_{cat}/K_m$ (M <sup>-1</sup> s <sup>-1</sup> )	$K_d$ ( $\mu$ M)
WT	0.42 $\pm$ 0.04	3.4 $\pm$ .12	8095 $\pm$ 822	0.60 $\pm$ 0.04
T348Y	0.42 $\pm$ 0.04	4.2 $\pm$ 0.15	10000 $\pm$ 1017	0.75 $\pm$ 0.06
S607Y	0.48 $\pm$ 0.03	4.5 $\pm$ 0.15	9375 $\pm$ 664	1.00 $\pm$ 0.04
D778Y	0.38 $\pm$ 0.02	3.8 $\pm$ 0.08	10000 $\pm$ 567	0.67 $\pm$ 0.04
D779A	0.38 $\pm$ 0.03	5.0 $\pm$ 0.14	13157 $\pm$ 1102	0.64 $\pm$ 0.05
D779Y	0.20 $\pm$ 0.03	0.02 $\pm$ 0.001	100 $\pm$ 15.8	0.65 $\pm$ 0.04
D779W	0.35 $\pm$ 0.15	0.003 $\pm$ 0.0005	8.6 $\pm$ 4.0	0.78 $\pm$ 0.05

<sup>a</sup>0.01-6 mM P5C, 0.2 mM NAD<sup>+</sup>, 600 mM NaCl, 0.25  $\mu$ M enzyme, 50 mM potassium phosphate, pH 7.5

<sup>b</sup>0.1-25  $\mu$ M NAD<sup>+</sup>, 0.25  $\mu$ M enzyme, 50 mM potassium phosphate, pH 7.5

folded properly in all of the mutants. Thus, it appears that the severe decrease in P5CDH activity in D779Y and D779W is caused by structural effects in the channel that may impede P5C movement.

### Single Turnover Rapid-reaction Kinetics

From the above analysis, it appears that in the D779Y and D779W mutants, both catalytic domains are folded properly but P5C is prevented from entering the P5CDH domain. To test whether a single molecule of P5C could efficiently traverse the channel in the D779Y mutant, a single turnover experiment was performed anaerobically without

an electron acceptor for the flavin cofactor. In this experiment, enzyme and  $\text{NAD}^+$  are rapidly mixed with proline and the absorbance spectrum from 700-300 nm is recorded (Figure 5). From the spectra, NADH formation (340 nm) and flavin reduction (451 nm) can be extracted and plotted as a function of time. Observed rate constants were estimated by single exponential fits of both reductions and are reported in Table 4. The observed rate constants for flavin reduction of wild-type and T348Y were 0.178 and 0.147  $\text{s}^{-1}$ , while D779Y was about 3-fold faster at 0.456  $\text{s}^{-1}$ . The rate of NADH formation was similar between wild-type BjPutA and T348Y but was 10-fold slower (0.003  $\text{s}^{-1}$ ) in D779Y.

Table 4. Single turnover observed rate constants for BjPutA enzymes

<b>BjPutA Enzyme</b>	<b>FAD Reduction <math>k_{\text{obs}}</math> (<math>\text{s}^{-1}</math>)</b>	<b>NADH Formation <math>k_{\text{obs}}</math> (<math>\text{s}^{-1}</math>)</b>	<b>Lag Time (s)</b>
Wild-type	0.178	0.033	1
T348Y	0.147	0.035	1.5
D779Y	0.456	0.003	11

The  $k_{\text{obs}}$  values for flavin and  $\text{NAD}^+$  reduction for wild-type BjPutA and T348Y are similar to that reported previously for BjPutA using the same assay conditions (0.20<sup>-1</sup> and 0.025  $\text{s}^{-1}$ , respectively) (10). Additionally, Figure 5A and 5B show spectral traces for wild-type and T348Y, where there is a 1 and 1.5 sec lag in NADH formation, respectively. For D779Y shown in Figure 5C, the estimated lag time for NADH formation is about 11 sec. The longer delay and slower rate of NADH formation in D779Y is consistent with D779 being located at a point along the channel that is

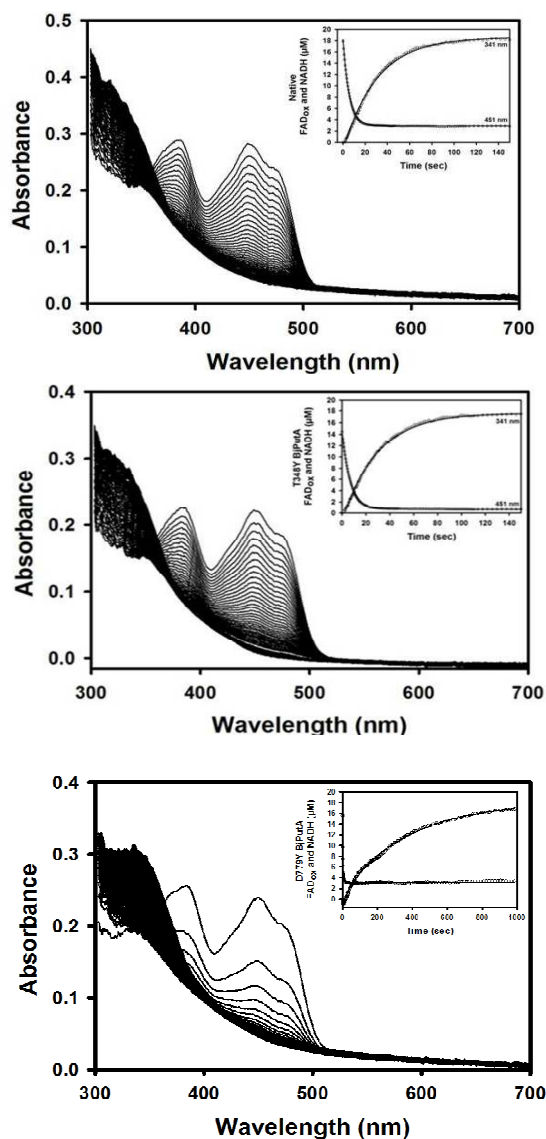


**Figure 5.** Single turnover rapid-reaction kinetic data for wild-type (A), T348Y (B), and D779Y (C). PutA (21.3  $\mu\text{M}$  wild-type, 17.8  $\mu\text{M}$  T348Y, 17.9  $\mu\text{M}$  D779Y) and 100  $\mu\text{M}$   $\text{NAD}^+$  were rapidly mixed with 40 mM proline (all concentrations reported as final) and monitored by stopped-flow multi-wavelength absorption (300-700 nm). Insets showing FAD (451 nm) and  $\text{NAD}^+$  (340 nm) reduction versus time were each fit to a single exponential equation to obtain the observed rate constant ( $k_{\text{obs}}$ ) of the respective reduction. Note the inset in (C) is on a different time scale.

narrower and thereby sensitive to large residue substitutions that potentially constrict the cavity and impair channeling activity.

### **Alternative P5CDH Substrates**

To further explore the narrowing of the cavity, smaller aldehyde substrates were assayed for their ability to navigate the channel. Table 5 compares the kinetic parameters of native substrate GSA (exogenous L-P5C), and smaller substrates succinate semialdehyde and propionaldehyde. Succinate semialdehyde contains one less carbon and no amino group, whereas propionaldehyde is a three carbon aldehyde. Table 5 compares the  $k_{\text{cat}}/K_m$  values of each substrate for wild-type, D779A, and channeling mutants D779Y and D779W. To determine whether smaller substrates enter the P5CDH domain more efficiently, the ratio of the  $k_{\text{cat}}/K_m$  of wild-type to the  $k_{\text{cat}}/K_m$  of each mutant was determined and is reported in Table 5. Using GSA, succinate semialdehyde, and propionaldehyde as substrates, D779A consistently reports a ratio close to one, indicating all three substrates were channeled similarly to wild-type. D779Y and D779W had  $k_{\text{cat}}/K_m$  values for GSA that were 81 and 941 fold lower than wild-type. However, when using succinate semialdehyde, these ratios improved to 30 for D779Y and 38 for D779W. If succinate semialdehyde was impaired to the same extent as the normal substrate, a 200-fold decrease in  $k_{\text{cat}}/K_m$  would be expected. Instead, the  $k_{\text{cat}}/K_m$  values only decreased by 70 and 8-fold for D779Y and D779W, respectively. Because the reaction mechanism is anticipated to be similar with succinate semialdehyde in all of the BjPutA enzymes, the 40-fold difference between wild-type BjPutA and D779Y/W indicates movement of

succinate semialdehyde in the channel is impaired, but to a much lesser extent than GSA/P5C. Propionaldehyde was shown to be an even poorer substrate for wild-type BjPutA with a  $k_{\text{cat}}/K_m$  of  $6.2 \text{ M}^{-1}\text{s}^{-1}$ . The ratio of  $k_{\text{cat}}/K_m$  for D779Y and D779W were 34 and 115, respectively. Although still an improvement over GSA, they were not improved relative to succinate semialdehyde. It should also be noted that propionaldehyde

Table 5. Alternative substrate kinetic comparisons

	Glutamic Semialdehyde		Succinate Semialdehyde		Propionaldehyde	
Enzyme	$k_{\text{cat}}/K_m$ $\text{M}^{-1}\text{s}^{-1}$	$k_{\text{cat}}/K_m$ Ratio WT:MT	$k_{\text{cat}}/K_m$ $\text{M}^{-1}\text{s}^{-1}$	$k_{\text{cat}}/K_m$ Ratio WT:MT	$k_{\text{cat}}/K_m$ $\text{M}^{-1}\text{s}^{-1}$	$k_{\text{cat}}/K_m$ Ratio WT:MT
WT	8095	--	42.2	--	6.2	--
D779A	13157	0.62	42.1	1	4.6	1.3
D779Y	100	81	1.4	30	0.18	34
D779W	8.6	941	1.1	38	0.054	115

All assays contained  $0.2 \text{ mM NAD}^+$ ,  $50 \text{ mM potassium phosphate}$ ,  $25 \text{ mM NaCl}$ ,  $\text{pH } 7.5$

inhibited all four enzymes in a similar fashion ( $K_I$  values between  $123$  and  $234 \text{ mM}$ ), suggesting D779Y and D779W are interrupting the channel and not disrupting the active site. Taken together, these results indicate that, while smaller substrates do not retain

activity of wild-type, there are marked improvements in the ability to reach the second active site, especially in the larger mutant D779W.

## **DISCUSSION**

Six mutations were made at three different points along the putative substrate channel of BjPutA. Of the six mutations made, only D779Y and D779W appear to disrupt P5CDH activity. Further kinetic results show that the PRODH and P5CDH domains are folded properly, which is also confirmed by X-ray crystal structures of both mutants (Tanner, personal communication). Finally, using smaller P5CDH domain substrates appears to increase the efficiency of the P5CDH active site relative to wild-type, especially for the more bulky D779W mutation. The results of this study verify that the cavity connecting the two active sites is used to shuttle P5C from the PRODH site to the P5CDH site, and that blockage of the channel decreases P5CDH activity.

Three separate mutations were made at D779 that provide details about the channel. First, mutating the aspartic acid to tyrosine dramatically decreases the catalytic efficiency of GSA by over 80-fold. Adding more bulk in the form of a tryptophan decreases the catalytic efficiency by over 940-fold, suggesting that larger residues at this position have a great effect on channeling P5C/GSA. Conversely, the alanine mutant at the same position displays similar kinetics at both active sites and channels similarly to wild-type. Additionally, results with D779A show that loss of the carboxyl group did not impact channeling, indicating charge at this location is not critical.

It is interesting to note that the position of the mutation along the channel is very important for channel disruption. D778Y is adjacent to D779Y/W and crystal structures

show it slightly orients into the cavity, though not enough to constrict the channel. Consistent with the structural predictions, the D778 mutant channels similarly, if not slightly better than wild-type. Additionally T348 and S607 appear to point into bottleneck regions of the channel, but the tyrosine mutations do not affect activity at either active site or the overall channeling reaction. In terms of T348Y and S607Y, we cannot rule out that hydrogen bonding occurs between the tyrosine and either the backbone or side chains of other local residues. Such an event would flatten the tyrosine against the sidewall of the cavity rather than pointing into the channel and possibly causing an obstruction.

One outstanding question that is answered in this study is how P5C/GSA accesses the P5CDH active site. Previously it was unknown whether P5C/GSA exclusively used the channel to enter the second catalytic site or whether it could enter directly from bulk solvent. Experiments using D779Y and D779W with both exogenously added and endogenously produced P5C showed decreased P5CDH activity. In channeling assays using proline as a substrate, both D779Y and D779W showed very little NADH formation (Figure 2). Likewise, using exogenous L-P5C to determine kinetic parameters for the P5CDH domain revealed significantly lower  $k_{\text{cat}}/K_m$  values, predominantly due to the large decreases in  $k_{\text{cat}}$ . If P5C/GSA were able to enter the P5CDH active site from a location other than the channel, the kinetic results would not have deviated from wild-type, especially when using exogenous P5C. It should be noted that both D779 mutants bind  $\text{NAD}^+$  similarly to wild-type and crystal structures show no global disruptions in protein folding (Dr. John Tanner, personal communication). Thus, the mutations did not structurally change or perturb a P5C entry/exit point that may have been near the P5CDH

domain. Ultimately these results indicate that P5C must access the P5CDH domain using the channel. It also suggests that if exogenous P5C is able to enter the cavity from a site other than through the PRODH domain, it must do so upstream of the D779 residue.

A second elusive question in the PutA field is where and how hydrolysis of P5C takes place. It has been proposed that the large internal cavity is large enough to house several P5C and water molecules and may provide an environment for hydrolysis (9). Based on the alternative substrate work using D779Y and D779W, it is tempting to suggest that P5C-GSA equilibrium favors the cyclic P5C at the point of these mutations in the channel. While succinate semialdehyde is missing a carbon and an amino group, perhaps the channeling improvement is due more to the linearity of the substrate rather than the shorter length. The larger D779W mutant shows nearly a 25-fold improvement when comparing the wild-type: mutant  $k_{\text{cat}}/K_{\text{m}}$  ratios for GSA and succinate semialdehyde. This may suggest the ringed structure is more sterically hindered than the linear substrate, which is able to navigate the obstruction more efficiently. Based on the structure, D779 is located within the first third of the channel, leaving plenty of room for a hydrolysis reaction to occur downstream.

Making mutations along substrate channels is not new; other studies have reported similar experiments to validate or expand understanding of substrate channeling. Recently, two mutations were made along a surface crevice connecting two active sites in the *Arabidopsis* bifunctional enzyme dethiobiotin synthetase (DTBS)-diaminopelargonic acid aminotransferase (DAPAT-AT) (17). The crevice is thought to channel the intermediate from DAPA-AT to DTBS. Mutants S360Y and I793W were made to

obstruct the external crevice, and progress curves were monitored. The results showed the mutations caused a lag time of 10-12 minutes, whereas wild-type experienced no such lag, suggesting channeling of the intermediate was disrupted. Channel obstructions ( $\beta$ C170F,  $\beta$ C170W) have also been made in tryptophan synthase, causing the rate of intermediate channeling to slow 10-fold in the phenylalanine mutant and over 1000-fold in the tryptophan mutant (34). Steady-state and transient kinetic results indicated the  $\beta$ C170W not only hindered passage of intermediate between active sites, but also affected crosstalk between subunits (34). In both examples substrate channeling was disrupted by placing bulky mutations along the channel, which provides precedence and validation for the research reported here.

Finally, the structures presented here show a snapshot of a cavity connecting two active sites, but it is necessary to think about the channel as being dynamic. It is well known that PutA undergoes a conformational change upon flavin reduction, and it has been proposed that a conserved ion pair (R456-E197) acts as a gate between the PRODH domain and the main cavity (10, 35). These two examples illustrate how the overall enzyme fluctuates, and it is reasonable that the topography of the channel changes as well. Future structural studies of the enzyme at different points of catalysis may show how the channel changes and could help further describe how P5C moves between active sites.

## REFERENCES

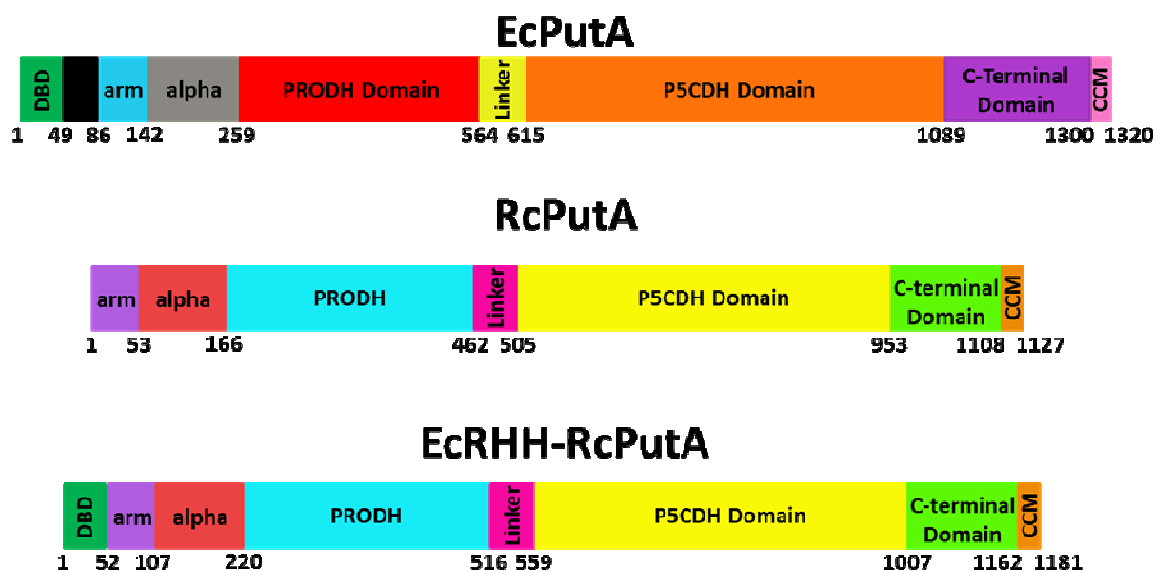
1. Nakajima, K., Inatsu, S., Mizote, T., Nagata, Y., Aoyama, K., Fukuda, Y., and Nagata, K. (2008) Possible involvement of put A gene in *Helicobacter pylori* colonization in the stomach and motility, *Biomed Res* 29, 9-18.
2. Krishnan, N., Doster, A. R., Duhamel, G. E., and Becker, D. F. (2008) Characterization of a *Helicobacter hepaticus* putA mutant strain in host colonization and oxidative stress, *Infect Immun* 76, 3037-3044.
3. van Weelden, S. W., Fast, B., Vogt, A., van der Meer, P., Saas, J., van Hellemond, J. J., Tielens, A. G., and Boshart, M. (2003) Procyclic *Trypanosoma brucei* do not use Krebs cycle activity for energy generation, *J Biol Chem* 278, 12854-12863.
4. Bringaud, F., Riviere, L., and Coustou, V. (2006) Energy metabolism of trypanosomatids: adaptation to available carbon sources, *Mol Biochem Parasitol* 149, 1-9.
5. Crawford, J. M., Kontnik, R., and Clardy, J. (2010) Regulating alternative lifestyles in entomopathogenic bacteria, *Curr Biol* 20, 69-74.
6. Willis, A., Bender, H. U., Steel, G., and Valle, D. (2008) PRODH variants and risk for schizophrenia, *Amino Acids* 35, 673-679.
7. Chakravarti, A. (2002) A compelling genetic hypothesis for a complex disease: PRODH2/DGCR6 variation leads to schizophrenia susceptibility, *Proc Natl Acad Sci U S A* 99, 4755-4756.
8. Phang, J. M., Donald, S. P., Pandhare, J., and Liu, Y. (2008) The metabolism of proline, a stress substrate, modulates carcinogenic pathways, *Amino Acids* 35, 681-690.
9. Tanner, J. J., and Becker, D. F. (2013) PutA and proline metabolism, In *Handbook of Flavoproteins* (Hille, R., Miller, S. M., and Palfey, B., Eds.), pp 31-56, Walter de Gruyter, Boston.
10. Srivastava, D., Schuermann, J. P., White, T. A., Krishnan, N., Sanyal, N., Hura, G. L., Tan, A., Henzl, M. T., Becker, D. F., and Tanner, J. J. (2010) Crystal structure of the bifunctional proline utilization A flavoenzyme from *Bradyrhizobium japonicum*, *Proc Natl Acad Sci U S A* 107, 2878-2883.
11. Ovadi, J. (1991) Physiological significance of metabolic channelling, *Journal of theoretical biology* 152, 1-22.
12. Anderson, K. S. (1999) Fundamental mechanisms of substrate channeling, *Methods Enzymol* 308, 111-145.
13. Huang, X., Holden, H. M., and Raushel, F. M. (2001) Channeling of substrates and intermediates in enzyme-catalyzed reactions, *Annu Rev Biochem* 70, 149-180.
14. Hyde, C. C., Ahmed, S. A., Padlan, E. A., Miles, E. W., and Davies, D. R. (1988) Three-dimensional structure of the tryptophan synthase alpha 2 beta 2 multienzyme complex from *Salmonella typhimurium*, *J Biol Chem* 263, 17857-17871.
15. Knighton, D. R., Kan, C. C., Howland, E., Janson, C. A., Hostomska, Z., Welsh, K. M., and Matthews, D. A. (1994) Structure of and kinetic channelling in

- bifunctional dihydrofolate reductase-thymidylate synthase, *Nat Struct Biol* 1, 186-194.
16. Stroud, R. M. (1994) An electrostatic highway, *Nat Struct Biol* 1, 131-134.
  17. Cobessi, D., Dumas, R., Pautre, V., Meinguet, C., Ferrer, J. L., and Alban, C. (2012) Biochemical and structural characterization of the Arabidopsis bifunctional enzyme dethiobiotin synthetase-diaminopelargonic acid aminotransferase: evidence for substrate channeling in biotin synthesis, *The Plant cell* 24, 1608-1625.
  18. Perham, R. N. (2000) Swinging arms and swinging domains in multifunctional enzymes: catalytic machines for multistep reactions, *Annu Rev Biochem* 69, 961-1004.
  19. Easterby, J. S. (1981) A generalized theory of the transition time for sequential enzyme reactions, *Biochem J* 199, 155-161.
  20. Rudolph, J., and Stubbe, J. (1995) Investigation of the mechanism of phosphoribosylamine transfer from glutamine phosphoribosylpyrophosphate amidotransferase to glycylamide ribonucleotide synthetase, *Biochemistry* 34, 2241-2250.
  21. Arentson, B. W., Sanyal, N., and Becker, D. F. (2012) Substrate channeling in proline metabolism, *Front Biosci (Landmark Ed)* 17, 375-388.
  22. Bearne, S. L., and Wolfenden, R. (1995) Glutamate gamma-semialdehyde as a natural transition state analogue inhibitor of Escherichia coli glucosamine-6-phosphate synthase, *Biochemistry* 34, 11515-11520.
  23. Bearne, S. L., Hekmat, O., and Macdonnell, J. E. (2001) Inhibition of Escherichia coli CTP synthase by glutamate gamma-semialdehyde and the role of the allosteric effector GTP in glutamine hydrolysis, *Biochem J* 356, 223-232.
  24. Thoden, J. B., Huang, X., Raushel, F. M., and Holden, H. M. (1999) The small subunit of carbamoyl phosphate synthetase: snapshots along the reaction pathway, *Biochemistry* 38, 16158-16166.
  25. Farrant, R. D., Walker, V., Mills, G. A., Mellor, J. M., and Langley, G. J. (2001) Pyridoxal phosphate de-activation by pyrroline-5-carboxylic acid. Increased risk of vitamin B6 deficiency and seizures in hyperprolinemia type II, *J Biol Chem* 276, 15107-15116.
  26. Surber, M. W., and Maloy, S. (1998) The PutA protein of Salmonella typhimurium catalyzes the two steps of proline degradation via a leaky channel, *Arch Biochem Biophys* 354, 281-287.
  27. Krishnan, N., and Becker, D. F. (2005) Characterization of a bifunctional PutA homologue from Bradyrhizobium japonicum and identification of an active site residue that modulates proline reduction of the flavin adenine dinucleotide cofactor, *Biochemistry* 44, 9130-9139.
  28. Moxley, M. A., Tanner, J. J., and Becker, D. F. (2011) Steady-state kinetic mechanism of the proline:ubiquinone oxidoreductase activity of proline utilization A (PutA) from Escherichia coli, *Arch Biochem Biophys* 516, 113-120.
  29. Williams, I., and Frank, L. (1975) Improved chemical synthesis and enzymatic assay of delta-1-pyrroline-5-carboxylic acid, *Analytical biochemistry* 64, 85-97.

30. Moxley, M. A., and Becker, D. F. (2012) Rapid reaction kinetics of proline dehydrogenase in the multifunctional proline utilization A protein, *Biochemistry* 51, 511-520.
31. Patil, P. V., and Ballou, D. P. (2000) The use of protocatechuate dioxygenase for maintaining anaerobic conditions in biochemical experiments, *Anal Biochem* 286, 187-192.
32. Chovancova, E., Pavelka, A., Benes, P., Strnad, O., Brezovsky, J., Kozlikova, B., Gora, A., Sustr, V., Klvana, M., Medek, P., Biedermannova, L., Sochor, J., and Damborsky, J. (2012) CAVER 3.0: a tool for the analysis of transport pathways in dynamic protein structures, *PLoS Comput Biol* 8, e1002708.
33. Schrodinger, LLC. (2010) The PyMOL Molecular Graphics System, Version 1.3r1.
34. Anderson, K. S., Kim, A. Y., Quillen, J. M., Sayers, E., Yang, X. J., and Miles, E. W. (1995) Kinetic characterization of channel impaired mutants of tryptophan synthase, *J Biol Chem* 270, 29936-29944.
35. Brown, E. D., and Wood, J. M. (1993) Conformational change and membrane association of the PutA protein are coincident with reduction of its FAD cofactor by proline, *J Biol Chem* 268, 8972-8979.

## CHAPTER 3

# Fusing the DNA-binding Domain of *Escherichia coli* Proline Utilization A (PutA) onto the Bifunctional PutA Enzyme from *Rhodobacter capsulatus* Nearly Mimics a Genuine Trifunctional PutA



Note: Results appearing in this chapter are being prepared for manuscript: Arentson, Benjamin W., Farmer, Erin, Zhu, Weidong, Tanner, John J., Becker, Donald F. “Fusing the DNA-binding Domain of *Escherichia coli* Proline Utilization A (PutA) onto the Bifunctional PutA Enzyme from *Rhodobacter capsulatus* Nearly Mimics a Genuine Trifunctional PutA” *manuscript in preparation*.

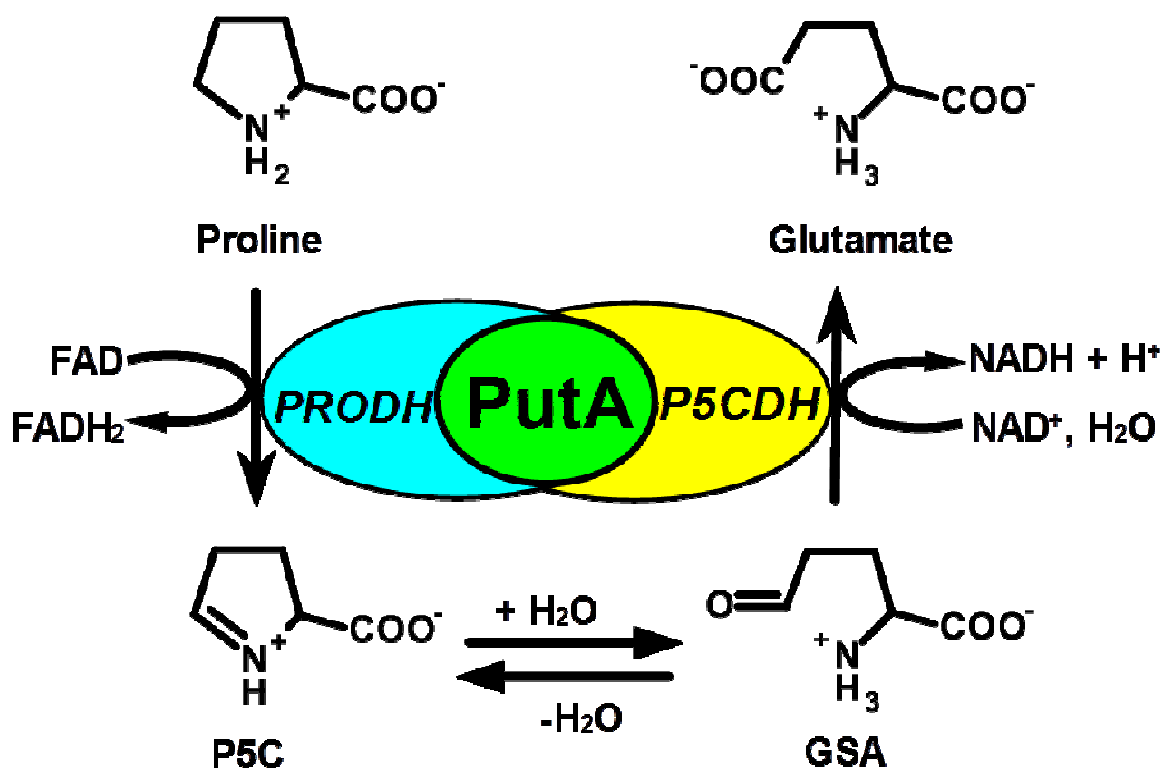
## ABSTRACT

Proline utilization A (PutA) is a bifunctional flavoenzyme with proline dehydrogenase (PRODH) and  $\Delta^1$ -pyrroline-5-carboxylate dehydrogenase domains that catalyze the two-step oxidation of proline to glutamate. A subset of PutA proteins also have an N-terminal ribbon-helix-helix (RHH) DNA-binding domain and are considered trifunctional, such as PutA from *Escherichia coli* (EcPutA). EcPutA moonlights as an autogenous transcriptional repressor of the *put* regulon and switches to a membrane-bound enzyme in response to cellular nutritional needs and proline availability. In this work, we explored whether a trifunctional PutA could be engineered by fusing the RHH DNA-binding domain of EcPutA onto the bifunctional PutA enzyme from *Rhodobacter capsulatus* (RcPutA). The resulting EcRHH-RcPutA chimera was characterized along with RcPutA and compared to EcPutA. RcPutA is shown to purify as a monomer whereas EcRHH-RcPutA forms a stable dimer analogous to EcPutA. Despite unique quaternary structures, RcPutA and EcRHH-RcPutA have comparable steady-state kinetic parameters and show evidence of substrate channeling. *In vitro* assays show EcRHH-RcPutA binds *put* control DNA and exhibits significantly increased lipid binding in the presence of proline. These results are consistent with properties of EcPutA and mirror the mechanism of EcPutA functional switching which is driven by proline-dependent activation of membrane binding. EcRHH-RcPutA, however, is not observed to act as transcriptional repressor in cell-based reporter assays. Thus, although EcRHH-RcPutA displays characteristics of functional switching *in vitro*, it does not fully mimic the *in vivo* properties of EcPutA.

## INTRODUCTION

The proline metabolic pathway converts proline into glutamate via two consecutive steps catalyzed by proline dehydrogenase (PRODH) and  $\Delta^1$ -pyrroline-5-carboxylate (P5C) dehydrogenase (P5CDH) (Scheme 1). In the first reaction, PRODH forms the intermediate P5C through the flavin-dependent, two-electron oxidation of proline. P5C then undergoes a non-enzymatic hydrolysis step, forming glutamate- $\gamma$ -semialdehyde (GSA), which is oxidized to glutamate by NAD<sup>+</sup>-dependent P5CDH. The above central reactions of proline metabolism impact a broad array of physiological processes in different organisms (1-4) and have underlying roles in human diseases such as cancer (5, 6) and schizophrenia (7-9). Proline is also a critical respiratory substrate for *Helicobacter pylori* during infection (10, 11) and in the fungal pathogen, *Cryptococcus neoformans*, proline catabolism was recently shown to be required for virulence in mice (12).

PRODH and P5CDH are separate enzymes in eukaryotes and Gram-positive bacteria, whereas in Gram-negative bacteria the enzymes are encoded as a bifunctional polypeptide known as proline utilization A (PutA) (13, 14). In addition to catalytic activities, a subset of Gram-negative bacteria such as *Escherichia coli* and *Salmonella typhimurium* encode PutAs with a DNA-binding domain, which allows PutA to bind DNA and repress transcription of *putA* and *putP* (proline transporter) genes (15, 16). The DNA binding domain in these so-called trifunctional PutAs provides a unique coupling between proline availability and proline metabolic gene expression (15, 16).



**Scheme 1.** Reactions catalyzed by the bifunctional PutA enzyme. Proline dehydrogenase (PRODH) domain catalyzes the conversion of proline to  $\Delta^1$ -pyrroline-5-carboxylate (P5C) using a flavin cofactor as an electron acceptor. P5C undergoes a non-enzymatic hydrolysis, resulting in glutamate- $\gamma$ -semialdehyde (GSA). The P5C dehydrogenase domain (P5CDH) catalyzes the NAD<sup>+</sup>-dependent oxidation of GSA to glutamate thereby generating NADH

In *S. typhimurium* and *E. coli*, PutA switches from a DNA-bound transcriptional repressor to a membrane-bound enzyme based on intracellular proline levels and the redox state of the flavin cofactor (16-18). Proline reduction of the flavin cofactor significantly increases PutA membrane binding affinity while diminishing PutA-DNA binding affinity by only two-fold (18-22). The DNA-binding domain of trifunctional PutAs is located at the N-terminus and has been shown by X-ray crystallography to be a ribbon-helix-helix (RHH) fold (15, 23, 24), whereas the membrane-binding domain of PutA is not known. Recent studies of PutA from *E. coli* (EcPutA) have identified conformational changes in the flavin cofactor and active site residues of the PRODH domain that are critical for mediating redox activation of PutA membrane interactions. Additionally, proline-dependent conformational changes occur outside the PRODH domain, which correlate with increased PutA membrane binding (20). How conformational changes in PutA enhance membrane interactions remains unclear.

Phylogenetic analysis of PutA proteins divides PutAs into two main branches. Branch 1 is composed of trifunctional and bifunctional PutAs whereas Branch 2 is composed entirely of bifunctional PutAs (13, 14, 25). Trifunctional PutAs (Branch 1A) are generally 1300 residues in length, which in addition to the PRODH and P5CDH domains, contain a N-terminal DNA-binding domain and a C-terminal domain (CTD) of unknown function (13, 14, 25). The bifunctional enzymes of Branch 1 can be subdivided into short (~ 1000 residues) and long (~ 1200 residues) bifunctional PutAs (13, 14, 25). The best characterized short bifunctional PutA (Branch 1A) is from *Bradyrhizobium japonicum* (BjPutA), from which the first X-ray crystal structure of a full-length PutA was solved (26). The X-ray crystal structure of BjPutA showed a dimer/tetramer oligomeric state

and revealed a 40 Å cavity linking the PRODH and P5CDH domains (26). The cavity allows channeling of the P5C intermediate between the two enzyme active sites. Long bifunctional PutAs (Branch 1B) are more closely related to trifunctional PutAs in that they contain the CTD of unknown function (13).

The aim of this study was to examine whether appending the DNA-binding domain of EcPutA onto a long bifunctional PutA would generate a bona fide trifunctional PutA. For this purpose, we chose to fuse the RHH domain of EcPutA (NCBI RefSeq NP\_415534.1) onto the N-terminus of the long bifunctional PutA from *Rhodobacter capsulatus* (RcPutA) (NCBI RefSeq code YP\_003578784.1, 1127 amino acids) to create an EcRHH-RcPutA chimera. RcPutA and EcPutA are 47% identical (61% similar) between the regions of the arm domain and the CTD of unknown function (Figure 1), making RcPutA a suitable candidate for studying the effects of adding a N-terminal DNA-binding domain (27). X-ray crystal structures of the EcPutA RHH domain (residues 1-47) show it is a dimer that binds a 9-bp sequence, which is conserved in the *put* promoter regions of Gram-negative bacteria that encode trifunctional PutAs (15). Figure 1 summarizes the domain organization of EcPutA, RcPutA, and the resulting EcRHH-RcPutA chimera.

Here, we report the functional properties of RcPutA and the EcRHH-RcPutA chimera and analyze the quaternary structures of these enzymes by analytical ultracentrifugation. We show that RcPutA is a monomer and demonstrate that the RHH domain of EcPutA induces dimerization of EcRHH-RcPutA. These results provide novel insights into the diverse quaternary structures of PutAs. The RHH domain is also shown to promote functional switching of RcPutA, however, other factors appear necessary for EcRHH-RcPutA switching *in vivo*.

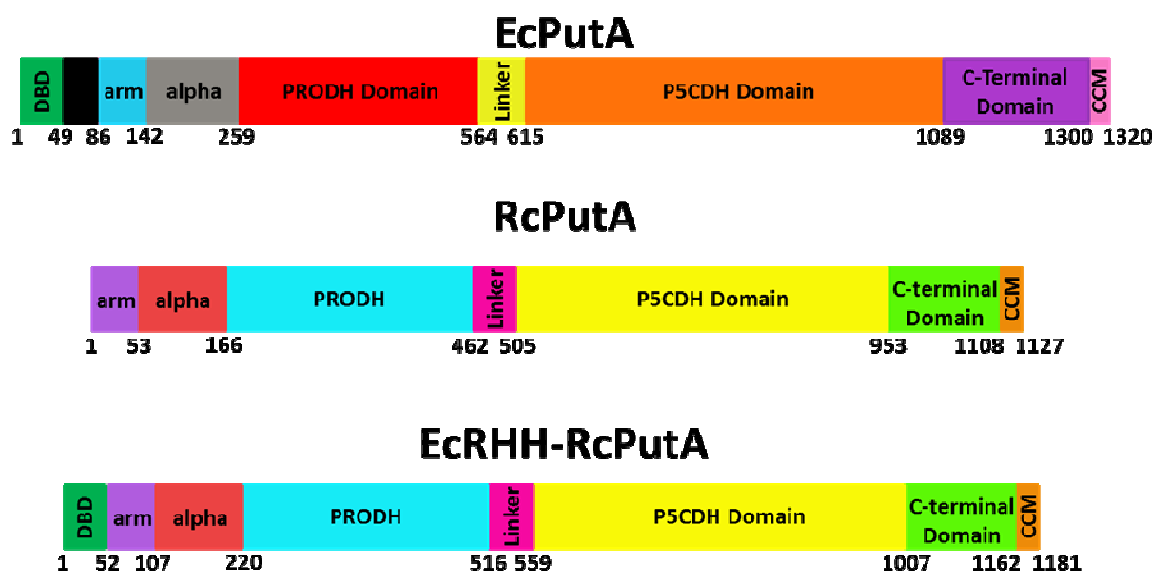


**Figure 1.** Domain organization maps of *E. coli* PutA, *R. capsulatus* PutA, and EcRHH-RcPutA. The DNA-binding domain (DBD) of *E. coli* PutA was fused immediately upstream of *R. capsulatus* PutA, resulting in the EcRHH-RcPutA enzyme. Numbers below the domain map indicate amino acid position. CCM, conserved C-terminal motif.

## MATERIALS AND METHODS

### Materials

Unless noted, all chemicals were purchased from Sigma-Aldrich or Fisher Scientific. Nanopure water was used in all experiments

### Expression Constructs and Protein Purification

The *putA* gene from *R. capsulatus* was PCR amplified and inserted into a pET28 vector (Novagen) using NdeI and XhoI restriction sites. The EcRHH-RcPutA enzyme was created by PCR amplification of the DNA-binding domain (residues 1-52) of EcPutA from a pET14b-EcPutA construct described previously (28). NdeI restriction sites were incorporated at both ends of the PCR product using primers 5'-CGGCGCCATATGATGACCGACCTTCCGCCCTTGG-3' and 5'-CGCCGCCATATGCTCCGGCAGAGTATCGCTGTTTTCC-3'. The PCR product was then ligated into the pET28a-RcPutA construct immediately upstream of RcPutA gene (NdeI and XhoI). The resulting pET28-EcRHH-RcPutA construct was confirmed by DNA sequencing (Eurofins MWG Operon).

EcPutA was overexpressed and purified as previously described (21, 29). RcPutA (1127 amino acids) and EcRHH-RcPutA (1180 amino acids), both in a pET28a vector, were overexpressed in BL21(DE3) pLysS cells (Promega). Starter cultures (5 ml) were grown overnight in LB medium (25 µg/ml kanamycin, 34 µg/ml chloramphenicol) and used to inoculate 4-L cultures of LB medium plus antibiotics. Once cultures reached

OD<sub>600</sub> of 0.8, 0.5 mM IPTG was added, and cultures were grown overnight at 20°C before harvesting by centrifugation and freezing the cell pellets at -80 °C.

The frozen cell pellets were resuspended in 50 ml binding buffer (20 mM Tris-base, 0.5 M NaCl, 5 mM imidazole, 10% glycerol, pH 7.9) at 4°C containing FAD (0.1 mM) and protease inhibitors  $\epsilon$ -amino-N-caproic acid (3 mM), phenylmethylsulfonyl fluoride (0.3 mM), leupeptin (1  $\mu$ M), tosyl phenylalanyl chloromethyl ketone (48  $\mu$ M), and tosyllysine chloromethyl ketone hydrochloride (78  $\mu$ M). Cells were disrupted by sonication at 4°C. The solubility of the proteins was optimized by adding 0.25 mM Triton X-100 to the cell lysate and incubating at 4°C with slow stirring for 30 min. The cell lysate was centrifuged for 1 h at 19,000 rpm in a JA-20 rotor (Beckman). The supernatant was filtered (0.2  $\mu$ m filter, VWR) and loaded onto a Ni<sup>2+</sup> affinity column (Superflow resin, Qiagen) equilibrated with Tris-base binding buffer (pH 7.9). Wash buffer (Tris base with 60 mM imidazole) followed by elution buffer (Tris base with 500 mM imidazole) were then applied to the column. Elution fractions containing PutA protein were then dialyzed overnight at 4°C into 50 mM Tris (pH 7.5) buffer containing 10 mM NaCl, 0.5 mM EDTA, and 10% glycerol. The protein was then loaded onto an anion exchange column (HiTrap Q HP column, GE Life Sciences) equilibrated with the Tris buffer above. A linear gradient of 0-1 M NaCl in Tris buffer (pH 7.5, 0.5 mM EDTA, 10% glycerol) was used to elute PutA. Purified RcPutA and EcRHH-RcPutA were then dialyzed into 50 mM Tris (pH 7.5) containing 50 mM NaCl, 0.5 mM EDTA, and 10 % glycerol and stored at -80°C. Protein purity was analysed by SDS-PAGE. Protein concentration was determined by the 660 nm Protein Assay (Thermo Scientific) using bovine serum albumin as the standard. The amount of bound flavin adenine

dinucleotide (FAD) cofactor in purified RcPutA and EcRHH-RcPutA were determined as previously described (17). The N-terminal hexahistidine tag was retained after purification.

### **PRODH Kinetic Assays**

All steady-state assays were performed at 23°C. Kinetic parameters for proline were determined using coenzyme Q<sub>1</sub> (CoQ<sub>1</sub>) as an electron acceptor and monitoring CoQ<sub>1</sub> reduction by the decrease in absorbance at 278 nm ( $\epsilon = 14,500 \text{ M}^{-1} \text{ cm}^{-1}$ ) (29).  $K_m$  and  $k_{cat}$  for proline were determined for RcPutA and EcRHH-RcPutA (0.25  $\mu\text{M}$ ) by varying proline (0-100 mM) and fixing CoQ<sub>1</sub> at 300  $\mu\text{M}$ . Likewise, the  $K_m$  and  $k_{cat}$  for CoQ<sub>1</sub> were determined by varying CoQ<sub>1</sub> (10-450  $\mu\text{M}$ ) while holding proline constant at 200 mM. The above assays were conducted in 50 mM potassium phosphate (pH 7.5) and 25 mM NaCl. Data was collected using a 0.15 cm pathlength on a Hi-Tech Scientific SF-61DX2 stopped-flow instrument. Kinetic parameters were determined by fitting initial velocities to the Michaelis-Menton equation (SigmaPlot 12.0).

### **DNA-binding**

The DNA-binding activity of the different proteins was determined by gel mobility shift assays using fluorescently labeled *put* control DNA as previously described (23). A dissociation constant of EcRHH-RcPutA with *put* control DNA was determined by best-fit analysis to eq 1 (Sigma Plot 12), where  $n$  is the number of binding sites and  $[L]$  is total concentration of protein (17).

$$\text{Fraction of DNA Bound} = n[L]/(Kd + [L]) \quad (1)$$

### **PRODH-P5CDH Coupled Assay**

PRODH-P5CDH coupled activity, in which proline is converted to glutamate, was measured for RcPutA and EcRHH-RcPutA as described previously (26). Briefly, 0.25  $\mu\text{M}$  enzyme was mixed with 200  $\mu\text{M}$  CoQ<sub>1</sub>, 40 mM proline, and 200  $\mu\text{M}$  NAD<sup>+</sup> in 50 mM potassium phosphate (pH 7.5) containing 25 mM NaCl. The progress of the reaction was followed by NAD<sup>+</sup> reduction at 340 nm ( $\epsilon = 6200 \text{ M}^{-1} \text{ cm}^{-1}$ ).

### **Oligomeric Structure Determination**

The oligomeric states of RcPutA and EcRHH-RcPutA were determined by gel filtration chromatography and sedimentation equilibrium. The purified proteins were loaded onto a Superdex 200 10/300 GL column (GE Life Sciences) and eluted by FPLC in 50 mM Tris buffer (pH 7.5) containing 100 mM NaCl, 0.5 mM EDTA, and 10% glycerol at a flow rate of 0.5 ml/min. The molecular weight of each protein was determined using thyroglobulin (669 kDa), apoferritin (443 kDa),  $\beta$ -amylase (200 kDa), bovine serum albumin (66 kDa), and carbonic anhydrase (29 kDa) as molecular weight standards.

Sedimentation equilibrium was performed using an Optima XL-I analytical ultracentrifuge (Beckman Coulter, Inc.) equipped with an eight-hole An50 Ti rotor. RcPutA (2 mg/ml) and EcRHH-RcPutA (2 mg/ml) were dialyzed in 50 mM Tris buffer (pH 7.5) containing 100 mM NaCl, 0.5 mM EDTA, and 5% glycerol. The dialyzed proteins were then diluted to 0.2, 0.5, and 0.8 mg/ml and loaded at 110  $\mu\text{l}$  each into the sample cells. The reference cell was loaded (125  $\mu\text{l}$ ) with the dialysate buffer. Radial scans with a spacing of 0.001 cm were collected at 280 nm at 22 and 24 h after

equilibration at 8000 rpm. The scans are an average of 10 measurements at each radial position. Origin 6.0 software was used to best-fit the data to a single ideal species model using a solvent density of 1.018 g/ml and a partial specific volume of 0.742 ml/g estimated from the RcPutA and EcRHH-RcPutA polypeptides by Sednterp software.

### **Membrane Interactions and Lipid Pull-down Assays**

Membrane interactions of RcPutA and EcRHH-RcPutA were tested *in vivo* using an *E. coli* BL21(DE3) strain that lacks PutA. A PutA deficient (*putA*<sup>-</sup>) *E. coli* strain of BL21(DE3) was generated by disrupting the *putA* gene with a kanamycin cassette (TargetTron Gene Knockout System, Sigma). The specific primers used were IBS 5'

AAAAAAGCTTATAATTATCCTTACGCCTCCCGCAGGTGCGCCCAGA

TAGGGTG 3', EBS1d

5'CAGATTGTACAAATGTGGTGATAACAGATAAGTCCCGCA

GCC TAACTTACCTTTCTTTGT 3' and EBS2

5'TGAACGCAAGTTTCTAATTTCGGTTA

GGCGTCGATAGAGGAAAGTGTCT. The kanamycin cassette was introduced after 355 bp of *putA* gene. Subsequent PCR analysis of the *putA* gene showed a band of 547 bp which contains 219 bp of the kanamycin cassette demonstrating the successful insertion of the kanamycin cassette into the *putA* gene. Western blot analysis of cell lysates using an antibodies generated against the RHH domain as previously described (30) confirmed the lack of *putA* gene expression. The resulting BL21(DE3) *putA*<sup>-</sup> Kan<sup>r</sup> was then used for testing functional membrane interactions of the different proteins. For these experiments, EcPutA, RcPutA and EcRHH-RcPutA were subcloned into a pET21a vector (Novagen)

by introducing NdeI and XhoI sites at the N-terminus and C-terminus, respectively, by PCR. The following primers were used: EcPutA, (Fwd) 5' CGGCGCCATATGGGAACCACCACCATGG-3' and (Rev) 5' CGGCGCCTCGAGTTAACCTATAGTCATTAAGC-3'; RcPutA, (Fwd) 5' CGGCGCCATATGACCGACCTTTCCGCCC-3', (Rev) 5'-CGGCGCCTCGAGTCACCCGGCCAGCAAAGCCGC-3'; and EcRHH-RcPutA, EcPutA Fwd and RcPutA Rev primers. A stop codon was placed upstream of the XhoI site so that the PutA proteins were expressed without a histidine tag. The resulting constructs EcPutA-pET21a, RcPutA-pET21a, and EcRHH-RcPutA-pET21a were confirmed by DNA sequencing (Eurofins MWG Operon). The PutA constructs and pET21a empty vector were transformed into BL21(DE3) *putA*<sup>-</sup> Kan<sup>r</sup>. Liquid cultures (5 ml) of cells containing the different constructs were grown in LB medium and cell lysates were made to test for PutA protein expression. SDS-PAGE of total protein showed equivalent expression levels of EcPutA, RcPutA, and EcRHH-RcPutA without (leaky expression) and with IPTG (250 μM). To test for functional membrane interactions, cultures were grown in LB medium to an OD<sub>600</sub> of 0.5 and streaked on minimal agar plates containing triphenyltetrazolium chloride (TTC) and proline (0.5%) or glycerol (0.5%). Agar plates were made by autoclaving 0.7% K<sub>2</sub>HPO<sub>4</sub>, 0.3% KH<sub>2</sub>PO<sub>4</sub>, 0.01% MgSO<sub>4</sub>, 0.2% protease peptone, 2.0% agar, then after cooling adding filter-sterilized 0.5% proline or 0.5% glycerol, 0.005% L-tryptophan, 0.0001% thiamine, and 0.0025% triphenyl tetrazolium chloride (all wt/vol %).

Lipid pull-down assays were performed anaerobically under a nitrogen atmosphere in a anaerobic chamber (Belle Technology Glovebox) as described previously using *E. coli*

polar lipids (Avanti Polar Lipids) (31). In these assays 50 mM proline was used to reduce the flavin cofactor in the PutA proteins (0.3 mg/ml) during the incubation with lipid vesicles.

### **Cell-based Functional Switching Assays**

EcPutA-pET21a, RcPutA-pET21a, and EcRHH-RcPutA-pET21a and pET21a empty vector were transformed into *E. coli* strain JT31 *putA-lacZ*-containing *putC:lacZ* (pUT03) as described previously (28, 31). Cells transformed with the various PutA constructs were grown at 37°C in M9 minimal medium containing 0.005% L-tryptophan, 0.05% thiamine, 50 µg/ml ampicillin, 34 µg/ml chloramphenicol, 25 µg/ml kanamycin, and 0, 0.1, and 15 mM proline. PutA expression was induced with 250 µM IPTG at OD<sub>600</sub> 0.2 and cells were grown until OD<sub>600</sub> 0.8-1. β-galactosidase activity is reported in Miller units (32) and was determined as previously described (31) except for the following minor changes. Cells (500 µl) were diluted two-fold to 1 ml in Z buffer and assays were run for 45 sec. Optical densities and absorbance readings were recorded using a Biotek Powerwave XS plate reader (200 µl assays). Results are reported as an average of four independent experiments.

## **RESULTS**

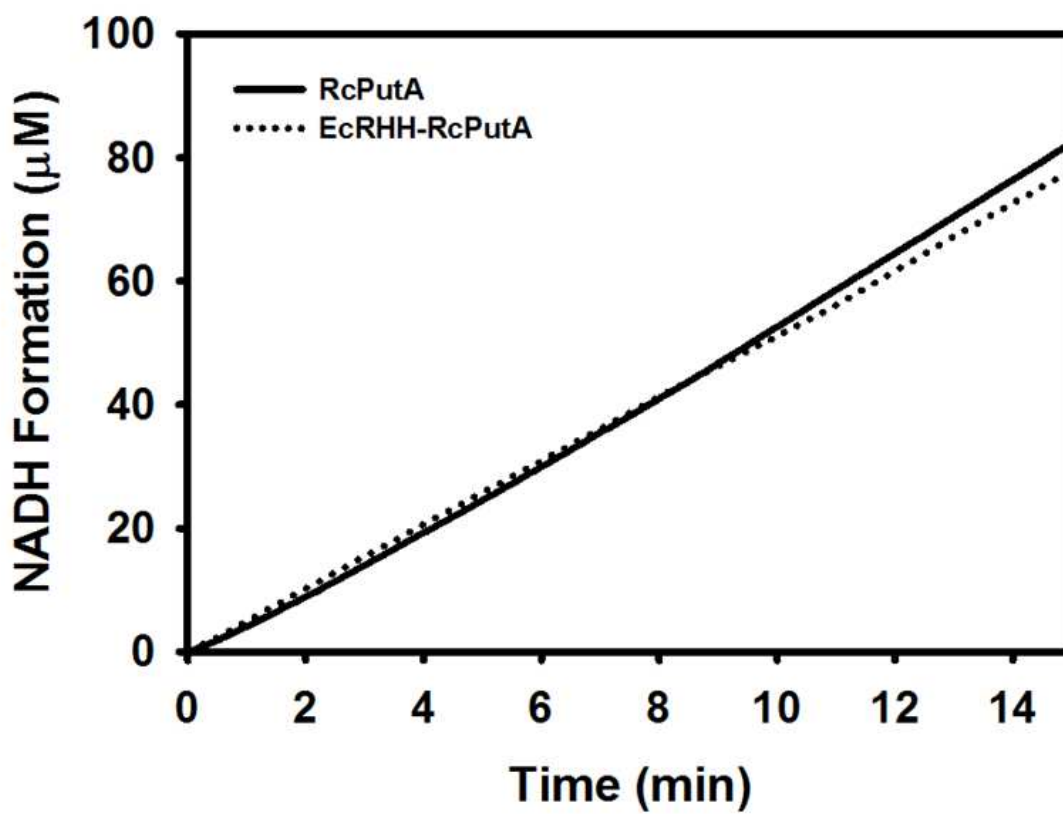
### **General Properties and Steady-state Kinetic Parameters**

RcPutA and EcRHH-RcPutA purified as soluble proteins with molecular sizes on SDS-PAGE consistent with the predicted molecular weights of 119,460 Da (RcPutA) and 125,529 Da (EcRHH-RcPutA). The UV-visible spectra of the RcPutA and EcRHH-

RcPutA were similar with maximum absorbance bands at 380 nm and 451 nm. Based on the flavin absorbance spectra, the flavin content is 97% and 92% for RcPutA and EcRHH-RcPutA, respectively.

The PRODH steady-state kinetic parameters for RcPutA and EcRHH-RcPutA were determined and are reported in Table 1. The  $K_m$  values for proline (5.6 mM) and CoQ<sub>1</sub> (93  $\mu$ M) in RcPutA are lower than that of EcPutA with the most significant difference observed in the  $K_m$  for proline. The  $k_{cat}$  for RcPutA is also significantly lower than EcPutA. However, the resulting  $k_{cat}/K_m$  values for RcPutA vary by only 2-3 fold from that of EcPutA. For EcRHH-RcPutA, the  $k_{cat}/K_m$  of 167.9 M<sup>-1</sup> s<sup>-1</sup> with proline was the same as RcPutA. When holding proline constant and varying CoQ<sub>1</sub>, a  $k_{cat}/K_m$  value of 6832 M<sup>-1</sup> s<sup>-1</sup> was determined which is about two-fold lower than RcPutA. Overall, the PRODH steady-state kinetic parameters are similar for RcPutA and EcRHH-RcPutA with both enzymes exhibiting a slower  $k_{cat}$  than that of EcPutA. Thus, it appears that fusing the EcRHH domain onto RcPutA does not significantly affect the PRODH kinetic parameters.

To further explore the kinetic properties of RcPutA and EcRHH-RcPutA, coupled PRODH-P5CDH assays were performed. These assays report on the activity of both the PRODH and P5CDH active sites by monitoring NADH formation, which is used as a read-out of the overall conversion of proline to glutamate. Figure 2 shows a PRODH-P5CDH coupled assay for RcPutA and EcRHH-RcPutA. The steady-state velocities of NADH formation are similar for RcPutA and EcRHH-RcPutA under the assay conditions, thus providing additional evidence that the fusion of the EcPutA DNA-binding domain does not disrupt the overall kinetic properties of RcPutA. In addition, no



r EcPutA, RcPutA, and EcRHH-RcPut

Proline			
$k_{\text{cat}}$ ( $\text{s}^{-1}$ )	$k_{\text{cat}}/K_m$ ( $\text{M}^{-1} \text{s}^{-1}$ )	$K$	
$8.0 \pm 0.2$	$68.4 \pm 6.7$	162	
$1.0 \pm 0.1$	$178.6 \pm 3.9$	93.	
$0.89 \pm 0.1$	$167.9 \pm 5.2$	161	

50 mM potassium phosphate, 25 mM N

**Figure 2.** PRODH-P5CDH coupled activity assays of RcPutA and EcRHH-RcPutA.

Assays were performed using 200  $\mu$ M CoQ<sub>1</sub>, 40 mM proline, 0.25  $\mu$ M enzyme (RcPutA or EcRHH-RcPutA) in 50 mM potassium phosphate (pH 7.5) and 25 mM NaCl. NADH formation was monitored at 340 nm.

lag phase is apparent in these assays suggesting that the intermediate L-P5C/GSA does not equilibrate with bulk solvent but instead is channeled between the PRODH and P5CDH active sites (26). These results are consistent with that previously described for BjPutA (26).

**Oligomeric State Determination**

The domain organization of RcPutA provides an excellent opportunity to explore the impact of the RHH and CTD domains of EcPutA on the oligomeric organization of PutAs. RcPutA has a conserved CTD but lacks the RHH DNA binding domain of EcPutA. The oligomeric states of RcPutA and EcRHH-RcPutA were first analyzed by gel filtration chromatography. Figure 3A shows a striking difference between the two proteins. The elution profile of EcRHH-RcPutA estimates a molecular mass ( $M$ ) of  $\sim$  315 kDa whereas RcPutA elutes at an apparent  $M$  of  $\sim$  122 kDa. These results indicate that RcPutA purifies as a monomer whereas EcRHH-RcPutA is a dimer ( $\sim$ 252 kDa) or a trimer ( $\sim$ 378 kDa) species.

RcPutA and EcRHH-RcPutA were then analyzed by analytical ultracentrifugation. Sedimentation equilibrium experiments were performed using three different protein concentrations. The equilibrium data for RcPutA (Figure 3B) and EcRHH-RcPutA (Figure 3C) were best-fit to an ideal single-species model which yielded  $M$  values of 130 kDa (125.5 kDa theoretical) and 256 kDa (251 kDa theoretical), respectively. These results confirm that RcPutA is a monomer and that EcRHH-RcPutA is a dimer, suggesting that the EcPutA RHH domain induces dimerization of RcPutA.

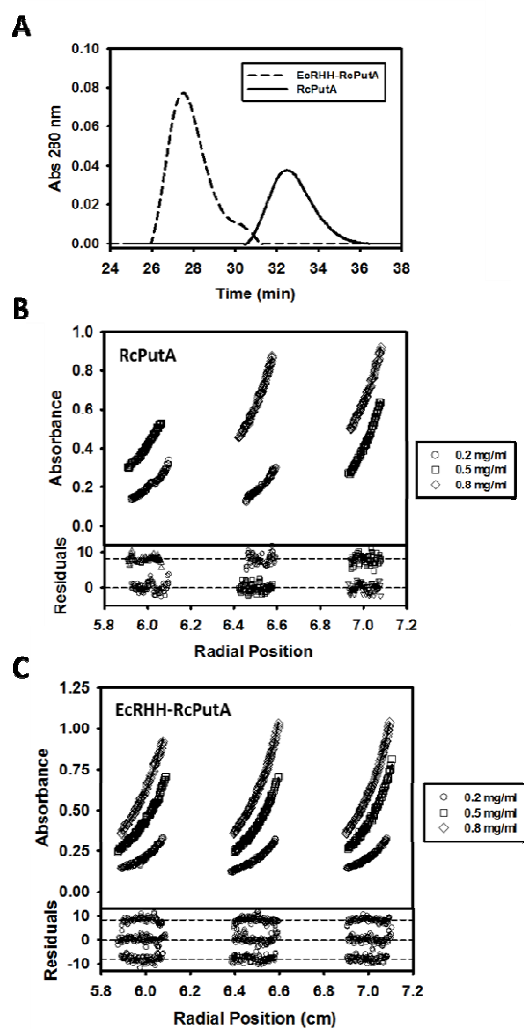


**Figure 3.** Oligomeric structure analysis of RcPutA and EcRHH-RcPutA. (A) Gel filtration elution profiles (monitored at 280 nm) of RcPutA (solid trace) and EcRHH-RcPutA (dotted trace). (B) Sedimentation equilibrium analysis of RcPutA. Global fit analysis of three different protein concentrations at 8000 rpm to an ideal single-species model yielding a 130 kDa species (theoretical 126 kDa). (C) Sedimentation equilibrium analysis of EcRHH-RcPutA. Global fit analysis of three different protein concentrations at 8000 rpm to an ideal single-species model yielding a 256 kDa species (theoretical 251 kDa). A vertical offset was applied to the residuals which are shown for each fit in the bottom panel. Molecular weight values are reported at a 95% confidence interval.

### **DNA-binding and Lipid Pull-down Assays of EcRHH-RcPutA**

From the analysis above, it appears EcRHH-RcPutA adopts a similar oligomeric state as that of EcPutA. We next sought to determine if EcRHH-RcPutA exhibited the functional switching properties of EcPutA. The DNA-binding activities of EcPutA, RcPutA, and EcRHH-RcPutA were compared using gel mobility shift DNA-binding assays. Figure 4A shows that RcPutA does not bind DNA as expected whereas EcRHH-RcPutA binds *put* control DNA similarly to EcPutA. A dissociation constant ( $K_d$ ) for EcRHH-RcPutA with *put* control DNA was determined by varying EcRHH-RcPutA concentration in the binding assays as shown in Figure 4B. Figure 4C shows a plot of the fraction of bound DNA versus EcRHH-RcPutA concentration fit to eq 1 ( $n = 1.2$ ), from which a  $K_d$  value of  $39 \pm 16$  nM was estimated. This value is equivalent to that determined previously for EcPutA ( $K_d = 45$  nM) (17).

Lipid pull-down assays were used to test whether the membrane binding properties of RcPutA and EcRHH-RcPutA are regulated by proline reduction of the flavin cofactor as

observed for EcPutA (21, 31). RcPutA, EcRHH-RcPutA, and EcPutA were incubated with *E. coli* polar lipid vesicles in the absence and presence of 50 mM proline. After incubation for 1 h, the soluble and lipid fractions were separated by centrifugation and analyzed by SDS-PAGE to monitor PutA partitioning in the soluble and lipid fractions. Figure 5 clearly shows that in the absence of proline (i.e., oxidized state) RcPutA and EcRHH-RcPutA are mainly in the soluble fraction similar to EcPutA. In the presence of proline, RcPutA and EcRHH-RcPutA significantly partition into the lipid fraction, indicating that membrane interactions are favored in a reducing environment as seen with

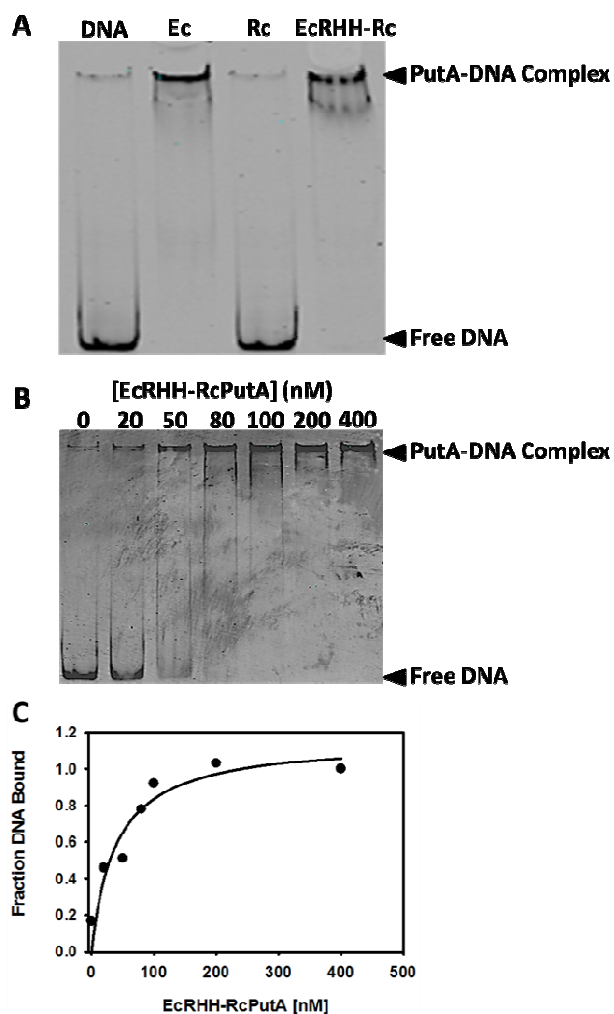


**Figure 4.** DNA-binding assays. (A) Gel mobility shift assays of EcPutA (200 nM), RcPutA (200 nM), and EcRHH-RcPutA (200 nM) added to binding mixtures containing 2 nM of fluorescent labeled (IRDye-700 label) *put* control DNA (420 bp) and 100 ug/ml of nonspecific calf thymus DNA. Free DNA and PutA-DNA complexes were separated on a nondenaturing 4% polyacrylamide gel. (B) Representative gel mobility shift assay with increasing concentrations (0-400 nM) of EcRHH-RcPutA with fluorescently labeled *put* control DNA (2 nM). (C) Plot of EcRHH-RcPutA concentration versus fraction of DNA bound from two independent gel-shift assays. Data were fit to eq 1 to yield a dissociation constant ( $K_d$ ) of  $39 \pm 16$  nM.

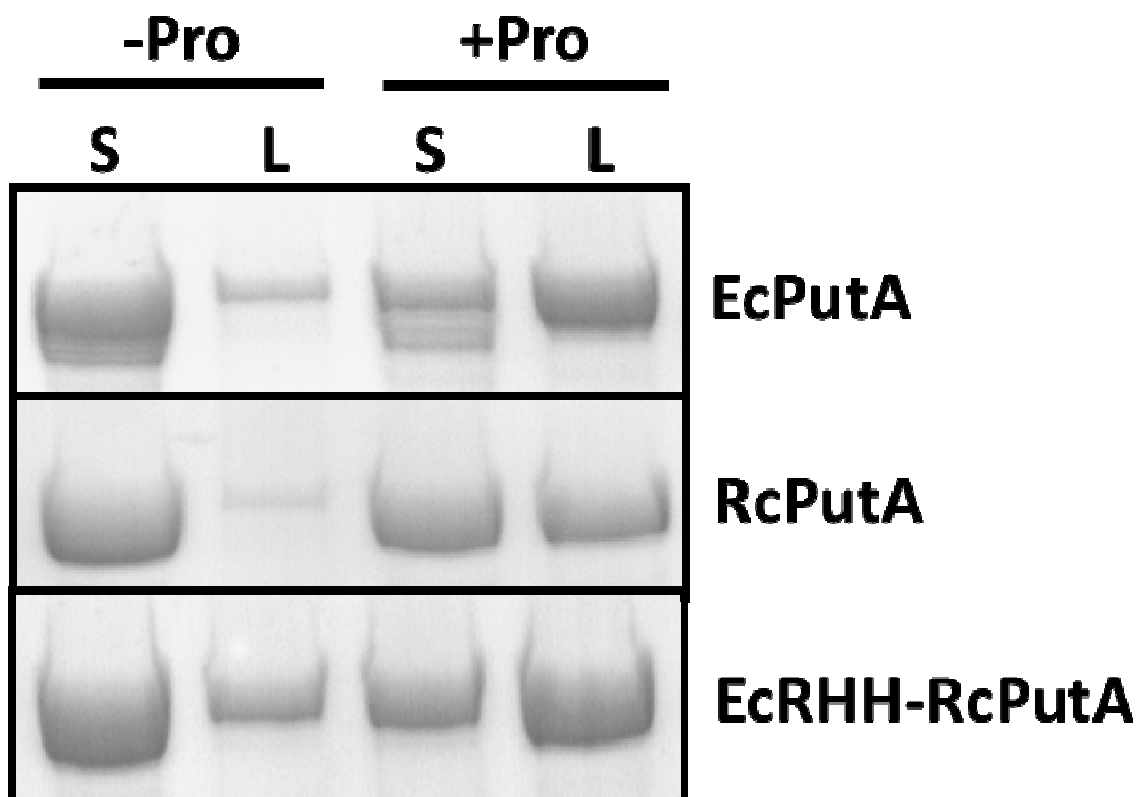


**Figure 5.** Lipid pull-down assays. EcPutA, RcPutA, and EcRHH-RcPutA (0.3 mg/ml each) were incubated with or without proline in HEPES buffer (pH 7.5, 150 mM NaCl) with freshly prepared *E. coli* polar lipid vesicles (0.8 mg/mL) for 1 h at room temperature. Following incubation, soluble and lipid fractions were separated by Air-fuge ultracentrifugation and analyzed via SDS-PAGE.

EcPutA. These results are consistent with redox functional switching of RcPutA-membrane associations as described previously for EcPutA.

### **Cell-based Testing of EcRHH-RcPutA Functional Switching**

The assays described above show that EcRHH-RcPutA and EcPutA exhibit similar properties suggesting that only the DNA binding domain of EcPutA is required to convert RcPutA into a trifunctional protein. To confirm that EcRHH-RcPutA is a genuine trifunctional protein, cell-based membrane interactions and transcriptional repressor assays were performed. The ability of RcPutA and EcRHH-RcPutA to couple proline utilization with the respiratory chain was tested in *E. coli putA*<sup>-</sup> cells on minimal medium agar plates containing TTC, a redox dye that acts as an electron acceptor for dehydrogenases and complex 1 at the membrane (33, 34). Figure 6A shows that plates streaked with cells containing EcPutA, RcPutA, and EcRHH-RcPutA show a strong red color, whereas cells containing the empty vector show only a faint red color after 20 h of growth. These results indicate that EcRHH-RcPutA interacts functionally with the membrane *in vivo*.

The ability of EcRHH-RcPutA to switch between DNA binding and membrane binding was assessed using a cell-based  $\beta$ -galactosidase reporter assay as previously described (28, 31). Figure 6B shows that  $\beta$ -galactosidase activity increases 3-fold in cells containing EcPutA when proline is added to the growth media. This increase in  $\beta$ -galactosidase activity is similar to that which has been reported previously for EcPutA (31). In cells with RcPutA, the  $\beta$ -galactosidase activity matched that of cells

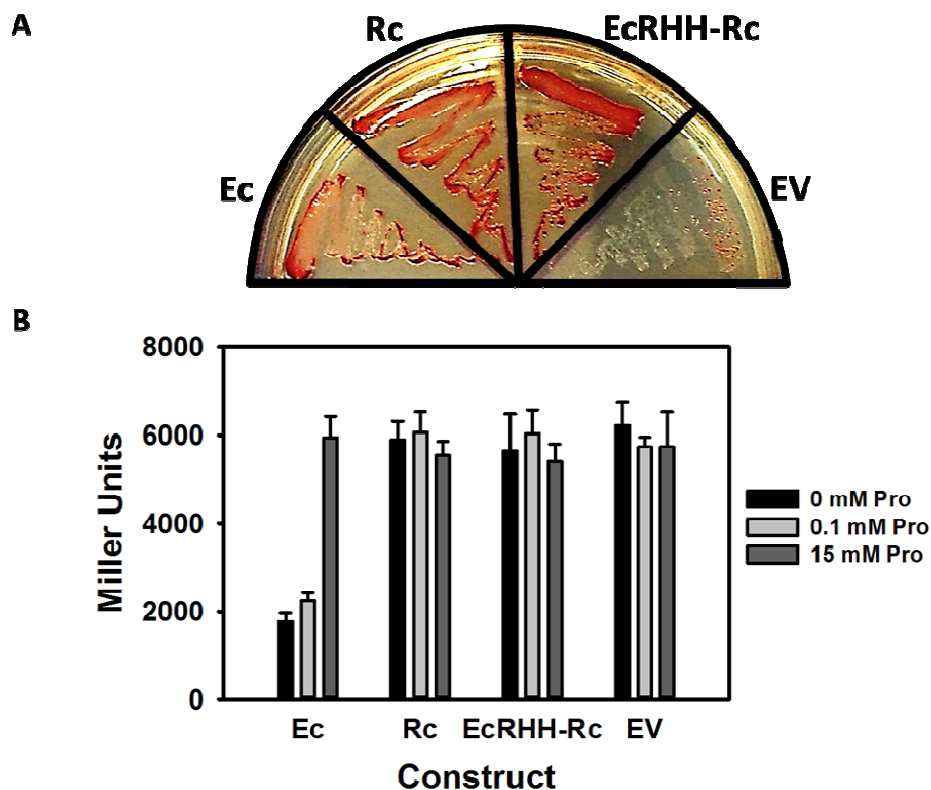


**Figure 6.** Cell-based functional switching assays. (A) *In vivo* membrane interaction assays were performed with BL21DE3 PutA<sup>-</sup> Kan<sup>R</sup> cells containing EcPutA, RcPutA, EcRHH-RcPutA and pET-21a empty vector. Cells were plated on minimal media agar containing proline and TTC and grown for 20 h at 37 °C. The appearance of a red color indicates utilization of proline as respiratory substrate and functional PutA-membrane interactions. A control experiment using minimal media plus glycerol showed red colonies for all four constructs (data not shown). (B) Cell-based transcriptional repressor assays in *E. coli* strain JT31 *putA*<sup>-</sup> *lacZ* cells containing the *putC*:*lacZ* reporter gene plasmid and EcPutA, RcPutA, EcRHH-RcPutA and the pET-21a empty vector. Cells were grown at 37 °C in minimal media supplemented with 0 mM, 0.1 mM, and 15 mM proline.  $\beta$ -galactosidase activity is reported as the average of four independent experiments  $\pm$  standard errors.

containing the empty vector with and without proline consistent with RcPutA not binding *put* control DNA (Figure 6B) and thereby not being able to repress transcription of the *putC:lacZ* reporter gene. Unexpectedly, cells containing EcRHH-RcPutA exhibited the same level of  $\beta$ -galactosidase activity as RcPutA cells with and without proline. The high levels of  $\beta$ -galactosidase activity in the absence of proline indicate that unlike EcPutA, EcRHH-RcPutA does not repress transcription of the *putC:lacZ* reporter gene. Thus, although EcRHH-RcPutA appears to have all of the properties necessary for functional switching, the chimeric protein is unable to act as transcriptional repressor *in vivo*.

## DISCUSSION

Purification of RcPutA provided an opportunity to characterize a PutA enzyme with a unique quaternary structure, which in contrast to BjPutA and EcPutA, purifies as monomer. The CTD of RcPutA must interfere with the dimerization interface observed previously for BjPutA. BjPutA is a shorter enzyme that lacks the CTD and was observed by X-ray crystallography to form a dimer of dimers or a tetrameric species.<sup>(26)</sup> Relative to EcPutA, RcPutA lacks the RHH-DNA-binding domain, which has also been shown to be responsible for dimerization of EcPutA. Thus, RcPutA represents an intermediate form between the two different dimeric species of BjPutA and EcPutA.

The observation that RcPutA follows a substrate channeling mechanism in the coupled PRODH-P5CDH reaction indicates a dimeric structure is not required for substrate channeling. The progress curve of the coupled PRODH-P5CDH assay is consistent with substrate channeling, as no lag phase is detected indicating that the

P5C/GSA intermediate is channeled from the PRODH active site to the P5CDH domain in RcPutA. Substrate channeling is best characterized for BjPutA in which the X-ray crystal structure of the full-length enzyme revealed a cavity linking the PRODH and P5CDH active sites (26). In assays using a mixture of monofunctional variants of BjPutA which lack either PRODH or P5CDH activity, a ~ 8 min lag was observed before reaching steady-state formation of NADH thereby mimicking a non-channeling PRODH-P5CDH coupled reaction (26). The progress curve of RcPutA and the EcRHH-RcPutA clearly do not show a lag, which is consistent with a substrate channeling mechanism.

Discovering that the monomeric form of RcPutA does not prohibit substrate channeling suggests another function for the CTD. The X-ray crystal structure of the BjPutA showed a domain swap dimer is formed via the P5CDH domain (26). A  $\beta$ -flap from each protomer forms strong interactions with the neighboring protomer in BjPutA (26). This interaction not only helps stabilize the dimeric structure but also helps form part of the cavity wall (26). It seems likely that the CTD of RcPutA must somehow substitute for these domain swap interactions thus helping form the channel cavity while stabilizing the P5CDH domain within the RcPutA monomer. An unexpected finding was the enhanced membrane binding of RcPutA in the presence of proline. Previously, BjPutA membrane-binding affinity was shown not to be increased by proline (35). Here, the membrane-binding of RcPutA was significantly enhanced by proline similar to that of EcPutA. This indicates a potentially important role of the CTD in the regulation of PutA-membrane interactions. The physiological rationale for regulating RcPutA membrane interactions is not clear, as RcPutA does not have a transcriptional repressor function. In *R. capsulatus*, *putA* expression is activated in response to proline by the PRODH

activator, PutR (36). PutR contains a helix-turn-helix motif and is a member of the Lrp/AsnC family of DNA binding proteins (36).

Fusing the EcRHH domain with RcPutA imparts *in vitro* DNA-binding activity in EcRHH-RcPutA that is similar to EcPutA. In addition, EcRHH-RcPutA forms a stable dimer providing further evidence that dimerization in trifunctional PutAs is mediated through the DNA-binding domain (23, 37). The lipid-pull down assays show EcRHH-RcPutA exhibits a strong increase in membrane binding consistent with EcPutA. Thus, the *in vitro* characterization of EcRHH-RcPutA suggests that RcPutA has been successfully converted into a trifunctional PutA protein. In the cell-based reporter assays, however, we did not detect transcriptional repression of the *putC:lacZ* reporter gene nor did we observe a proline-dependent increase in  $\beta$ -galactosidase activity. Because EcRHH-RcPutA shows evidence of functional membrane interactions in the TTC assays and no evidence for repression of the *putC:lacZ* reporter gene, we propose that the failure of EcRHH-RcPutA to functionally switch *in vivo* is due to significantly weaker DNA binding in the cell.

The inability of EcRHH-RcPutA to act as a transcriptional repressor *in vivo* was unexpected. Previously, the EcRHH DNA-binding domain alone was shown to strongly repress transcription of the *putC:lacZ* reporter gene in cell based assays (23, 31). Thus, residues outside the RHH domain are not required for EcPutA transcriptional repressor activity. Comparing the shape reconstructions generated by SAXS of EcPutA and EcRHH-RcPutA may provide some insights into the lack of transcriptional repressor activity in EcRHH-RcPutA.

The reason EcRHH-RcPutA exhibits DNA-binding *in vitro* and apparently not in the cell-based assay may be due to differences in DNA configuration. A relaxed linear DNA fragment is used in the gel-mobility shift assays whereas in the cell-based assays the *putC:lacZ* reporter gene is on plasmid DNA that is presumably supercoiled. The supercoiled or condensed DNA structure may impact the accessibility of the *put* control region to the EcRHH domain in EcRHH-RcPutA. In EcPutA, the spacing of the catalytic lobes must be wide enough to allow the RHH domain to interact with different DNA configurations. In EcRHH-RcPutA, the spacing is narrower, possibly restricting the ability of the RHH domain to access condensed DNA. The structure of the EcRHH-RcPutA dimer, however, allows the RHH domain to still interact with relaxed DNA. As a result, fusing only the EcRHH domain onto RcPutA does not generate a fully trifunctional protein. EcRHH-RcPutA shares many characteristics of EcPutA but fails in the cell-based test of functional switching.

Comparison of the domain organization (Figure 1) between EcPutA and RcPutA shows that EcPutA has a region of 34 amino acids (residues 49-86) that links the RHH and arm domains. This linker region is not conserved in RcPutA and was not included in the design of the EcRHH-RcPutA chimera. Whether this linker region is of structural importance for stabilization and shape of the proposed DNA-binding cleft in EcPutA remains unclear. It has previously been suggested that the aforementioned 34 residues are involved in a hinge mechanism that can narrow or widen the DNA-binding cleft based on global conformational changes caused by flavin reduction. From this study, it appears that these 34 residues may indeed be critical for *in vivo* EcPutA DNA binding and

EcPutA transcriptional repressor activity. Future studies will explore the role of the 34-amino acid linker region in the functional switching mechanism of EcPutA.

## REFERENCES

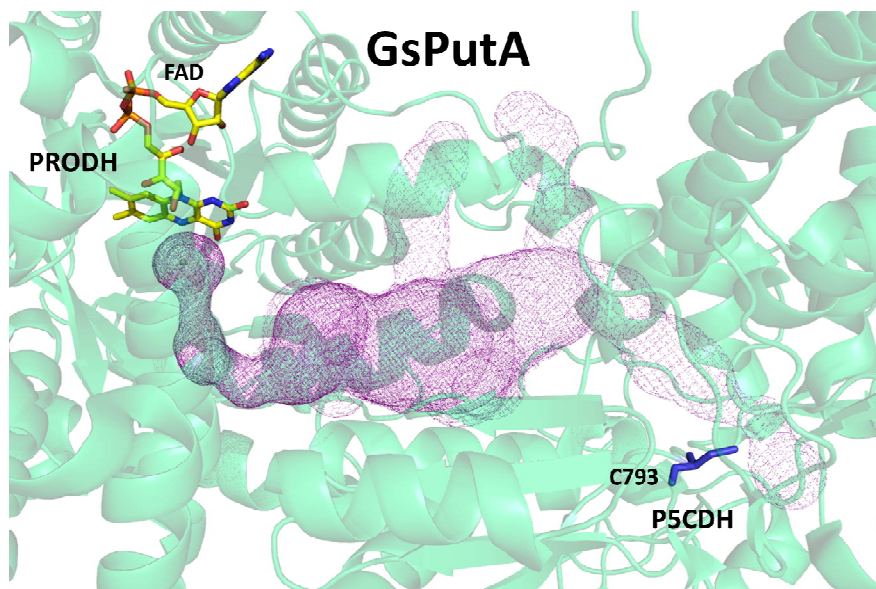
1. Liang, X., Zhang, L., Natarajan, S. K., and Becker, D. F. (2013) Proline mechanisms of stress survival, *Antioxidants & redox signaling* 19, 998-1011.
2. Szabados, L., and Savoure, A. (2010) Proline: a multifunctional amino acid, *Trends in plant science* 15, 89-97.
3. Wood, J. M., Bremer, E., Csonka, L. N., Kraemer, R., Poolman, B., van der Heide, T., and Smith, L. T. (2001) Osmosensing and osmoregulatory compatible solute accumulation by bacteria, *Comparative biochemistry and physiology. Part A, Molecular & integrative physiology* 130, 437-460.
4. Natarajan, S. K., Zhu, W., Liang, X., Zhang, L., Demers, A. J., Zimmerman, M. C., Simpson, M. A., and Becker, D. F. (2012) Proline dehydrogenase is essential for proline protection against hydrogen peroxide-induced cell death, *Free radical biology & medicine* 53, 1181-1191.
5. Phang, J. M., Liu, W., and Zabornyk, O. (2010) Proline metabolism and microenvironmental stress, *Annual review of nutrition* 30, 441-463.
6. Liu, W., Le, A., Hancock, C., Lane, A. N., Dang, C. V., Fan, T. W. M., and Phang, J. M. (2012) Reprogramming of proline and glutamine metabolism contributes to the proliferative and metabolic responses regulated by oncogenic transcription factor c-MYC, *P Natl Acad Sci USA* 109, 8983-8988.
7. Willis, A., Bender, H. U., Steel, G., and Valle, D. (2008) PRODH variants and risk for schizophrenia, *Amino Acids* 35, 673-679.
8. Chakravarti, A. (2002) A compelling genetic hypothesis for a complex disease: PRODH2/DGCR6 variation leads to schizophrenia susceptibility, *Proceedings of the National Academy of Sciences of the United States of America* 99, 4755-4756.
9. Zarchi, O., Carmel, M., Avni, C., Attias, J., Frisch, A., Michaelovsky, E., Patya, M., Green, T., Weinberger, R., Weizman, A., and Gothelf, D. (2013) Schizophrenia-like neurophysiological abnormalities in 22q11.2 deletion syndrome and their association to COMT and PRODH genotypes, *Journal of psychiatric research*.
10. Nakajima, K., Inatsu, S., Mizote, T., Nagata, Y., Aoyama, K., Fukuda, Y., and Nagata, K. (2008) Possible involvement of put A gene in Helicobacter pylori colonization in the stomach and motility, *Biomedical research* 29, 9-18.
11. Krishnan, N., Doster, A. R., Duhamel, G. E., and Becker, D. F. (2008) Characterization of a Helicobacter hepaticus putA mutant strain in host colonization and oxidative stress, *Infection and immunity* 76, 3037-3044.
12. Lee, I. R., Lui, E. Y., Chow, E. W., Arras, S. D., Morrow, C. A., and Fraser, J. A. (2013) Reactive oxygen species homeostasis and virulence of the fungal pathogen Cryptococcus neoformans requires an intact proline catabolism pathway, *Genetics* 194, 421-433.
13. Tanner, J. J. (2008) Structural biology of proline catabolism, *Amino Acids* 35, 719-730.
14. Singh, R. K., and Tanner, J. J. (2012) Unique structural features and sequence motifs of proline utilization A (PutA), *Frontiers in bioscience* 17, 556-568.

15. Zhou, Y., Larson, J. D., Bottoms, C. A., Arturo, E. C., Henzl, M. T., Jenkins, J. L., Nix, J. C., Becker, D. F., and Tanner, J. J. (2008) Structural basis of the transcriptional regulation of the proline utilization regulon by multifunctional PutA, *Journal of molecular biology* 381, 174-188.
16. Ostrovsky de Spicer, P., and Maloy, S. (1993) PutA protein, a membrane-associated flavin dehydrogenase, acts as a redox-dependent transcriptional regulator, *Proc. Natl. Acad. Sci. U. S. A.* 90, 4295-4298.
17. Becker, D. F., and Thomas, E. A. (2001) Redox properties of the PutA protein from *Escherichia coli* and the influence of the flavin redox state on PutA-DNA interactions, *Biochemistry* 40, 4714-4721.
18. Wood, J. M. (1987) Membrane association of proline dehydrogenase in *Escherichia coli* is redox dependent, *Proc. Natl. Acad. Sci. U. S. A.* 84, 373-377.
19. Brown, E. D., and Wood, J. M. (1993) Conformational change and membrane association of the PutA protein are coincident with reduction of its FAD cofactor by proline, *J Biol Chem* 268, 8972-8979.
20. Zhu, W., and Becker, D. F. (2003) Flavin redox state triggers conformational changes in the PutA protein from *Escherichia coli*, *Biochemistry* 42, 5469-5477.
21. Zhang, W., Zhou, Y., and Becker, D. F. (2004) Regulation of PutA-membrane associations by flavin adenine dinucleotide reduction, *Biochemistry* 43, 13165-13174.
22. Muro-Pastor, A. M., Ostrovsky, P., and Maloy, S. (1997) Regulation of gene expression by repressor localization: biochemical evidence that membrane and DNA binding by the PutA protein are mutually exclusive, *Journal of bacteriology* 179, 2788-2791.
23. Gu, D., Zhou, Y., Kallhoff, V., Baban, B., Tanner, J. J., and Becker, D. F. (2004) Identification and characterization of the DNA-binding domain of the multifunctional PutA flavoenzyme, *The Journal of biological chemistry* 279, 31171-31176.
24. Larson, J. D., Jenkins, J. L., Schuermann, J. P., Zhou, Y., Becker, D. F., and Tanner, J. J. (2006) Crystal structures of the DNA-binding domain of *Escherichia coli* proline utilization A flavoprotein and analysis of the role of Lys9 in DNA recognition, *Protein science : a publication of the Protein Society* 15, 2630-2641.
25. Tanner, J. J., and Becker, D. F. (2013) PutA and proline metabolism, In *Handbook of Flavoproteins* (Hille, R., Miller, S. M., and Palfey, B., Eds.), pp 31-56, Walter de Gruyter, Boston.
26. Srivastava, D., Schuermann, J. P., White, T. A., Krishnan, N., Sanyal, N., Hura, G. L., Tan, A., Henzl, M. T., Becker, D. F., and Tanner, J. J. (2010) Crystal structure of the bifunctional proline utilization A flavoenzyme from *Bradyrhizobium japonicum*, *Proceedings of the National Academy of Sciences of the United States of America* 107, 2878-2883.
27. Altschul, S. F., Gish, W., Miller, W., Myers, E. W., and Lipman, D. J. (1990) Basic local alignment search tool, *J Mol Biol* 215, 403-410.
28. Zhang, W., Zhang, M., Zhu, W., Zhou, Y., Wanduragala, S., Rewinkel, D., Tanner, J. J., and Becker, D. F. (2007) Redox-induced changes in flavin structure and roles of flavin N(5) and the ribityl 2'-OH group in regulating PutA--membrane binding, *Biochemistry* 46, 483-491.

29. Moxley, M. A., Tanner, J. J., and Becker, D. F. (2011) Steady-state kinetic mechanism of the proline:ubiquinone oxidoreductase activity of proline utilization A (PutA) from *Escherichia coli*, *Archives of biochemistry and biophysics* 516, 113-120.
30. Zhou, Y., Zhu, W., Bellur, P. S., Rewinkel, D., and Becker, D. F. (2008) Direct linking of metabolism and gene expression in the proline utilization A protein from *Escherichia coli*, *Amino Acids* 35, 711-718.
31. Zhu, W., Haile, A. M., Singh, R. K., Larson, J. D., Smithen, D., Chan, J. Y., Tanner, J. J., and Becker, D. F. (2013) Involvement of the beta3-alpha3 Loop of the Proline Dehydrogenase Domain in Allosteric Regulation of Membrane Association of Proline Utilization A, *Biochemistry* 52, 4482-4491.
32. Miller, J. H. (1972) *Experiments in molecular genetics*, Cold Spring Harbor Laboratory, Cold Spring Harbor, N.Y.
33. Berridge, M. V., Herst, P. M., and Tan, A. S. (2005) Tetrazolium dyes as tools in cell biology: new insights into their cellular reduction, *Biotechnology annual review* 11, 127-152.
34. Rich, P. R., Mischis, L. A., Purton, S., and Wiskich, J. T. (2001) The sites of interaction of triphenyltetrazolium chloride with mitochondrial respiratory chains, *FEMS microbiology letters* 202, 181-187.
35. Zhang, W., Krishnan, N., and Becker, D. F. (2006) Kinetic and thermodynamic analysis of *Bradyrhizobium japonicum* PutA-membrane associations, *Archives of biochemistry and biophysics* 445, 174-183.
36. Keuntje, B., Masepohl, B., and Klipp, W. (1995) Expression of the putA gene encoding proline dehydrogenase from *Rhodobacter capsulatus* is independent of NtrC regulation but requires an Lrp-like activator protein, *Journal of bacteriology* 177, 6432-6439.
37. Singh, R. K., Larson, J. D., Zhu, W., Rambo, R. P., Hura, G. L., Becker, D. F., and Tanner, J. J. (2011) Small-angle X-ray Scattering Studies of the Oligomeric State and Quaternary Structure of the Trifunctional Proline Utilization A (PutA) Flavoprotein from *Escherichia coli*, *The Journal of biological chemistry* 286, 43144-43153.

## CHAPTER 4

### Kinetic Exploration of the Proline Dehydrogenase Active Sites of *Geobacter sulfurreducens* Proline Utilization A and *Deinococcus radiodurans* Proline Dehydrogenase



Note: The GsPutA results presented in this chapter are currently part of a manuscript and will be published alongside crystal structures.

The DrPRODHD results have been published: Reproduced in part with permission from (Luo, M., Arentson, B. W., Srivastava, D., Becker, D. F., and Tanner, J. J. (2012) Crystal structures and kinetics of monofunctional proline dehydrogenase provide insight into substrate recognition and conformational changes associated with flavin reduction and product release, *Biochemistry* 51, 10099-10108).

Copyright (2012) American Chemical Society.

<http://pubs.acs.org/doi/abs/10.1021/bi301312f>

## ABSTRACT

This chapter is divided into two sections. The first will kinetically explore the proline dehydrogenase (PRODH) active site of *Geobacter sulfurreducens* PutA (GsPutA), using a new ubiquinone analog menadione bisulfite. Additionally, proline:ubiquinone oxidoreductase activity is shown to use a two-site ping pong mechanism as previously reported in *E. coli* PutA. Finally a coupled channeling assay was used to show that GsPutA channels P5C, verifying that all known PutAs to date channel.

The second part of Chapter 4 will kinetically explore the monofunctional proline dehydrogenase from *Deinococcus radiodurans*, revealing wild-type has a high  $K_m$  for proline. Additionally two highly conserved residues (G63A, E64A) were mutated and kinetically characterized. Results indicate that Gly63 is important for the flexibility of the  $\beta 1$ - $\alpha 1$  loop, and Glu64 is important for stabilizing the closed active site.

Both sections are based on crystal structures generated by the lab of Dr. John J. Tanner, University of Missouri-Columbia. Kinetic characterizations were performed to help interpret structural evidence.

## PART I: GsPutA Characterization

### INTRODUCTION

Proline metabolism occurs through two enzymatic steps (*1*). First, the flavin-dependent proline dehydrogenase catalyzes the two electron oxidation of proline to  $\Delta^1$ -pyrroline-5-carboxylate (P5C). P5C undergoes a non-enzymatic hydrolysis, which opens the five-member ring and results in glutamate- $\gamma$ -semialdehyde (GSA). GSA is a substrate

for NAD<sup>+</sup>-dependent P5C dehydrogenase (P5CDH), which catalyzes a second two electron oxidation to generate glutamate. In Gram-positive bacteria and eukaryotes PRODH and P5CDH are expressed as separate enzymes; however, in Gram negative bacteria the domains are fused into a single polypeptide called proline utilization A (PutA) (2, 3).

The crystal structure of *Bradyrhizobium japonicum* (BjPutA) has been determined, but it contains sulfate ions in both active sites and does not reveal how the structure changes during catalysis (4). Recently however, several crystal structures of minimalist PutA from *Geobacter sulfurreducens* were determined by Harkewal Singh of the Tanner Lab (personal correspondence), revealing snapshots of different catalytic states. In particular, a structure of the oxidized enzyme with no ligands bound demonstrated for the first time a PutA in a resting state. Additionally, a GsPutA structure with proline inhibitors THFA and lactate bound at the PRODH active site were the first full length PutAs bound with proline analogs (personal correspondence). A structure exhibiting the flavin-reduced state provided, for the first time, a structure of the PRODH domain after release of P5C into the channel and before quinone binding (Tanner, personal communication). Finally, a looming question in PutA biochemistry was answered by a structure revealing the putative ubiquinone binding site.

N-propargylglycine (PPG) is a known mechanistic inhibitor of the PRODH active site, where it reduces the flavin then becomes catalytically stuck through the formation of a covalent bond between the active site lysine and N5 of the flavin (5). Using this inhibitor, crystals with GsPutA locked into a reduced state were soaked with ubiquinone analog menadione bisulfite (MB). MB was chosen both due to its high solubility in water

and because menaquinones are the predominant respiratory quinones in *Geobacter* (6). A subsequent structure revealed the binding site of MB, and presumably all quinone-based flavin electron acceptors. As expected, the structure shows MB surrounded by several non-polar and aromatic residues, including L147, L385, Y406, P408, Y309, and Y418 (personal correspondence). These residues provided points of mutation to potentially disrupt the quinone binding site, so Gs L385A and Gs Y418A were made. Other mutations to GsPutA were attempted, but solubility proved difficult. A second structure of a minimalist PutA from *Bdellovibrio bacteriovorus* (BbPutA) was solved alongside GsPutA, which also showed MB bound to the PRODH active site. Using the BbPutA-MB complex, mutations Bb Y304A, Bb L380A, Bb Y401A, and Bb Y413A were made. Of these mutations, only Gs Y418A, Bb Y413A, and Bb L380A will be discussed in this chapter.

## **MATERIALS AND METHODS**

### **Chemicals**

All chemicals were purchased from Sigma-Aldrich or Fisher Scientific.

Nanopure water was used in all experiments. All enzymes were purified in the lab of Dr. John J Tanner, University of Missouri-Columbia.

### **Steady State Kinetic Assays**

All PRODH kinetic data was collected on a Hi-Tech Scientific SF-61DX2 model stopped-flow spectrometer at 23 °C in 50 mM HEPES, 25 mM NaCl, pH 7.4 using 0.25  $\mu$ M enzyme. For kinetic determinations, the reduction of ubiquinone (CoQ<sub>1</sub>) ( $\epsilon = 14,500$

$\text{M}^{-1} \text{cm}^{-1}$ ), menadione ( $\epsilon = 14,000 \text{ M}^{-1} \text{cm}^{-1}$ ) or MB ( $\epsilon = 8,200 \text{ M}^{-1} \text{cm}^{-1}$ ) was monitored at wavelengths 278, 262 and 266 nm, respectively. Using GsPutA, the  $K_m$  and  $k_{\text{cat}}$  for CoQ<sub>1</sub>, menadione, or MB were determined by varying CoQ<sub>1</sub> (2.5-400  $\mu\text{M}$ ), menadione (2-400  $\mu\text{M}$ ), or MB (2.5-200  $\mu\text{M}$ ), while holding proline constant at 350 mM. Likewise the  $K_m$  and  $k_{\text{cat}}$  for proline were determined by varying proline (10-750 mM), while holding CoQ<sub>1</sub> (300  $\mu\text{M}$ ), menadione (100  $\mu\text{M}$ ), or MB (150  $\mu\text{M}$ ) constant.

Using BbPutA, the  $K_m$  and  $k_{\text{cat}}$  of CoQ<sub>1</sub>, menadione, and MB were determined by varying CoQ<sub>1</sub> (2.5-500  $\mu\text{M}$ ), menadione (2.5-150  $\mu\text{M}$ ), or MB (2.5-250  $\mu\text{M}$ ), while holding proline constant at 350 mM. The  $K_m$  and  $k_{\text{cat}}$  for proline were determined by varying proline (1-350 mM), while holding CoQ<sub>1</sub> (250  $\mu\text{M}$ ), menadione (100  $\mu\text{M}$ ), or MB (100  $\mu\text{M}$ ) constant.

Three mutations at the putative ubiquinone binding site were made, L380A and Y413A in BbPutA, and Y418A in GsPutA. All mutants were characterized using variable proline (1-950 mM) while keeping menadione constant at 100  $\mu\text{M}$ , or variable menadione (0-200  $\mu\text{M}$ ) while holding proline at 350 mM. Enzyme concentration was 0.25  $\mu\text{M}$  for L380A and Y413A for BbPutA and 2.5  $\mu\text{M}$  for Y418A in GsPutA in all assays.

P5CDH kinetic constants were determined by following  $\text{NAD}^+$  reduction at 340 nm, using a Powerwave XS microplate spectrophotometer (Bio-Tek). Assays consisted of a buffer composed of 50 mM potassium phosphate, 25 mM NaCl, pH 7.5, where L-P5C was varied (25-4000  $\mu\text{M}$ ), while holding  $\text{NAD}^+$  constant at 0.2 mM (0.75  $\mu\text{M}$  enzyme). The effective concentration of P5C and GSA at pH 7.5 was estimated as previously reported (4, 7). All above initial velocity data was fit to the Michaelis-Menten

equation using SigmaPlot 12.0.

### **Product Inhibition Assays**

The proline:ubiquinone oxidoreductase mechanism was explored by determining the product inhibition pattern of L-P5C, as previously reported (8). Briefly four different concentrations of L-P5C (0, 0.5, 1.5, and 2.84 or 3 mM) were used while varying either proline or MB. When varying proline (10-750 mM), 100  $\mu$ M of MB was added (GsPutA 0.25  $\mu$ M), and while varying MB (2.5-200  $\mu$ M), proline was held at 250 mM (GsPutA 0.5  $\mu$ M). The product inhibition pattern was also performed while varying proline (10-750 mM) in the presence of menadione (100  $\mu$ M) to verify the natural electron acceptor has the same inhibition pattern as MB (GsPutA 0.25  $\mu$ M). Each data set was fit globally to non-linear forms of the competitive, non-competitive, uncompetitive, and mixed inhibition models, then best-fit models were reported.

### **Channeling Assays**

Assays designed to detect a lag phase in the progress curve for the production of NADH from proline were also performed. The observation of a lag phase in the progress curve would be inconsistent with channeling. The channeling assay was performed on a Cary 50 UV-Vis spectrophotometer in 50 mM potassium phosphate, 25 mM NaCl, pH 7.5 using 40 mM proline, 150  $\mu$ M menadione, 0.2 mM  $\text{NAD}^+$ , and 0.75  $\mu$ M GsPutA. Assays were performed in the presence and absence of  $\text{NAD}^+$ , then progress curves were subtracted to account for spectral interference of menadione at 340 nm. For comparison, the progress curve for two non-interacting PRODH and P5CDH enzymes was simulated using the free diffusion model described by equation 1 (9).

$$[\text{NADH}] = v_1 t + (v_1/v_2)K_m(e^{-v_2 t/K_m} - 1) \quad (1)$$

In this equation,  $v_1$  is the rate of PRODH activity under the reaction conditions. The parameters  $v_2$  and  $K_m$  are the steady-state kinetic parameters for P5CDH activity of GsPutA.

## RESULTS AND DISCUSSION

### Kinetic Characterization of GsPutA

Steady-state kinetic measurements were performed with MB and menadione to verify that 1,4-naphthoquinones lacking an isoprenoid chain are electron acceptors of GsPutA and to explore the mechanism of the oxidative half reaction (Table 1). The  $K_m$  and  $k_{\text{cat}}$  values for MB at a fixed proline concentration of 350 mM are 10.5  $\mu\text{M}$  and 0.66  $\text{s}^{-1}$ , respectively. Those of menadione are 8.2  $\mu\text{M}$  and 0.97  $\text{s}^{-1}$ . The catalytic efficiencies of the two quinones thus agree within a factor of two (60,000  $\text{M}^{-1}\text{s}^{-1}$  for MB and 120,000

**Table 1.** Steady-state kinetic parameters of GsPutA

Variable substrate	Fixed substrate	$K_m$ ( $\mu\text{M}$ )	$k_{\text{cat}}$ ( $\text{s}^{-1}$ )	$k_{\text{cat}} / K_m$ ( $\text{M}^{-1}\text{s}^{-1}$ )
menadione bisulfite	proline <sup>*</sup>	$10.5 \pm 1.2$	$0.66 \pm 0.018$	$62857 \pm 7385$
menadione	proline <sup>*</sup>	$8.2 \pm 0.89$	$0.97 \pm 0.029$	$118292 \pm 13317$
proline	menadione bisulfite <sup>†</sup>	$63010 \pm 8047$	$0.85 \pm 0.027$	$13.5 \pm 1.8$
proline	menadione <sup>†</sup>	$89400 \pm 12700$	$0.67 \pm 0.027$	$7.5 \pm 1.1$

<sup>\*</sup>Fixed proline concentration of 350 mM.

<sup>†</sup>Fixed menadione concentration of 100  $\mu\text{M}$ ; fixed menadione bisulfite concentration of 150  $\mu\text{M}$ .

$\text{M}^{-1}\text{s}^{-1}$  for menadione). Likewise, the kinetic constants for proline at a fixed quinone concentration are similar (Table 1). These results show MB and menadione are efficient

*in vitro* electron acceptors for GsPutA and suggest that the two quinones bind at the same site on GsPutA.

### **Kinetic Mechanism of Proline:ubiquinone Oxidoreductase**

In addition, the kinetic mechanism of the proline:ubiquinone oxidoreductase activity was investigated, as EcPutA was recently reported to use a two-site ping-pong mechanism when using CoQ<sub>1</sub> as an electron acceptor (8). To verify that a two-site ping-pong mechanism was also present when using MB in GsPutA, the product inhibition pattern of L-P5C was explored. Using proline as a variable substrate, assays were performed under different L-P5C concentrations to verify L-P5C competitively inhibits proline when using MB as a flavin electron acceptor (Figure 1A). The same experiment was performed using menadione as an electron acceptor also revealed L-P5C competitively inhibits proline, further suggesting MB binds at the same site as menadione (data not shown). Similarly MB concentrations were varied as L-P5C was held at different concentrations, revealing L-P5C is an uncompetitive inhibitor of MB (Fig. 1B). Taken together, the inhibition pattern of L-P5C parallels what is seen in EcPutA using electron acceptor CoQ<sub>1</sub>, implying MB binds in the same fashion as CoQ<sub>1</sub>. Furthermore, these results suggest all PutAs may use a two-site ping-pong mechanism when oxidizing proline to L-P5C.

### **Coupled Channeling Assay**

After determining GsPutA is kinetically active and displays a two-site ping pong mechanism when using MB as an electron acceptor, a channeling assay was performed to see whether GsPutA channels P5C between active sites. Initiating the coupled reaction

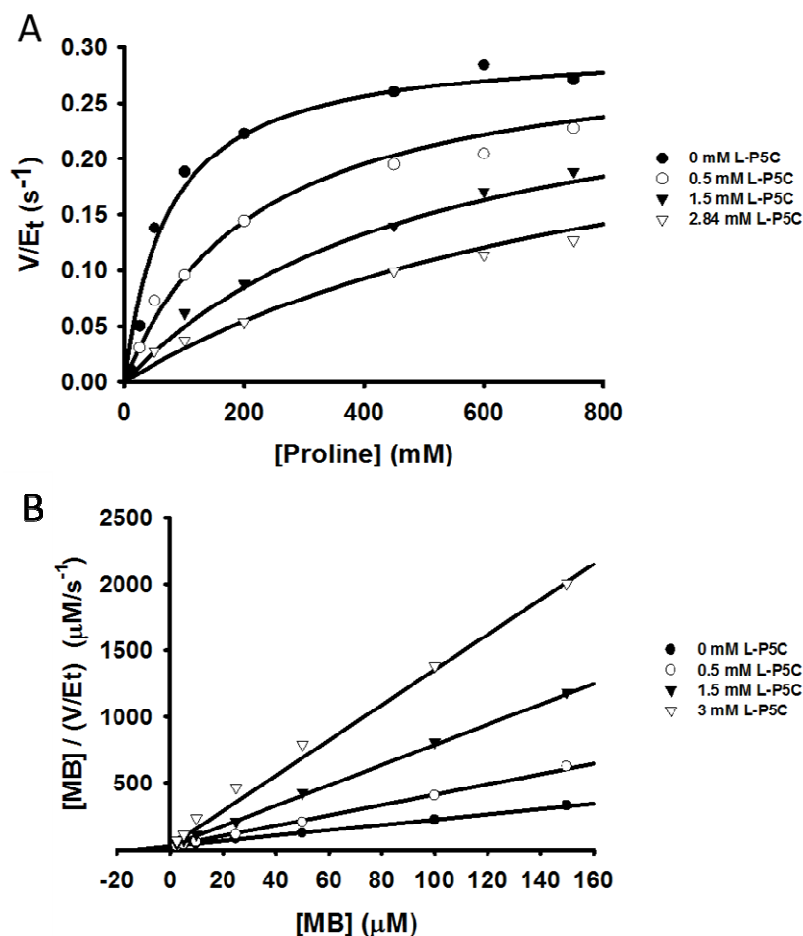


**Figure 1.** Verification of proline:ubiquinone oxidoreductase kinetic mechanism by determining the product inhibition pattern of L-P5C. (A) L-P5C vs proline. A non-linear fit to a competitive inhibition model. Variable proline as L-P5C held at: closed circles 0 mM L-P5C, open circles 0.5 mM L-P5C, closed triangles 1.5 mM L-P5C, open triangles 2.84 mM L-P5C. Best fit parameters were  $k_{cat} = 0.30 \pm 0.009 s^{-1}$ ,  $K_m = 73.1 \pm 8.8$  mM proline, and  $K_I = 0.25 \pm 0.03$  mM L-P5C. (B) L-P5C vs MB. A non-linear fit to an uncompetitive model shown here as a Hanes-Woolf plot. Variable MB as L-P5C held at: closed circles 0 mM L-P5C, open circles 0.5 mM L-P5C, closed triangles 1.5 mM L-P5C, open triangles 3 mM L-P5C. Best fit parameters were  $k_{cat} = 0.50 \pm 0.01 s^{-1}$ ,  $K_m = 12.9 \pm 0.9$   $\mu M$  MB, and  $K_I = 0.53 \pm 0.025$  mM L-P5C.

with 40 mM proline, NADH formation was followed at 340 nm. Shown in Figure 2, NADH formation occurs instantaneously at the start of the steady-state assay, which suggests the occurrence of substrate channeling. Additionally a simulation using a free diffusional model described by equation 1 was used to model a non-channeling PutA. In equation 1,  $v_1$  is the rate of PRODH activity ( $2.78 \mu\text{M min}^{-1}$ ) using menadione as a flavin electron acceptor, while  $v_2$  ( $5.6 \mu\text{M min}^{-1}$ ) and  $K_{m\text{GSA}}$  ( $35.5 \mu\text{M}$ ) are the steady-state parameters of the P5CDH domain using exogenous L-P5C. Applying the above kinetic parameters to equation 1, the dotted line in Figure 2 represents a progress curve of a non-channeling PutA. A non-channeling PutA is predicted to display a lag phase with transient time,  $\tau$ , equal to the ratio of  $K_m$  to  $V$  of the second enzyme, which is estimated at 6.3 minutes. Taken together, the data suggests the native enzyme channels based on the lack of a lag phase in the native enzyme and the non-channeling simulation using native steady-state rates.

### **BbPutA Proline:ubiquinone Oxidoreductase Activity**

PRODH domain kinetic data using proline and three ubiquinone analogs was also collected for BbPutA. Table 2 depicts  $k_{\text{cat}}$  and  $K_m$  of proline and ubiquinone analogs CoQ<sub>1</sub>, menadione, and MB. GsPutA and *E. coli* PutA (EcPutA) are also shown as points of comparison. Notably, when using CoQ<sub>1</sub>, menadione, or MB, BbPutA has a  $K_m$  for proline in the low millimolar range (1.0-6.9 mM), which is the lowest proline  $K_m$  of any PutA to date. Typically proline  $K_m$  values using these analogs are in range of 30-70 mM, as shown with EcPutA, BjPutA, and now GsPutA (4, 8). Also, based on turnover

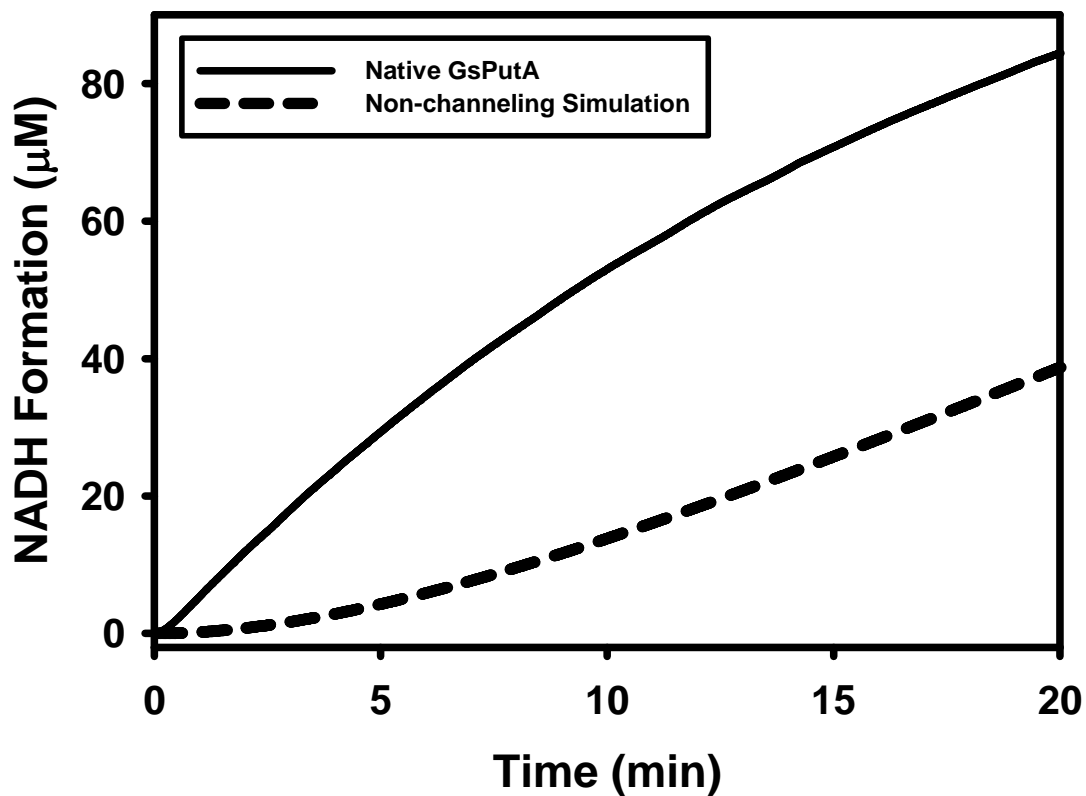


**Figure 2.** Channeling assay depicting the production of NADH from proline by GsPutA. The solid curve represents NADH formation of native GsPutA, while the dashed curve represents a simulation of non-interacting PROD<sub>H</sub> and P5CD<sub>H</sub> based on experimentally determined kinetic values (equation 1). See text for experimentally determined values.

e) BbPutA, and EcPutA using three ubiquinone analogs

	Menadione			Proline (Menadione)		
	$K_m$ ( $\mu\text{M}$ )	$k_{cat}$ ( $\text{s}^{-1}$ )	$k_{cat}/K_m$ ( $\text{M}^{-1} \text{s}^{-1}$ )	$K_m$ (mM)	$k_{cat}$ ( $\text{s}^{-1}$ )	$k_{cat}/K_m$ ( $\text{M}^{-1} \text{s}^{-1}$ )
Bb WT	8.2	0.97	118292	89	0.67	7.5
Bb Y413A	44.6	4.6	103139	6.9	3.0	434
Bb Y413M	79*	3.5*	44000*	67*	2.4*	36*

Fig. 3. (2011) Steady-state kinetic mechanism of the proline ubiquinone oxidoreductase

number and catalytic efficiency, menadione is the preferred electron acceptor for flavin, with well over a two-fold increase in  $k_{cat}$  over other analogs.

### Ubiquinone Active Site Mutants

Using the above PRODH kinetic results, as well as the GsPutA crystal structure with MB bound at the PRODH active site, two BbPutA mutants and one GsPutA mutant were made in attempt to disrupt ubiquinone binding. Bb Y413A, Bb L380A, and Gs Y418A were all made based on the GsPutA and BbPutA crystal structures of the Dr. Jack Tanner lab that showed these native residues interacting with or in close proximity to bound MB. Multiple sequence alignments reveal these same residues are conserved in EcPutA, as Gs Y418 and Bb Y413 align with Ec Y552.

Table 3. Kinetic parameters of Gs and Bb PutA Putative ubiquinone binding site mutants

Enzyme	Menadione			Proline (Menadione)		
	$K_m$ ( $\mu\text{M}$ )	$k_{cat}$ ( $\text{s}^{-1}$ )	$k_{cat}/K_m$ ( $\text{M}^{-1} \text{s}^{-1}$ )	$K_m$ (mM)	$k_{cat}$ ( $\text{s}^{-1}$ )	$k_{cat}/K_m$ ( $\text{M}^{-1} \text{s}^{-1}$ )
Bb WT	44.6	4.6	103139	6.9	3.0	434

L380A	60.9	1.7	27914	163	2.1	12.9
Y413A	14.5**	0.07**	4827**	--	--	0.044***
<b>Gs WT</b>	8.2	0.97	118292	89	0.67	7.5
Y418A	BD*	BD*	BD*	BD*	BD*	BD*

\*Below detection limit.

\*\* [Proline] is 350 mM, which is not saturating.

\*\*\*Unable to saturate with proline (up to 950 mM)

The oxidoreductase activity of these mutants was characterized by determining kinetic parameters using proline or menadione as a variable substrates (Table 3). In the case of Bb L380A, the  $K_m$  for menadione (44.6  $\mu\text{M}$ ) is similar to wild-type (60.9  $\mu\text{M}$ ); however, the  $K_m$  for proline is over 20-fold higher than wild-type at (163 to 6.9 mM), suggesting proline binding is affected by this mutant.

Bb Y413A and Gs Y418A were also characterized. The  $K_m$  for proline of Bb Y413A was unable to be determined due to a lack of saturation even at nearly 1 M proline, but the  $k_{\text{cat}}/K_m$  was calculated to be  $0.044 \text{ M}^{-1}\text{s}^{-1}$ , which is nearly 10,000 times lower than wild-type. When determining kinetic parameters using menadione as a variable substrate, the  $K_m$  and  $k_{\text{cat}}$  were unable to be successfully estimated because proline was not at saturating levels. Similarly, kinetic data for the homologous residue in GsPutA, Y418A, was unable to be collected due to a lack of activity, even at enzyme concentrations of 2.5  $\mu\text{M}$ . Taken together, all three mutants seem to have a marked effect on proline binding, especially Bb Y413A and Gs Y418A.

While menadione binding was not directly affected by the active site mutations, it is interesting to point out that the GsPutA crystal structures reveal both ubiquinone (MB) and proline bind at the *si* face of the flavin (personal correspondence). Previous

structural evidence suggests they also share active site residues, as Bb Y413 and Gs Y418 are homologous to *E. coli* Y552, which interacts with proline analog L-tetrahydro-2-furoic acid (THFA) through van der Waals interactions (10, 11). Conversely, the mechanism of the proline:ubiquinone oxidoreductase reaction was shown to be a two-site ping-pong mechanism, suggesting proline and ubiquinone bind at separate sites. However, these observations are both possible because the substrates associate with different conformations of the enzyme. The GsPutA structures suggest proline binds and the ion gate closes to sequester the active site, but when MB is bound the PRODH site remains open. In this scenario, it is possible to share active site residues and still have a two-site ping pong mechanism.

What the kinetic results do not convey is whether ubiquinone binding is affected, especially in the case of Bb Y413A and presumably Gs Y418A. In BbY413 proline binding is clearly affected, but we cannot conclude any definitive kinetic information from menadione because menadione binding is dependent on proline oxidation. Further studies to determine the menadione dissociation constant using wild-type and mutants may provide insight into the effectiveness of the mutants in binding menadione. Additionally, identifying residues that interact with menadione further from the proline binding site may provide more kinetic support for the putative ubiquinone binding site.

## **SUMMARY**

Kinetic characterization of GsPutA showed MB is a comparable substrate to menadione, as menadione and MB have similar kinetic parameters. MB also was shown to follow a two-site ping pong mechanism previously shown in EcPutA with CoQ<sub>1</sub>, suggesting MB binds to the same site as other quinones. Ubiquinone binding mutants

were inconclusive as to their effect on ubiquinone binding due to the weakened affinity of proline to the enzyme. Finally, GsPutA was shown to channel P5C, which provides a second kinetic and structural example of a channeling PutA.

## **PART II: DrPRODH Characterization**

### **INTRODUCTION**

The second project presented in this chapter involves the recently solved crystal structure of *Deinococcus radiodurans* PRODH (DrPRODH) solved by Min Luo of the Tanner Lab (12). The DrPRODH structure is of interest because the conformational changes between the oxidized and reduced states of corresponding PRODHs and PutAs have not been established structurally (though limited proteolysis experiments suggest conformational change (13)). A structure of oxidized PutA (BjPutA) exists, but the reduced structure does not (4). Likewise, the structure of TtPRODH has been determined without substrate bound, but the substrate-bound reduced structure is unknown (14). Structures both of oxidized and reduced DrPRODH bound by THFA were determined, allowing conclusions to be made about conformational changes both within the active site and peripherally in PRODH enzymes (12).

Interestingly, the oxidized structure displays flavin in two different conformations, both of which bind THFA. In the THFA-bound reduced structure, the flavin undergoes a large conformational change, going from a planar isoalloxazine to a bent conformation, which has also been observed in *E. coli* PutA (15). However, unlike the oxidized state, the flavin occupies a single conformation. Flavin reduction also changes global protein conformation. One such change involves  $\beta_1\alpha_1$  loop (residues 62-

69) and  $\alpha_8$  helix (residues 285-295), which interact through ion pair R291-E64 in the oxidized state (Figure 3). In the reduced state the linkage is ruptured, opening the active site to solvent. Based on this observation, the  $\beta_1\alpha_1$  loop was explored. A well-conserved glycine-glutamate motif (G63 and E64 in DrPRODHD) seen in all monofunctional PRODHDs and PutAs was identified, and mutants G63A and E64A were made using site-directed mutagenesis (14). Here Part II will explore the kinetic characterization of wild-type as well as these mutants, which will help draw conclusions regarding the

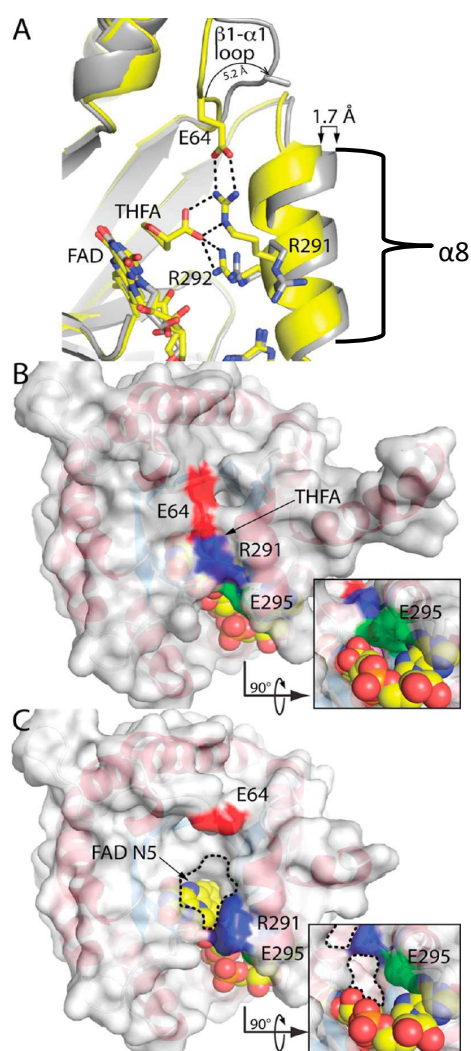


**Figure 3.** Structure of DrPRODHD depicting the conformational changes induced by

flavin reduction. A. Superimposed oxidized structure (yellow) and reduced structure (grey), which shows the shift in helix 8 and the  $\beta 1$ - $\alpha 1$  loop. Black dotted lines depict electrostatic interactions of the oxidized structure. B. Surface representation of the oxidized structure. FAD is shown as yellow spheres, THFA shown as pink spheres. The E64 and R291 electrostatic interaction is shown in red and blue, respectively. C. Surface representation of the reduced structure, where dashed lines indicate the opening in the active site. Coloring is the same as B. Figure adapted from (12).

involvement of G63 and E64 in catalysis.

## **MATERIALS AND METHODS**

### **Enzyme Activity Assays**

All chemicals used during kinetic characterization were purchased from Fischer Scientific or Sigma-Aldrich. All steady-state assays were conducted at 23 °C in 50 mM potassium phosphate, 25 mM NaCl at pH 7.5. For all assays, Coenzyme Q<sub>1</sub> (CoQ<sub>1</sub>) was used as the electron acceptor with CoQ<sub>1</sub> reduction monitored by the decrease in absorbance at 278 nm using a molar extinction coefficient of 14.5 mM<sup>-1</sup> cm<sup>-1</sup> (8). The  $K_m$  for proline and  $k_{cat}$  for wild-type DrPROD<sub>H</sub> (0.25  $\mu$ M) were determined by varying the concentration of proline (0 - 500 mM) while keeping CoQ<sub>1</sub> constant (200  $\mu$ M). Inhibition of wild-type DrPROD<sub>H</sub> (0.25  $\mu$ M) by THFA was analyzed by varying proline (10 - 500 mM) and THFA (0 - 200 mM), while keeping CoQ<sub>1</sub> constant (200  $\mu$ M). These assays were performed in a total volume of 200  $\mu$ l per assay using a Powerwave XS microplate spectrophotometer (Bio-Tek). The  $K_m$  for CoQ<sub>1</sub> and  $k_{cat}$  for wild-type DrPROD<sub>H</sub> (0.25  $\mu$ M) were determined by varying CoQ<sub>1</sub> (0 - 200  $\mu$ M) and keeping proline constant (500

mM). For the DrPRODHD mutants G63A (11  $\mu\text{M}$ ) and E64A (6.3  $\mu\text{M}$ ), the  $K_m$  for proline and  $k_{\text{cat}}$  were determined by varying proline (0 - 1000 mM) and holding CoQ<sub>1</sub> constant (200  $\mu\text{M}$ ). The  $K_m$  for CoQ<sub>1</sub> and  $k_{\text{cat}}$  for the DrPRODHD mutants were determined by varying CoQ<sub>1</sub> (10 - 450  $\mu\text{M}$ ) and holding proline constant (500 mM). These assays were performed in a total volume of 150  $\mu\text{l}$  by mixing enzyme and substrate solutions using a Hi-Tech Scientific SF-61DX2 stopped flow instrument equipped with a 0.15 cm path length cell. Steady-state parameters were calculated by fitting initial rate data to the Michaelis-Menten equation and inhibition data were globally fit to a competitive inhibition model using Enzyme Kinetic Wizard (SigmaPlot 12.0).

## RESULTS AND DISCUSSION

The kinetic parameters for wild-type DrPRODHD were first determined (Table 4). The values of  $k_{\text{cat}}$  and  $K_m$  using proline as the variable substrate with fixed CoQ<sub>1</sub> are 8.7 s<sup>-1</sup> and 290 mM, respectively, resulting in a  $k_{\text{cat}}/K_m$  of 30 s<sup>-1</sup>M<sup>-1</sup>. For comparison, the corresponding parameters of the closely related TtPRODHD (47% identical to DrPRODHD) are  $k_{\text{cat}} = 13 \text{ s}^{-1}$ ,  $K_m = 27 \text{ mM proline}$  (16). Those of the *E. coli* PutA are  $k_{\text{cat}} = 5.2 \text{ s}^{-1}$ ,  $K_m = 42 \text{ mM proline}$  (8). Thus, the  $K_m$  for proline of DrPRODHD is higher than expected. The kinetic parameters were also determined using CoQ<sub>1</sub> as the variable substrate at fixed proline concentration. These values are  $k_{\text{cat}} = 14 \text{ s}^{-1}$ ,  $K_m = 155 \mu\text{M}$ . The corresponding values for TtPRODHD are not available. Those of the *E. coli* PutA are  $k_{\text{cat}} = 3.4 \text{ s}^{-1}$ ,  $K_m = 110 \mu\text{M CoQ}_1$  (8). Finally, THFA was found to inhibit DrPRODHD competitively with proline. The estimated  $K_I$  value of 38 mM is over 10 times higher than those of TtPRODHD (1 mM, (16)) and PutA (1.6 mM, (8)). These results suggest that the affinity of DrPRODHD for proline is atypically low. One explanation is the dual conformations of

FAD in the active site. Perhaps one conformation is an inactive state that must undergo conformational change in order to be active. Additional structures of the DrPRODH enzyme could address this.

Catalytic activity is severely impaired in the mutants G63A and E64A (Table 4). The  $k_{\text{cat}}$  values of  $0.08 \text{ s}^{-1}$  and  $0.055 \text{ s}^{-1}$  for G63A and E64A, respectively, are over 100 times lower than that of DrPRODH. The catalytic efficiencies of G63A and E64A are therefore 140-fold and 27-fold lower than that of DrPRODH. Using  $\text{CoQ}_1$  as the varying

**TABLE 4.**  
**Kinetic Parameters for DrPRODHD and DrPRODHD Mutant Enzymes Using Proline and CoQ1 as the Substrates**

	$k_{cat}$ ( $s^{-1}$ )	$K_m$ (mM)	$k_{cat}/K_m$ ( $s^{-1}M^{-1}$ )	Variational Effect ( $k_{cat}/K_m$ of mutant) ( $k_{cat}/K_m$ of DrPRODHD)
DrPRODHD	$8.7 \pm 0.58$	$290 \pm 39$	$30 \pm 4.5$	
G63A	$0.080 \pm 0.006$	$384 \pm 68$	$0.21 \pm 0.04$	$0.007 \pm 0.002$
E64A	$0.055 \pm 0.001$	$50 \pm 6$	$1.1 \pm 0.13$	$0.037 \pm 0.007$
			Proline as the variable substrate <sup>a</sup>	
DrPRODHD	$14 \pm 1$	$0.155 \pm 0.04$	$90323 \pm 24185$	
G63A	$0.043 \pm 0.003$	$0.028 \pm 0.01$	$1535 \pm 559$	$0.017 \pm 0.008$
E64A	$0.046 \pm 0.003$	$0.032 \pm 0.01$	$1438 \pm 458$	$0.016 \pm 0.007$
			CoQ1 as the variable substrate <sup>b</sup>	

<sup>a</sup>[CoQ1] was fixed at 200  $\mu$ M.

<sup>b</sup>[Proline] was fixed at 500 mM.

substrate, the  $k_{\text{cat}}$  values are  $0.043 \text{ s}^{-1}$  and  $0.046 \text{ s}^{-1}$  for G63A and E64A, respectively. These values are 300-fold lower than the  $k_{\text{cat}}$  for DrPRODHD. The kinetic analysis of G63A and E64A confirms the significance of the conserved sequence motif and is consistent with the structures, which suggest that Gly63 is important for the flexibility of the  $\beta 1$ - $\alpha 1$  loop, and Glu64 is important for stabilizing the closed active site.

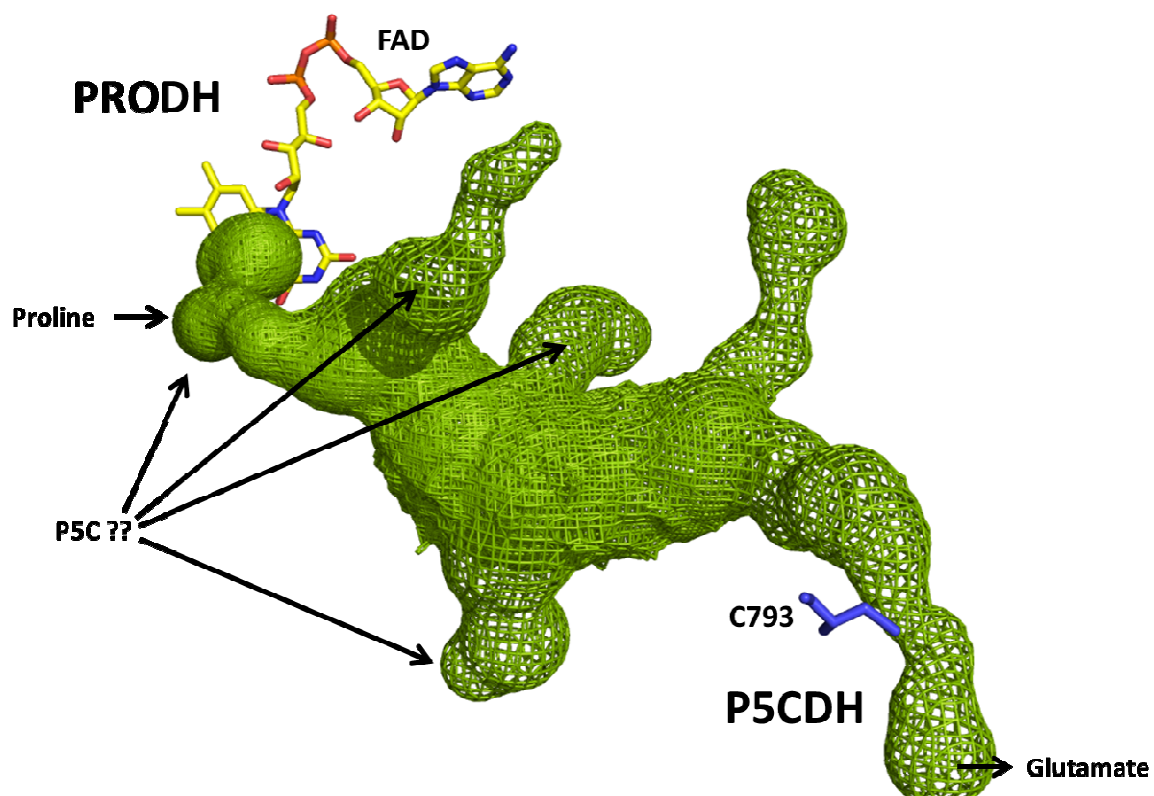
**REFERENCES**

1. Adams, E. (1970) Metabolism of proline and of hydroxyproline, *International review of connective tissue research* 5, 1-91.
2. Singh, R. K., and Tanner, J. J. (2012) Unique structural features and sequence motifs of proline utilization A (PutA), *Frontiers in bioscience : a journal and virtual library* 17, 556-568.
3. Tanner, J. J., and Becker, D. F. (2013) PutA and proline metabolism, In *Handbook of Flavoproteins* (Hille, R., Miller, S. M., and Palfey, B., Eds.), pp 31-56, Walter de Gruyter, Boston.
4. Srivastava, D., Schuermann, J. P., White, T. A., Krishnan, N., Sanyal, N., Hura, G. L., Tan, A., Henzl, M. T., Becker, D. F., and Tanner, J. J. (2010) Crystal structure of the bifunctional proline utilization A flavoenzyme from *Bradyrhizobium japonicum*, *Proceedings of the National Academy of Sciences of the United States of America* 107, 2878-2883.
5. Srivastava, D., Zhu, W., Johnson, W. H., Jr., Whitman, C. P., Becker, D. F., and Tanner, J. J. (2010) The structure of the proline utilization a proline dehydrogenase domain inactivated by N-propargylglycine provides insight into conformational changes induced by substrate binding and flavin reduction, *Biochemistry* 49, 560-569.
6. Hedrick, D. B., Peacock, A. D., Lovley, D. R., Woodard, T. L., Nevin, K. P., Long, P. E., and White, D. C. (2009) Polar lipid fatty acids, LPS-hydroxy fatty acids, and respiratory quinones of three *Geobacter* strains, and variation with electron acceptor, *J Ind Microbiol Biotechnol* 36, 205-209.
7. Bearne, S. L., and Wolfenden, R. (1995) Glutamate gamma-semialdehyde as a natural transition state analogue inhibitor of *Escherichia coli* glucosamine-6-phosphate synthase, *Biochemistry* 34, 11515-11520.
8. Moxley, M. A., Tanner, J. J., and Becker, D. F. (2011) Steady-state kinetic mechanism of the proline:ubiquinone oxidoreductase activity of proline utilization A (PutA) from *Escherichia coli*, *Archives of biochemistry and biophysics* 516, 113-120.
9. Meek, T. D., Garvey, E. P., and Santi, D. V. (1985) Purification and characterization of the bifunctional thymidylate synthetase-dihydrofolate reductase from methotrexate-resistant *Leishmania tropica*, *Biochemistry* 24, 678-686.
10. Zhang, M., White, T. A., Schuermann, J. P., Baban, B. A., Becker, D. F., and Tanner, J. J. (2004) Structures of the *Escherichia coli* PutA proline dehydrogenase domain in complex with competitive inhibitors, *Biochemistry* 43, 12539-12548.
11. Tanner, J. J. (2008) Structural biology of proline catabolism, *Amino Acids* 35, 719-730.
12. Luo, M., Arentson, B. W., Srivastava, D., Becker, D. F., and Tanner, J. J. (2012) Crystal structures and kinetics of monofunctional proline dehydrogenase provide insight into substrate recognition and conformational changes associated with flavin reduction and product release, *Biochemistry* 51, 10099-10108.

13. Zhu, W., and Becker, D. F. (2003) Flavin redox state triggers conformational changes in the PutA protein from *Escherichia coli*, *Biochemistry* 42, 5469-5477.
14. White, T. A., Krishnan, N., Becker, D. F., and Tanner, J. J. (2007) Structure and kinetics of monofunctional proline dehydrogenase from *Thermus thermophilus*, *J Biol Chem* 282, 14316-14327.
15. Zhang, W., Zhang, M., Zhu, W., Zhou, Y., Wanduragala, S., Rewinkel, D., Tanner, J. J., and Becker, D. F. (2007) Redox-induced changes in flavin structure and roles of flavin N(5) and the ribityl 2'-OH group in regulating PutA--membrane binding, *Biochemistry* 46, 483-491.
16. White, T. A., Krishnan, N., Becker, D. F., and Tanner, J. J. (2007) Structure and kinetics of monofunctional proline dehydrogenase from *Thermus thermophilus*, *J Biol Chem* 282, 14316-14327.

# CHAPTER 5

## Conclusions and Future Directions



## SUMMARY AND FUTURE DIRECTIONS

Proline metabolism has become an important area of study due to its involvement in many different cellular processes from bacterial abiotic stress survival and pathogenicity, to human tumor suppression and cellular redox control (1-6). This dissertation sought to further knowledge of proline catabolism through kinetic exploration of proline utilization A (PutA). First, substrate channeling was studied by making bulky mutations along a cavity connecting the PRODH and P5CDH domains (Chapter 2). Mutants D779Y and D779W showed a significant decrease in P5CDH activity when compared to wild-type. To rule out mis-folded active sites, kinetic parameters  $k_{\text{cat}}$  and  $K_m$  for the PRODH and P5CDH domains were obtained. The PRODH kinetics for both mutants were similar to wild-type, suggesting the PRODH site was unperturbed; however, the P5CDH domain  $k_{\text{cat}}$  for D779Y (140-fold slower) and D779W (1000-fold slower) were both significantly slower than wild-type. To distinguish between P5C interacting with the P5CDH active site and a mis-folded P5CDH domain,  $\text{NAD}^+$  dissociation constants were determined for all mutants. In all cases, the  $K_d$  values for  $\text{NAD}^+$  aligned well with those of wild-type, suggesting P5C was not efficiently arriving at the active site.

Next single-turnover reactions were performed to determine if P5C produced in the PRODH domain was bottlenecked by the mutations, preventing movement to the second active site. Results indicated that, even under single turnover conditions, D779Y did not adequately transfer P5C through the channel. Together, these results all suggest D779Y and D779W orient into the channel and hinder passage of P5C to the P5CDH domain. Based on these results, other conclusions regarding the channel can also be

made. Kinetic results indicate both exogenous P5C and endogenous P5C generated by proline oxidation show decreased P5CDH activity in the mutants. This suggests that the entry/exit point of P5C is upstream of the mutation, and P5C cannot enter the P5CDH domain at the presumable NADH/glutamate entry/exit channel. This will be further discussed below for future directions.

An additional experiment performed determined kinetic constants of alternative substrates for the P5CDH domain. The hypothesis was that smaller substrates will be able to better navigate the obstruction caused by mutants D779Y and D779W. The D779Y/W  $k_{cat}/K_m$  of succinate semialdehyde and propionaldehyde were compared to wild-type and were shown to improve when using smaller substrates. These results may also suggest that the P5C-GSA equilibrium favors the ringed P5C at this point in the channel, as linear substrate succinate semialdehyde appears to move through the channel more efficiently.

To summarize, D779Y and D779W appear to impede passage of P5C to the P5CDH domain, allowing conclusions discussed above to be drawn about the usage of the channel. However, many questions still remain and will be targets of future experiments. As outlined above, we know the channel is leaky, but where P5C enters and exits remains a mystery. A future direction to answer this question involves mutant A987Y, which appears to block a channel (Channel 2, Figure 1) to bulk solvent near the D779Y/W mutation site. To determine if this is an entry exit point for P5C, mechanistic inhibitor N-propargylglycine (PPG) will be used to inactivate the PRODH domain (7). Next P5CDH activity assays will be performed in the presence and absence of the inhibitor and either wild-type or A987Y. From this experiment we will be able to

determine whether exogenous P5C uses the same channel proline uses to access the channel, or whether P5C uses the channel blocked by the A987Y mutation. Additional work to determine the where the P5C/GSA hydrolysis takes place may also be possible, especially with the work described above.

Chapter 3 discusses the creation of an artificial trifunctional PutA using long bifunctional PutA *R. capsulatus* and the DNA-binding domain of *E. coli*. Characterization of this trifunctional PutA showed both PRODH activity and overall channeling activity was similar to wild-type RcPutA. When determining DNA-binding ability *in vitro*, the EcRHH-RcPutA enzyme had a similar disassociation constant to wild-type *E. coli* PutA. Additionally *in vitro* EcRHH-RcPutA interacted with the membrane in the presence and absence of proline similar to *E. coli* PutA. When assaying the chimera in cell-based assays, membrane interaction in the presence of proline showed similar phenotypes to RcPutA and EcPutA; however, the chimera did not interact with DNA. Although not presented in this dissertation, Dr. Jack Tanner's group at University of Missouri-Columbia determined small-angle X-ray scattering (SAXS) structure of the chimera enzyme and found that it was a V-shaped dimer in solution, similarly to what was previously reported for EcPutA (8). However, the EcRHH-RcPutA trench is not as wide or as deep as EcPutA. This may be due to a shorter separation of the catalytic lobes, meaning more EcPutA residues may be necessary to create a groove that resembles EcPutA. As a future direction, we are currently working to add 34 additional EcPutA residues to the DNA-binding domain. In EcPutA, the additional residues are part of a linker region between the RHH domain and the arm domain. Performing a cell-based assay with a DNA-binding domain containing the additional 34 residues will provide

further structure-function knowledge of the DNA-binding portion of functional switching.

Chapter 4 explores the kinetics of *G. sulfurreducens* PutA (GsPutA), the structure of which was recently solved by the lab of Dr. Jack Tanner. Of great interest to PutA biochemists are the different structures that were solved. Previously the only full length PutA was that of BjPutA (9). As discussed in Chapter 4, the new structures provide snapshots never before seen at different points of catalysis. Additionally, the ubiquinone binding site was determined with ubiquinone analog menadione bisulfite bound at the *si* face of flavin. In the work presented here, we verified menadione bisulfite was a substrate of GsPutA through kinetic characterizations. Results indicated that it was a substrate, having similar catalytic efficiencies to known substrate menadione. Following substrate verification, the kinetic mechanism of the proline:ubiquinone oxidoreductase activity was investigated. Previously it was shown that EcPutA uses a two-site ping-pong mechanism when using CoQ<sub>1</sub> as an electron acceptor. To verify menadione bisulfite uses the same mechanism in GsPutA, product inhibition of L-P5C was explored. Results indicated that GsPutA also uses a two-site ping-pong mechanism. Substrate channeling was also studied in GsPutA. Channeling assays showed no lag in NADH formation, while a simulation of non-interacting PROD<sub>H</sub> and P5CD<sub>H</sub> using experimentally determined values showed a lag of 6.3 minutes. Finally of note, Chapter 4 contains kinetic results for GsPutA, BbPutA, and EcPutA for flavin electron acceptors CoQ<sub>1</sub>, menadione, and menadione bisulfite.

Future directions for GsPutA are many, as crystal structures reveal several different snapshots of enzyme catalysis. It would be very interesting to look at changes

in channel topography with respect to different stages of catalysis. Perhaps other tunnels to bulk solvent become evident, or the channel constricts or expands during turnover.

The structures also revealed several channels from the cavity to the surface that potentially can be blocked with mutagenesis to determine if they have a role in supplying the cavity with water for hydrolysis of P5C/GSA or whether exogenous P5C can use the tunnels for an entry-exit point.

**REFERENCES**

1. Nakajima, K., Inatsu, S., Mizote, T., Nagata, Y., Aoyama, K., Fukuda, Y., and Nagata, K. (2008) Possible involvement of put A gene in *Helicobacter pylori* colonization in the stomach and motility, *Biomed Res* 29, 9-18.
2. Krishnan, N., Doster, A. R., Duhamel, G. E., and Becker, D. F. (2008) Characterization of a *Helicobacter hepaticus* putA mutant strain in host colonization and oxidative stress, *Infect Immun* 76, 3037-3044.
3. Szabados, L., and Savoure, A. (2010) Proline: a multifunctional amino acid, *Trends Plant Sci* 15, 89-97.
4. Wood, J. M., Bremer, E., Csonka, L. N., Kraemer, R., Poolman, B., van der Heide, T., and Smith, L. T. (2001) Osmosensing and osmoregulatory compatible solute accumulation by bacteria, *Comp Biochem Physiol A Mol Integr Physiol* 130, 437-460.
5. Yoshihara, Y., Kiyosue, T., Katagiri, T., Ueda, H., Mizoguchi, T., Yamaguchi-Shinozaki, K., Wada, K., Harada, Y., and Shinozaki, K. (1995) Correlation between the induction of a gene for delta 1-pyrroline-5-carboxylate synthetase and the accumulation of proline in *Arabidopsis thaliana* under osmotic stress, *Plant J* 7, 751-760.
6. Krishnan, N., Dickman, M. B., and Becker, D. F. (2008) Proline modulates the intracellular redox environment and protects mammalian cells against oxidative stress, *Free Radic Biol Med* 44, 671-681.
7. Srivastava, D., Zhu, W., Johnson, W. H., Jr., Whitman, C. P., Becker, D. F., and Tanner, J. J. (2010) The structure of the proline utilization a proline dehydrogenase domain inactivated by N-propargylglycine provides insight into conformational changes induced by substrate binding and flavin reduction, *Biochemistry* 49, 560-569.
8. Singh, R. K., Larson, J. D., Zhu, W., Rambo, R. P., Hura, G. L., Becker, D. F., and Tanner, J. J. (2011) Small-angle X-ray scattering studies of the oligomeric state and quaternary structure of the trifunctional proline utilization A (PutA) flavoprotein from *Escherichia coli*, *J Biol Chem* 286, 43144-43153.
9. Srivastava, D., Schuermann, J. P., White, T. A., Krishnan, N., Sanyal, N., Hura, G. L., Tan, A., Henzl, M. T., Becker, D. F., and Tanner, J. J. (2010) Crystal structure of the bifunctional proline utilization A flavoenzyme from *Bradyrhizobium japonicum*, *Proc Natl Acad Sci U S A* 107, 2878-2883.